APPENDIX F: **Comparison of Two Geomechanical Analysis Codes for WIPP Disposal Room Modeling: SANCHO and SPECTROM-32**

F-2

Comparison of Two Geomechanical Analysis Codes for WIPP Disposal Room Modeling: SANCHO and SPECTROM-32

Topical Report RSI-0461

D.A. Labreche
RE/SPEC Inc.
4775 Indian School Rd., NE
Suite 300
Albuquerque, NM 87110

G.D. Callahan, K.L. DeVries, J.D. Osnes
RE/SPEC Inc.
P.O. Box 725
Rapid City, SD 57709

Comparison of Two Geomechanical Analysis Codes for WIPP Disposal Room Modeling: SANCHO and SPECTROM-32

D.A. Labreche
RE/SPEC Inc.
Albuquerque, NM 87110

G.D. Callahan, K.L. DeVries, J.D. Osnes
RE/SPEC Inc.
Rapid City, SD 57709

ABSTRACT

Two geomechanical stress analysis computer programs, **SANCHO** and **SPECTROM-32**, have been used extensively to simulate disposal room problems at the Waste Isolation Pilot Plant (WIPP). Past attempts to compare results obtained with these programs have met with varying degrees of success. In this study, the material models used to represent the host salt formation, backfill material, and TRU waste were examined for the two codes. Where significant material model differences existed, **SPECTROM-32** was modified to include the material models contained in **SANCHO**. The same material models may now be executed for the host salt and the TRU waste in the two codes although the deviatoric portion of the creep consolidation model used for the crushed salt backfill is different. A fundamental difference exists between the codes; **SANCHO** is based on a finite strain formulation while **SPECTROM-32** is based on a small strain formulation. Verification problems and a waste disposal room problem are presented. For a typical WIPP waste disposal room, the results from the two codes compare reasonably well despite their remaining differences.

CONTENTS

Tables

Tables (Continued)

Figures

1.0 INTRODUCTION

The Waste Isolation Pilot Plant (WIPP) is a research and development facility constructed to demonstrate the safe management, storage, and eventual disposal of transuranic (TRU) waste generated by the U.S. Department of Energy. The WIPP, located in southeastern New Mexico at a depth of approximately 655 m (2,150 ft) in bedded halites, consists of a series of underground drifts, panels, and disposal rooms. Each disposal room, measuring roughly $4 \times 10 \times 91$ m ($13 \times 33 \times 300$ ft), will be filled with containers holding TRU waste of various forms. After the containers are placed in a room, a majority of the remaining space will be backfilled, sealed, and left to consolidate with time.

This consolidation or closure process is a complex series of events (Butcher and Mendenhall, in preparation) which involves changes in the void spaces within the waste and backfill, deformation of the surrounding salt, brine migration into the room, and the potential for gas generation within the TRU waste. Of interest in this report are those aspects of the closure process that depend on in situ stresses and the mechanical properties of the engineering materials within and around the room. The mechanical and physical changes in the disposal room contents and the surrounding salt are studied by means of computer simulations with appropriate mathematical models of the material response to changes in stress or strain over time. These mathematical models are contained within computer programs developed to obtain solutions to properly defined boundary value problems.

Two specific computer programs (codes) have been involved in a majority of the WIPP disposal room modeling efforts up to the present time — **SANCHO** (Stone et al., 1985) and **SPECTROM-32** (Callahan et al., 1990). Both codes are based on the finite element method, although there are several differences in the implementation of the numerical schemes (Butcher and Mendenhall, in preparation). The primary purpose of this report is to document some of the recent activities aimed at understanding the differences in simulation results calculated by these codes. This report does not constitute the final resolution on the comparison of **SANCHO** and **SPECTROM-32**, although it does extend the discussions contained in Butcher and Mendenhall (in preparation). Rather, this report is a status and a summary of activities conducted in an attempt to resolve some of the unanswered questions relevant to **SANCHO** and **SPECTROM-32** predictions of disposal room response.

This report begins with a presentation of the components of the disposal room numerical model, i.e., the computer program and its constitutive models, the physical and engineering

characteristics of the problem(s) of interest, and the modeling approach(es) used. The steps taken during a study of the computer code differences are summarized in Chapter 3 (Simulation Results) and the report concludes with several observations and recommendations relative to further activities and steps that can be taken to prevent creation of additional differences.

2.0 DESCRIPTION OF NUMERICAL MODEL COMPONENTS

In general terms, a numerical model is a mathematical representation of physical phenomena. There are numerous approaches to numerical modeling, although common approaches have developed around particular classes of phenomena, e.g., Eulerian finite difference codes for hypervelocity impact problems and Lagrangian finite difference codes for fluid flow in porous media. The finite element method (FEM) is a common approach used for solid mechanics applications, although within the FEM, there are a variety of numerical techniques for solving the equations developed for a particular problem. At a finer level of detail, within each code, there are special models (constitutive relations) that describe how a given material responds when a particular stress or strain state is imposed on it. And finally, at the center of each numerical model are various methods to represent the special set of conditions for which a solution is desired. Each of the above areas constitutes a component of the total numerical model. For the particular task of comparing the results of computer simulations from two different numerical models, discrepancies between any of these components has the potential to produce significant differences in the calculated output.

Understanding the differences between **SANCHO** and **SPECTROM-32** simulation results requires an understanding of each of the model components. The purpose of this chapter is to develop that understanding through a discussion of each component. A brief description of the computer programs **SANCHO** and **SPECTROM-32**, based on existing documentation, provides some insight into the framework within which each code has evolved and some of their unique features. Specific code differences relevant to the current interests are discussed. Next, a description of the constitutive models relevant to WIPP disposal room modeling and the materials represented in the comparison problems are discussed. As much as possible, generic descriptions of the constitutive models are provided. However, when assumptions are required for implementation, the **SPECTROM-32** approach is described. These assumptions are noted as the subtle areas wherein calculated differences may originate. At the conclusion of the discussions of the numerical tools, the general room modeling problem of interest to WIPP is briefly described and the relevant input parameters are presented.

2.1 Description of the Finite Element Codes

Two finite element programs are under consideration: **SPECTROM-32** and **SANCHO**. **SPECTROM-32** is a small-strain, thermomechanical structural analysis program developed by RE/SPEC Inc.,

and **SANCHO** is a large-strain, thermomechanical structural analysis program developed by Sandia National Laboratories.

2.1.1 SPECTROM-32

The following brief description of **SPECTROM-32** was adapted from the code documentation (Callahan et al., 1990).

SPECTROM-32 was written to evaluate the quasi-static infinitesimal strain, time-dependent, nonlinear deformation of two dimensional solids. Although it is a multi-purpose analysis code being designed for the specific needs of U.S. Government programs for high-level nuclear waste disposal in geologic formations, it is not a general purpose finite element program. Most of the options and nonlinear modeling features were incorporated to account for the specific geotechnical needs of the nuclear waste program. Many material component models are available[1], including thermoelastic, thermoviscoelastic, thermoelastic-plastic, and thermovisco-plastic options, as well as accommodation of limited-tension materials and jointed rock mass behavior. A variety of boundary conditions are available, as well as material anisotropy, sliding interfaces, excavation and addition of elements, arbitrary initial stresses, multiple material domains, and load incrementation. The program is formulated using the direct stiffness or displacement method with the basic equations being derived from the principle of virtual work. Potential energy is minimized over each element leading to a system of algebraic equations for each element in terms of nodal displacement and the applied forces on the element. For elastic problems, the system of linear equations is solved directly using the frontal solution process. For inelastic problems, the simple forward or Euler method is used to iterate to a vanishingly small residual force vector.

2.1.2 SANCHO

The following brief description of **SANCHO** was taken from the code documentation (Stone et al., 1985).

---

[1] Additional constitutive relations and capabilities have been added to the current version after publication of the **SPECTROM-32** documentation.

SANCHO is a special purpose, finite element program that has been developed in response to some of the perceived drawbacks with existing finite element software for nonlinear analysis. **SANCHO** was developed to solve the quasi-static, large deformation, inelastic response of two dimensional solids. The element library is based on a bilinear isoparametric quadrilateral with a constant bulk strain. The equilibrium solution strategy uses an iterative scheme designed around a self-adaptive dynamic relaxation algorithm. The iterative scheme is based on explicit central difference pseudo-time integration with artificial damping. The code is explicit in nature so that no stiffness matrix is formed or factorized which reduces the amount of computer storage necessary for execution. The explicit nature of the program also makes it attractive for future vectorization on vector processing machines. The code has a standard material model interface which is used with the three (five in the current version[2]) material models incorporated into the code. A finite strain elastic-plastic strain hardening model, a volumetric plasticity model, a metallic creep material model (a continuum joint model, and a nonlinear elastic creep consolidation model for crushed salt), are presently included. A sliding interface capacity, based on a master-slave algorithm, is also incorporated within **SANCHO**. The user-oriented data input scheme is based on keyword descriptors and utilizes a free field reader for ease of data entry. **SANCHO** is designed to work with a separate mesh generation program and to write a data file that can be used by various plot codes for graphical post processing of the data. The capability to write a restart file is also provided.

The capabilities of these two finite element codes are quite similar. The primary differences between these codes in terms of functionality are the wider variety of material models and element types available in **SPECTROM-32**. The primary differences between the codes in terms of formulation are the solution algorithms, the infinitesimal strain formulation used in **SPECTROM-32** versus the finite strain formulation used in **SANCHO**, and a difference in the approach to implementing the slide-lines.

2.2 Description of Constitutive Relations

This section presents the constitutive relations included in **SPECTROM-32** and **SANCHO** for intact salt, crushed salt backfill, TRU waste, and pressure from gas generation that are pertinent to WIPP disposal room analyses. Gas generation is not a constitutive relation but is a decoupled implementation methodology. Discussion is included here since gas generation is a phenomenon modeled in WIPP disposal room problems that requires definition of the equation of state.

---

[2] Additional constitutive relations have been added to the current version after publication of the **SANCHO** documentation.

Additional discussion of constitutive models for **SPECTROM-32** may be found in Callahan et al. (1990) and Callahan and DeVries (1991), and in Stone et al. (1985) for **SANCHO**.

2.2.1 Intact Salt

The total strain rate for the natural rock salt or intact salt constitutive model is assumed to include two components. The components consist of elastic and creep contributions, and the total strain rate is written as

$$\dot{\varepsilon}_{ij} = \dot{\varepsilon}_{ij}^e + \dot{\varepsilon}_{ij}^c \tag{2-1}$$

The elastic strains (ε_{ij}^e) are assumed to be linear elastic and given by Hooke's Law (e.g., Timoshenko and Goodier, 1970). The creep strains (ε_{ij}^c) are described by Krieg (1984) for a steady-state only model and by Munson et al. (1989) for a multi-mechanism model for transient and steady-state creep. Both creep formulations are available in **SPECTROM-32**; whereas, **SANCHO** contains only a steady-state model. Summaries of the linear elastic and creep portions of the model are given here for completeness.

2.2.1.1 LINEAR ELASTIC MODEL

The elastic strains, ε_{ij}^e, are the contribution from the stress field given by Hooke's law

$$\varepsilon_{ij}^e = C_{ijkl}\sigma_{kl} \tag{2-2}$$

where C_{ijkl} is the matrix of elastic constants and σ_{kl} is the stress tensor.

For an isotropic body, there are two independent elastic constants and Equation 2-2 can be written as

$$\varepsilon_{ij}^e = \frac{1}{E}\Big[(1 + \nu)\sigma_{ij} - \nu\sigma_{kk}\delta_{ij}\Big] \tag{2-3}$$

where the elastic material constants E and ν represent Young's modulus and Poisson's ratio. We may also write Equation 2-3 in terms of the bulk modulus (K) and shear modulus (G) for the material as

$$\varepsilon_{ij}^c = \frac{\sigma_m}{3K}\delta_{ij} + \frac{S_{ij}}{2G} \qquad (2\text{-}4)$$

where

$$\sigma_m = \frac{\sigma_{kk}}{3}, \text{ mean stress}$$

$$S_{ij} = \sigma_{ij} - \sigma_m\delta_{ij}, \text{ deviatoric stress} \qquad (2\text{-}5)$$

$$\delta_{ij} = \text{Kronecker delta.}$$

Equation 2-3 may be rearranged to give the elastic constitutive equations for stress in terms of strain

$$\sigma_{ij} = \frac{E}{(1+v)(1-2v)}\left[(1-2v)\varepsilon_{ij}^c + v\varepsilon_{kk}^c\delta_{ij}\right] \qquad (2\text{-}6)$$

2.2.1.2 MUNSON-DAWSON MULTI-MECHANISM CREEP MODEL

The inelastic creep strain rate, as defined by the modified Munson-Dawson material model, is written as

$$\dot{\varepsilon}_e^{ic} = F\dot{\varepsilon}_s \qquad (2\text{-}7)$$

where $\dot{\varepsilon}_e^{ic}$ is the invariant inelastic strain-rate measure and $\dot{\varepsilon}_s$ is the steady-state strain rate. The transient function F consists of three branches — a workhardening branch, an equilibrium branch, and a recovery branch and is written in that order as

$$F = \begin{cases} \exp\left[\Delta\left(1 - \dfrac{\zeta}{\varepsilon_t^f}\right)^2\right] & \zeta < \varepsilon_t^f \\[3mm] 1 & \zeta = \varepsilon_t^f \\[3mm] \exp\left[-\delta\left(1 - \dfrac{\zeta}{\varepsilon_t^f}\right)^2\right] & \zeta > \varepsilon_t^f \end{cases} \qquad (2\text{-}8)$$

Δ and δ are the workhardening and recovery parameters, respectively, and ε_t^f is the transient strain-rate limit. The internal variable ζ is governed by the evolutionary equation

$$\dot{\zeta} = (F - 1)\dot{\varepsilon}_s \qquad (2\text{-}9)$$

and the transient strain-rate limit is given by

$$\varepsilon_t^f = K_0 \exp(cT)\left(\frac{\sigma_e}{\mu}\right)^m \qquad (2\text{-}10)$$

The workhardening parameter is defined as a function of stress

$$\Delta = \alpha + \beta \log\left(\frac{\sigma_e}{\mu}\right) \qquad (2\text{-}11)$$

Because of insufficient data, the recovery parameter is taken to be a constant.

The steady-state strain rate is the sum of the three individual strain-rate mechanisms acting in parallel

$$\dot{\varepsilon}_s = \sum_{i=1}^{3} \dot{\varepsilon}_{s_i} \qquad (2\text{-}12)$$

The three contributing mechanisms — dislocation climb, an undefined mechanism, and glide are written respectively as

$$\dot{\varepsilon}_{s_1} = A_1 \left(\frac{\sigma_e}{\mu} \right)^{n_1} \exp\left(-\frac{Q_1}{RT} \right) \tag{2-13}$$

$$\dot{\varepsilon}_{s_2} = A_2 \left(\frac{\sigma_e}{\mu} \right)^{n_2} \exp\left(-\frac{Q_2}{RT} \right) \tag{2-14}$$

$$\dot{\varepsilon}_{s_3} = \left(B_1 e^{-Q_1/RT} + B_2 e^{-Q_2/RT} \right) \sinh\left[q\left(\frac{\sigma_e - \sigma_0}{\mu} \right) \right] H(\sigma_e - \sigma_0) \tag{2-15}$$

where

σ_e = invariant stress measure

μ = normalizing parameter

q = activation volume

$A_1, A_2, B_1, B_2, n_1, n_2, Q_1,$
$Q_2, \sigma_0, K_0, c, m, \alpha, \beta$ = experimental constants

R = universal gas constant

T = absolute temperature

$H(.)$ = Heaviside step function.

To generalize the Munson-Dawson model to three-dimensional states of stress, Fossum et al. (1988) are followed to define Mises and Tresca types of flow potential functions. The inelastic tensorial strain rate components may be written as

$$\dot{\varepsilon}_{ij}^c = \dot{\varepsilon}_e^c \frac{\partial \sigma_e^f}{\partial \sigma_{ij}} \tag{2-16}$$

where the invariant inelastic strain-rate measure is

$$\dot{\varepsilon}_e^c = \dot{\varepsilon}_e^c \left(T, \sigma_e, \varepsilon_e^c \right) \tag{2-17}$$

The two invariant stress measures in Equations 2-16 and 2-17 are given by

$$\sigma_c^f = \sigma_c^f(\sigma_m, J_2, J_3)$$

$$\sigma_e = \sigma_e(\sigma_m, J_2, J_3)$$

(2-18)

where the mean stress (σ_m), the second invariant of the deviator stress (J_2), and the third invariant of the deviator stress (J_3) are given by

$$\sigma_m = \frac{\sigma_{kk}}{3}$$

$$J_2 = \frac{1}{2}S_{ij}S_{ji}$$

(2-19)

$$J_3 = \frac{1}{3}S_{ij}S_{jk}S_{ki}$$

The Lode angle (ψ), which is a convenient alternative to J_3, is given by

$$\psi = \frac{1}{3}\sin^{-1}\left[\frac{-3\sqrt{3}\,J_3}{2J_2^{3/2}}\right], \quad \left(-\frac{\pi}{6} \leq \psi \leq \frac{\pi}{6}\right)$$

(2-20)

The partial derivative given in Equation 2-16 may be determined using the chain rule as

$$\frac{\partial\sigma_c^f}{\partial\sigma_{ij}} = \frac{\partial\sigma_c^f}{\partial\sigma_m}\frac{\partial\sigma_m}{\partial\sigma_{ij}} + \frac{\partial\sigma_c^f}{\partial J_2}\frac{\partial J_2}{\partial\sigma_{ij}} + \frac{\partial\sigma_c^f}{\partial\psi}\frac{\partial\psi}{\partial J_3}\frac{\partial J_3}{\partial\sigma_{ij}}$$

(2-21)

The derivatives of the invariants in Equation 2-21 are the same regardless of the invariant stress and strain measures selected. These derivatives (Callahan, 1982) are

$$\frac{\partial \sigma_m}{\partial \sigma_{ij}} = \frac{\delta_{ij}}{3}$$

$$\frac{\partial J_2}{\partial \sigma_{ij}} = S_{ij} \qquad (2\text{-}22)$$

$$\frac{\partial \psi}{\partial J_3}\frac{\partial J_3}{\partial \sigma_{ij}} = -\frac{\sqrt{3}}{2J_2^{3/2}\cos 3\psi}t_{ij}$$

where

$$t_{ij} = S_{ip}S_{pj} - \frac{2}{3}J_2\delta_{ij}$$

Therefore, to define completely the inelastic strain-rate measure required by Equation 2-16, the invariant stress and strain-rate measures need to be prescribed. The equivalent inelastic strain-rate measure is given by the Munson-Dawson material model in Equation 2-7. Two types of invariant stress measures are considered. These are termed the pressure-dependent and frictional forms of the invariant stress measure. The pressure-dependent form is similar to the Mises-Schleicher plastic potential, and the frictional form is similar to the Mohr-Coulomb plastic potential. Mathematically, these stress measures are

$$\sigma_c^f = 3\tau\sigma_m + \sqrt{3J_2} \quad \text{(pressure - dependent)} \qquad (2\text{-}23)$$

$$\sigma_e^f = 2\sin\tau\sigma_m + \left(\cos\psi - \frac{\sin\psi \; \sin\tau}{\sqrt{3}}\right)2\sqrt{J_2} \quad \text{(frictional)} \qquad (2\text{-}24)$$

The variable τ is a material constant termed the flow dilatancy parameter. The other invariant stress measure (σ_e) that needs to be described is taken to be identical to those given in Equations 2-23 and 2-24, except that the parameter τ is replaced by a different variable (θ), viz

$$\sigma_e = 3\theta\sigma_m + \sqrt{3J_2} \tag{2-25}$$

$$\sigma_e = 2\sin\theta\sigma_m + \left(\cos\psi - \frac{\sin\psi\,\sin\theta}{\sqrt{3}}\right)2\sqrt{J_2} \tag{2-26}$$

The variable θ is a material constant termed the frictional parameter. If $\theta = \tau$, then $\sigma_e = \sigma_e^f$; however, this is not required theoretically.

Equation 2-21 requires the partial derivatives of the invariant stress measures with respect to stress. Differentiation of Equations 2-23 and 2-24 provides these quantities for the pressure-dependent and frictional forms of the invariant stress measures. These quantities are as follows:

Pressure-Dependent

$$\frac{\partial\sigma_e^f}{\partial\sigma_m} = 3\tau$$

$$\frac{\partial\sigma_e^f}{\partial J_2} = \frac{\sqrt{3}}{2\sqrt{J_2}} \tag{2-27}$$

$$\frac{\partial\sigma_e^f}{\partial\psi} = 0$$

Frictional

$$\frac{\partial \sigma_e^f}{\partial \sigma_m} = 2 \sin \tau$$

$$\frac{\partial \sigma_e^f}{\partial J_2} = \left[\frac{\cos 2\psi}{\cos 3\psi} + \frac{\sin \tau}{\sqrt{3}} (\tan 3\psi \cos \psi - \sin \psi) \right] \frac{1}{\sqrt{J_2}} \qquad (2\text{-}28)$$

$$\frac{\partial \sigma_e^f}{\partial \psi} = -\left[\sin \psi + \frac{\cos \psi \sin \tau}{\sqrt{3}} \right] 2\sqrt{J_2}$$

By letting τ go to zero in Equations 2-23 and 2-24, we eliminate the mean stress dependence and obtain Mises- and Tresca-types of invariant stress measures, respectively. θ is also set to zero such that $\sigma_e = \sigma_e^f$. Thus, Equations 2-23 and 2-24 become

$$\sigma_e = \sqrt{3J_2} \qquad \text{(Mises)} \qquad (2\text{-}29)$$

$$\sigma_e = 2\cos \psi \sqrt{J_2} \qquad \text{(Tresca)} \qquad (2\text{-}30)$$

and the derivatives in Equations 2-27 and 2-28 become

Mises

$$\frac{\partial \sigma_e}{\partial \sigma_m} = 0$$

$$\frac{\partial \sigma_e}{\partial J_2} = \frac{\sqrt{3}}{2\sqrt{J_2}} \qquad (2\text{-}31)$$

$$\frac{\partial \sigma_e}{\partial \psi} = 0$$

Tresca

$$\frac{\partial \sigma_e}{\partial \sigma_m} = 0$$

$$\frac{\partial \sigma_e}{\partial J_2} = \left[\frac{\cos 2\psi}{\cos 3\psi}\right]\frac{1}{\sqrt{J_2}} \qquad (2\text{-}32)$$

$$\frac{\partial \sigma_e}{\partial \psi} = -2\sin\psi\sqrt{J_2}$$

Substituting Equations 2-31, 2-22, and 2-21 into Equation 2-16 gives the familiar generalization for the Mises flow potential

$$\dot{\varepsilon}_{ij}^c = \frac{3\,\dot{\varepsilon}_e^c}{2\sqrt{3J_2}}\,S_{ij} \qquad (2\text{-}33)$$

and substituting Equations 2-32, 2-22, and 2-21 into Equation 3-16 gives the generalization for the Tresca flow potential

$$\dot{\varepsilon}_{ij}^c = \dot{\varepsilon}_e^c\left\{\left[\frac{\cos 2\psi}{\cos 3\psi}\right]\frac{S_{ij}}{\sqrt{J_2}} + \left[\frac{\sqrt{3}\sin\psi}{J_2\cos 3\psi}\right]t_{ij}\right\} \qquad (2\text{-}34)$$

Finally, substitution of Equation 2-7 into Equations 2-33 and 2-34 gives the generalization of the Munson-Dawson model for Mises (octahedral shear) and Tresca (maximum shear) types of flow potentials, respectively. The Tresca flow generalization is typically used in the analysis of underground structures in natural salt formations.

Equation 2-34 is seen to be indeterminant as the Lode angle approaches ±30 degrees. In other words, the flow potential forms corners at $\psi = \pm30$ degrees and the direction of straining is not unique. To eliminate this problem computationally, Equation 2-34 is evaluated in the limit as $\psi \to \pm30$ degrees. Performing this limiting operation, Equation 2-34 becomes

$$\dot{\varepsilon}_{ij}^{c} = \dot{\varepsilon}_{e}^{c} \left\{ \frac{S_{ij}}{\sqrt{3J_2}} \mp \frac{t_{ij}}{2J_2} \right\} \qquad (2\text{-}35)$$

The Tresca flow potential implemented in **SPECTROM-32** uses Equation 2-35 when the Lode angle is within 0.25 degrees of ±30 degrees.

2.2.1.3 STEADY-STATE CREEP MODEL

The WIPP steady-state creep law defined by Krieg (1984) is a secondary creep (steady-state) model defining the creep strain rate $\dot{\varepsilon}_{ij}^{c}$ as

$$\dot{\varepsilon}_{ij}^{c} = \frac{3\,\dot{\varepsilon}_{e}^{c}}{2\sigma_e} S_{ij} \qquad (2\text{-}36)$$

where

$$\dot{\varepsilon}_{e}^{c} = \sqrt{\frac{2}{3}\,\dot{\varepsilon}_{ij}\,\dot{\varepsilon}_{ij}}$$

$$\sigma_e = \sqrt{\frac{3}{2}\,S_{ij}S_{ij}}$$

As written, Equation 2-36 implies selection of the Mises flow potential (cf. Equation 2-33). The effective creep strain rate $\dot{\varepsilon}_{e}^{c}$ is defined as

$$\dot{\varepsilon}_{e}^{c} = D\sigma_{e}^{n}\,\exp\left(-\frac{Q}{RT}\right) \qquad (2\text{-}37)$$

where

Q = activation energy, $\dfrac{\text{cal}}{\text{mol}}$

R = universal gas constant, $1.987\dfrac{\text{cal}}{\text{mol}\cdot\text{K}}$

T = temperature, K

D,n = material constants.

To implement the WIPP secondary creep law form in **SPECTROM-32**, the Munson-Dawson model is used with only one of the steady-state mechanisms active. The effective strain rate $\dot{\varepsilon}_s$, for the dislocation climb mechanism is written as (cf. Equation 2-13)

$$\dot{\varepsilon}_{s_1} = A_1 \left(\frac{\sigma_e}{\mu}\right)^{n_1} \exp\left(-\frac{Q_1}{RT}\right) \tag{2-38}$$

where

Q_1 = activation energy, $\dfrac{cal}{mol}$

μ = normalizing parameter, 12,400 MPa

A_1, n_1 = material constants.

Equations 2-37 and 2-38 are equivalent if $D = \dfrac{A_1}{\mu^{n_1}}$. If we redefine μ as 1, then a one-to-one correspondence exists between Equations 2-37 and 2-38, and the WIPP secondary creep law implementation is complete. The only remaining requirement is that the Mises flow potential be specified for execution.

2.2.2 Crushed Salt

The total strain rate for the crushed salt constitutive model is assumed to consist of two components. The components are nonlinear elastic and creep consolidation contributions and the total strain rate is written as

$$\dot{\varepsilon}_{ij} = \dot{\varepsilon}^e_{ij} + \dot{\varepsilon}^c_{ij} \tag{2-39}$$

The manner in which the nonlinear elastic, ε^e_{ij}, and creep consolidation strains, ε^c_{ij}, are obtained are described by Callahan (1990), Callahan and DeVries (1991), and Weatherby et al. (1991). Since these descriptions were written, the deviatoric portion of the creep consolidation model in **SPECTROM-32** has been modified; the modified **SPECTROM-32** model is described here. Both the nonlinear elastic and creep consolidation portions of the model describe the material behavior in bulk (volumetric) and in shear (deviatoric). Although other models exist and are under consideration to describe the behavior of crushed salt (e.g., Zeuch, 1988 and 1990), the nonlinear elastic and creep consolidation models for crushed salt were adapted from those given by Sjaardema and Krieg (1987) for use in **SANCHO** and **SPECTROM-32**.

2.2.2.1 NONLINEAR ELASTIC MODEL

The elastic model described in Section 2.2.1.1 is applicable to crushed salt with the following procedure used to incorporate the nonlinearity in a piecewise manner.

For the nonlinear elastic model, the functional forms of the elastic constants given by Sjaardema and Krieg (1987) are adopted. They propose bulk and shear moduli as exponential functions of the current density, ρ_s. Tensile stresses and extensile strains are assumed to be positive. Functional forms of the elastic constants are written in terms of the total volumetric strain, ε_v, using the relation

$$\rho_s = \frac{\rho_0}{1 + \varepsilon_v} \tag{2-40}$$

where ρ_0 is the initial or original density of the material. The bulk modulus and shear modulus (K_s and G_s) are given by

$$K_s = K_0 e^{\frac{K_1 \rho_n}{1 + \varepsilon_v}}$$

$$G_s = G_0 e^{\frac{G_1 \rho_n}{1 + \varepsilon_v}} \tag{2-41}$$

where K_0, K_1, G_0, and G_1 are material constants.

At any time, the current values of Young's modulus and Poisson's ratio are computed from the current values of bulk and shear modulus using the relations

$$E_s = \frac{9 K_s G_s}{3 K_s + G_s}$$

$$\nu_s = \frac{3 K_s - 2 G_s}{6 K_s + 2 G_s} \tag{2-42}$$

Equations 2-42 are used in Equation 2-3 to compute the elastic strains.

To solve the nonlinear elastic problem, the method of load incrementation is used to approximate the tangent modulus. The following set of simultaneous equations have to be solved in the direct stiffness finite element approach

$$[K_t]\{\delta\} + \{f\} = 0 \tag{2-43}$$

where f is the total load (or unload) vector, δ is the displacement, and the tangent stiffness matrix K_t is a function of displacement, i.e.,

$$K_t = K_t(\delta) \tag{2-44}$$

since $\{\varepsilon^e\} = [B]\{\delta\}$ and $\varepsilon_v = \varepsilon_{kk}$ with $[B]$ representing the strain-displacement matrix. The load vector is divided into a number of small increments Δf such that the series of tangent moduli will approximate a given stress-strain curve. K_t is first approximated assuming $\varepsilon_v = 0$, which means that $\Delta\delta^0 = 0$ and

$$\left[K_t^0\right]\{\Delta\delta^1\} + \{\Delta f^1\} = 0 \tag{2-45}$$

Repetition of this process for each of the load increments may be written as

$$\{\Delta\delta^n\} = -\left[K_t^{n-1}\right]^{-1}\{\Delta f^n\} \tag{2-46}$$

The process is continued for each of the load increments, and the displacement is accumulated, i.e.,

$$\{\delta\} = \{\delta\} + \{\Delta\delta^n\} \tag{2-47}$$

Clearly, the functional forms adopted for bulk and shear moduli (Equations 2-41) allow increase without bound. Therefore, maximum values for bulk modulus K_f and shear modulus G_f are introduced based on the fully consolidated or intact densities for the material. If either the bulk or shear modulus reaches its maximum value, the tangent modulus is no longer allowed to change, and the material is assumed to be intact and linear elastic.

2.2.2.2 CREEP CONSOLIDATION MODEL

To develop the creep consolidation constitutive equation, general considerations are first observed and then specific functional forms are guided by available laboratory data. From the application of thermodynamic concepts, the three-dimensional generalization for creep strain rates is given by Fossum et al. (1988). Following this approach, three[3] continuum internal variables

---

[3] SPECTROM-32 contains all three components in Equation 2-48; whereas, SANCHO contains the first and third components.

are assumed, the inelastic volumetric strain, $\varepsilon_{eq_1}^c$, and two equivalent inelastic shear strains, $\varepsilon_{eq_2}^c$ and $\varepsilon_{eq_3}^c$. The creep consolidation strain rates are then written as

$$\dot{\varepsilon}_{ij}^c = \dot{\varepsilon}_{eq_1}^c \frac{\partial \sigma_{eq_1}^f}{\partial \sigma_{ij}} + \dot{\varepsilon}_{eq_2}^c \frac{\partial \sigma_{eq_2}^f}{\partial \sigma_{ij}} + \dot{\varepsilon}_{eq_3}^c \frac{\partial \sigma_{eq_3}^f}{\partial \sigma_{ij}} \quad (2\text{-}48)$$

For the first portion (volumetric) of Equation 2-48, the invariant strain-rate measure is

$$\dot{\varepsilon}_{eq_1}^c = \dot{\varepsilon}_v^c(\sigma_m) \quad (2\text{-}49)$$

The volumetric strain rate $\dot{\varepsilon}_v^c$ is described empirically by Sjaardema and Krieg (1987) based on hydrostatic laboratory test data on crushed salt as

$$\dot{\varepsilon}_v^c = \frac{(1 + \varepsilon_v)^2}{\rho_0} B_0 \left[1 - \exp(-B_1 \sigma_m)\right] e^{\frac{A\rho_0}{1+\varepsilon}} \quad (2\text{-}50)$$

where

$\varepsilon_v = \varepsilon_{kk}$, total volumetric strain

$\dot{\varepsilon}_v^c = \dot{\varepsilon}_{kk}^c$, volumetric creep strain rate

$\sigma_m = \dfrac{\sigma_{kk}}{3}$, mean stress

ρ_0 = initial density

B_0, B_1, A = material constants.

The invariant stress measure is given by

$$\sigma_{eq_1}^f = \sigma_m \quad (2\text{-}51)$$

For the second portion (deviatoric) of Equation 2-48, the invariant strain-rate measure is taken to be

$$\dot{\varepsilon}_{eq_2}^c = \beta \, \dot{\varepsilon}_{eq_1}^c = \beta \, \dot{\varepsilon}_v^c(\sigma_m) \quad (2\text{-}52)$$

and the invariant stress is assumed to be a scalar multiple of the octahedral shear stress

$$\sigma_{eq_2}^f = \sigma_c = \sqrt{3J_2} \qquad (2\text{-}53)$$

where J_2 is the second invariant of the stress deviator ($J_2 = \frac{1}{2}S_{ij}S_{ij}$). For the moment, the third component defining the creep consolidation strain rate will be ignored because the description is more readily presented by first considering only two of the components. Substituting the definitions of the invariant stress measures into Equation 2-48 and performing the required differentiation gives

$$\dot{\varepsilon}_{ij}^c = \dot{\varepsilon}_v^c \frac{\delta_{ij}}{3} + \beta\, \dot{\varepsilon}_v^c \frac{3S_{ij}}{2\sigma_c} \qquad (2\text{-}54)$$

β is selected (ignoring the third component) such that in a uniaxial test, the lateral components of $\dot{\varepsilon}_{ij}^c$ equal zero; this requires that $\beta = -\frac{2}{3}$. Simple example problems that illustrate the creep consolidation behavior with and without the second portion of creep consolidation strain rate equation are given by Callahan (1990). The major effect of this deviatoric portion is that the lateral strain components are eliminated in a simulated uniaxial test and that the out-of-plane strain component is eliminated under plane strain conditions. Without this deviatoric component, large tensile stresses in the out-of-plane direction are generated with uniaxial loading. After substituting for $\dot{\varepsilon}_v^c$ in Equation 2-54 and ignoring for the moment the third continuum internal variable portion of the equation, the creep consolidation strain rate components are given by

$$\dot{\varepsilon}_{ij}^c = \frac{(1 + \varepsilon_v)^2}{\rho_0} B_0 \left[1 - \exp(-B_1\sigma_m) \right] \exp\left(\frac{A\rho_0}{1 + \varepsilon_v} \right) \left\{ \frac{\delta_{ij}}{3} - \frac{S_{ij}}{\sigma_c} \right\} \qquad (2\text{-}55)$$

The third component is selected to be identical to either the Munson-Dawson model or the WIPP secondary creep model for intact salt, depending on which model is used to represent the creep behavior of the intact salt. Thus, $\dot{\varepsilon}_{eq_3}^c$ and $\sigma_{eq_3}^f$ are either the Munson-Dawson or WIPP secondary creep model invariant strain-rate and stress measures described in Sections 2.2.1.2 and 2.2.1.3, respectively. However, one notable exception is included that involves modification of the invariant stress measure.

The exception noted above to the two forms of the intact salt creep model includes a modification made to the effective stress measure. This modification stems from envisioning that the porous crushed salt is composed of cylinders of salt, each of which exhibits the creep behavior of intact salt separated by areas of open space as suggested by Sjaardema and Krieg

(1987). The local stress acting on the salt cylinders is stated in terms of the average stress acting on the porous crushed salt. The cross-sectional area of the porous sample is expressed in terms of the net cross-sectional area of the salt cylinders. This implied areal ratio is the inverse of the fractional density. Amplification of the effective stress by the fractional density is analogous to implementation of damage (ω) into constitutive models. Typically, damage will appear in the denominator as $1 - \omega$ with a stress measure in the numerator. As damage accumulates, ω increases ($\omega \rightarrow 1$), magnifying the influence of the stress measure. The consolidation process is basically the reverse of damage; whereby the fractional density divisor serves as a "consolidation" parameter reducing the influence of the stress measure as the crushed salt consolidates. Therefore, in this model, the effective stress in the Munson-Dawson or WIPP secondary creep models is expressed as

$$\sigma_{eq_i}^f = \frac{\rho_f \sigma_e}{\rho} \qquad (2\text{-}56)$$

where

σ_e = Average effective stress measure

ρ = Density

ρ_f = Fully consolidated density.

Obviously, as the material approaches full consolidation, the fractional density approaches 1, and the Munson-Dawson or WIPP secondary creep deviatoric component becomes the same as that for intact salt. Simultaneously, the creep consolidation portion of the model diminishes as the material approaches full consolidation. Therefore, the newly described model provides a smooth transition from crushed salt to intact salt behavior.

With the third component included in the creep consolidation equation for crushed salt as described above, the equation becomes

$$\dot{\varepsilon}_{ij}^c = \frac{(1 + \varepsilon_v)^2}{\rho_0} B_0 \left[1 - \exp(-B_1 \sigma_m) \right] \exp\left(\frac{A\rho_0}{1 + \varepsilon_v} \right) \left\{ \frac{\delta_{ij}}{3} - \frac{S_{ij}}{\sigma_e} \right\}$$
$$+ \dot{\varepsilon}_{eq_i}^c \frac{\rho_f}{\rho} \frac{\partial \sigma_e}{\partial \sigma_{ij}} \qquad (2\text{-}57)$$

Two alternative forms of the crushed salt consolidation are obtained for the Munson-Dawson deviatoric component — one for the Mises flow potential

$$\dot{\varepsilon}_{ij}^{c} = \frac{(1 + \varepsilon_{v})^{2}}{\rho_{0}} B_{0} \left[1 - \exp(-B_{1}\sigma_{m}) \right] \exp\left(\frac{A\rho_{0}}{1 + \varepsilon_{v}} \right) \left\{ \frac{\delta_{ij}}{3} - \frac{S_{ij}}{\sigma_{e}} \right\} \tag{2-58}$$

$$+ \dot{\varepsilon}_{eq_1}^{c} \frac{\rho_f}{\rho} \frac{3S_{ij}}{2\sqrt{3J_2}}$$

and one for the Tresca flow potential

$$\dot{\varepsilon}_{ij}^{c} = \frac{(1 + \varepsilon_{v})^{2}}{\rho_{0}} B_{0} \left[1 - \exp(-B_{1}\sigma_{m}) \right] \exp\left(\frac{A\rho_{0}}{1 + \varepsilon_{v}} \right) \left\{ \frac{\delta_{ij}}{3} - \frac{S_{ij}}{\sigma_{e}} \right\} \tag{2-59}$$

$$+ \dot{\varepsilon}_{eq_1}^{c} \frac{\rho_f}{\rho} \left\{ \left[\frac{\cos 2\psi}{\cos 3\psi} \right] \frac{S_{ij}}{\sqrt{J_2}} + \left[\frac{\sqrt{3}\sin\psi}{J_2 \cos 3\psi} \right] t_{ij} \right\}$$

where $\dot{\varepsilon}_{eq_1}^{c}$ is defined by Equation 2-7 for the Munson-Dawson model. Typically, only Equation 2-58 is used for the WIPP secondary creep model, where $\dot{\varepsilon}_{eq_1}^{c}$ is defined by Equation 2-38.

Since the creep consolidation equation allows unlimited consolidation, a cap is introduced that eliminates further consolidation when the intact material density ρ_f is reached. Thus, when the condition

$$|\varepsilon_v| \geq \left| \frac{\rho_0}{\rho_f} - 1 \right| \tag{2-60}$$

is satisfied, no further creep consolidation occurs. A somewhat different cap is imposed in **SANCHO**. When the current density reaches 99.9 percent of the intact material density, creep consolidation is stopped, and the density is set equal to the intact density. In addition, creep consolidation is not permitted to generate tensile stresses in **SPECTROM-32**. The procedure used to eliminate any tensile stresses is the same as described by Callahan et al. (1990) for a limited-tension material. Also, an option is included that allows a consolidating material's constitutive model to be redefined following complete consolidation. For example, a crushed salt material can be prescribed to behave according to the intact salt constitutive relation following complete consolidation. This option does not exist as a switch in **SANCHO**, but material change effectively occurs by virtue of the crushed salt constitutive model when the intact material density is reached.

2.2.2.3 COMBINED CRUSHED SALT MODEL

The final two equations for the total strain rate in the constitutive model for crushed salt are obtained by substituting Equation 2-3 and either Equation 2-58 or 2-59 into Equation 2-39, which for a Mises flow potential, yields

$$\dot{\varepsilon}_{ij} = \frac{\dot{\sigma}_m}{3K}\delta_{ij} + \frac{\dot{S}_{ij}}{2G} + \frac{(1+\varepsilon_v)^2}{\rho_0} B_0 \left[1 - \exp(-B_1\sigma_m)\right] \exp\left(\frac{A\rho_0}{1+\varepsilon_v}\right)$$

$$\left\{\frac{\delta_{ij}}{3} - \frac{S_{ij}}{\sigma_e}\right\} + \dot{\varepsilon}^c_{eq_1} \frac{\rho_f}{\rho} \frac{3S_{ij}}{2\sqrt{3J_2}} \tag{2-61}$$

and for the Tresca flow potential, yields

$$\dot{\varepsilon}_{ij} = \frac{\dot{\sigma}_m}{3K}\delta_{ij} + \frac{\dot{S}_{ij}}{2G} + \frac{(1+\varepsilon_v)^2}{\rho_0} B_0 \left[1 - \exp(-B_1\sigma_m)\right] \exp\left(\frac{A\rho_0}{1+\varepsilon_v}\right)$$

$$\left\{\frac{\delta_{ij}}{3} - \frac{S_{ij}}{\sigma_e}\right\} + \dot{\varepsilon}^c_{eq_1} \frac{\rho_f}{\rho} \left\{\left[\frac{\cos 2\psi}{\cos 3\psi}\right]\frac{S_{ij}}{\sqrt{J_2}} + \left[\frac{\sqrt{3}\sin\psi}{J_2\cos 3\psi}\right]t_{ij}\right\} \tag{2-62}$$

where $\dot{\varepsilon}^c_{eq_1}$ is defined by Equation 2-7 for the Munson-Dawson model deviatoric form and by Equation 2-38 for the WIPP secondary creep model form.

The above equation may be collapsed to yield the total volumetric strain-rate ($\dot{\varepsilon}_v$) expression for the model. Performing this operation yields

$$\dot{\varepsilon}_v = \frac{\dot{\sigma}_m}{K} + \frac{(1+\varepsilon_v)^2}{\rho_0} B_0 \left[1 - \exp(-B_1\sigma_m)\right] \exp\left(\frac{A\rho_0}{1+\varepsilon_v}\right) \tag{2-63}$$

When the combined nonlinear elastic and creep consolidation model is used, the relative change in the Euclidean or L_2 norm of the volumetric strain is monitored over time and the stiffness is updated when the change is greater than a user prescribed tolerance. Further details may be found in Callahan (1990).

2.2.3 TRU Waste

The basic equations describing the TRU waste model as given by Stone et al. (1985) are presented in this section. The TRU waste model is an elastic-plastic model of the Drucker-Prager type with a flat volumetric cap coincident with the deviatoric plane in principal stress space. The deviatoric part of the model is elastic-perfectly plastic such that the surface of revolution in principal stress space is stationary (i.e., neither kinematic nor isotropic hardening is allowed). The cap portion of the model hardens with volumetric straining such that the cap moves outward along the hydrostatic axis during volumetric yielding. The deviatoric and volumetric hardening parts of the model are uncoupled. The deviatoric yield function is given by

$$F_d = J_2 - \left(a_0 - a_1\sigma_m + a_2\sigma_m^2\right) \tag{2-64}$$

where

$$J_2 = \frac{1}{2}S_{ij}S_{ij}$$

$$S_{ij} = \sigma_{ij} - \sigma_m\delta_{ij}, \text{ deviatoric stress}$$

$$\sigma_m = \frac{\sigma_{kk}}{3}, \text{ mean stress} \tag{2-65}$$

$$\delta_{ij} = \text{Kronecker delta}$$

$$a_o, \ a_1, \ a_2 = \text{material constants.}$$

At yield, $F_d = 0$ and we may write Equation 2-64 as

$$F_d = \sqrt{J_2} - \sqrt{\left(a_o - a_1\sigma_m + a_2\sigma_m^2\right)} = 0 \tag{2-66}$$

which can more readily be compared to a Drucker-Prager type yield function.

The volumetric yield function is simply

$$F_v = \sigma_m - f(\varepsilon_v) \tag{2-67}$$

where $\varepsilon_v = \varepsilon_{kk}$ is the volumetric strain and $f(\varepsilon_v)$ describes the volumetric hardening by a set of pressure-volumetric strain relations (i.e., data pairs entered in tabular form). As an option, SPECTROM-32 also includes a mean stress-porosity functional form by which the volumetric hardening can be evaluated. This function is written as

$$\sigma_m = \frac{1}{3\kappa} \ln\left(\frac{\phi}{\phi_0}\right) \tag{2-68}$$

where

$$\kappa = \text{material parameter}$$

$$\phi_0 = \text{initial porosity.}$$

In addition to the deviatoric and volumetric parts of the plastic constitutive model, a tensile limit is also imposed. Tensile fracture does not occur as long as a particular tensile pressure is not large enough to produce a zero or imaginary deviatoric yield stress. Mathematically, fracture has not occurred if

$$\sigma_m < p \tag{2-69}$$

where p is the minimum root of the polynomial $a_0 - a_1\sigma_m + a_2\sigma_m^2 = 0$. If Equation 2-69 is not satisfied, the mean stress is set equal to p.

The plastic strain increment vector $d\varepsilon_{ij}^p$ is given by the flow rule

$$d\varepsilon_{ij}^p = d\lambda \frac{\partial M}{\partial \sigma_{ij}} \tag{2-70}$$

where M is the plastic potential function. If the yield function (F_d) is equal to the plastic potential function, F_d replaces M in Equation 2-70, and it is termed an associative flow rule; otherwise, the term *nonassociative flow* is used. For associative flow, the normality rule is satisfied which ensures a unique solution for boundary-value problems. For the deviatoric portion of the model, **SANCHO** uses a nonassociative flow rule so that deviatoric strains produce no volume change. This requires that the plastic potential function for the deviatoric model be

$$M = \sqrt{J_2} \tag{2-71}$$

and Equation 2-70 becomes

$$d\varepsilon_{ij}^p = d\lambda \frac{S_{ij}}{2\sqrt{J_2}} \tag{2-72}$$

For the volumetric portion of the model, Drucker's stability postulate for work-hardening materials (linearity requirement) is considered (e.g., see Chen and Han, 1988), which requires that

$$de_{ij}^p = \frac{1}{h} \partial F_v \frac{\partial F_v}{\partial \sigma_{ij}} = \frac{1}{h} \frac{\partial F_v}{\partial \sigma_{ij}} \frac{\partial F_v}{\partial \sigma_{mn}} d\sigma_{mn} \tag{2-73}$$

where h is a scalar hardening function which may depend upon stress, strain, and loading history. Using Equation 2-67, $\frac{\partial F_v}{\partial \sigma_{ij}} = \frac{\delta_{ij}}{3}$, and $\partial F_v = d\sigma_m$, Equation 2-73 takes the form

$$de_{ij}^p = \frac{1}{h} \frac{\delta_{ij}}{3} d\sigma_m \tag{2-74}$$

Rewriting Equation 2-74 for the plastic volumetric strain gives

$$d\varepsilon_{kk}^p = \frac{1}{h} d\sigma_m \tag{2-75}$$

which may be rearranged to produce

$$h = \frac{d\sigma_m}{d\varepsilon_{kk}^p} \tag{2-76}$$

Therefore, the hardening modulus describes the relationship between increments in mean stress (pressure) and increments in volumetric strain. Rather than prescribe a specific hardening function, **SANCHO** requires a pressure-volumetric strain relationship to describe the volumetric hardening behavior $f(\varepsilon_v)$, which is shown by Stone et al. (1985) plotted schematically as σ_m versus $\ln(\frac{\rho}{\rho_0})$ with an initial bulk modulus of K_0.

The tangent bulk modulus described by Callahan and DeVries (1991) used to model the TRU waste as a nonlinear elastic material is given by

$$K_t = \frac{d\sigma_m}{d\varepsilon_v} \tag{2-77}$$

where the mean stress-volumetric strain is written in terms of the porosity ϕ as given in Equation 2-68. Therefore, from Equations 2-76 and 2-77, a basic equivalency exists between the nonlinear elastic tangent bulk modulus and the flat, volumetric, plastic-cap hardening modulus. Thus, the volumetric strain behavior produced by the nonlinear elastic and crushable foam plastic models should yield equivalent results as long as the same pressure-volumetric strain relationships are used to define the tangent bulk modulus and the plastic hardening modulus. This is also a conclusion of Sandler et al. (1976) who state that the behavior of a cap model with a vertical cap and a bulk modulus, K, which is the same for loading and unloading (i.e., $K_L = K_U$), is identical

to the uncapped model with $K_L < K_U$. This is readily seen because with an associative flow rule applied to the vertical cap, only plastic volume changes occur. The crushable foam model uses the initial bulk modulus K_0 for loading and unloading. The **SPECTROM-32** nonlinear elastic model uses the tangent bulk modulus for loading and unloading (loads and unloads along the same path). Therefore, if we neglect unloading, the crushable foam plastic and nonlinear elastic models should produce equivalent volumetric behavior. This conclusion is basically true but is violated in plane strain types of problems because of the nature of the out-of-plane behavior in elastic and plastic types of problems. In elastic problems, the out-of-plane stress created by loading is equal to Poisson's ratio times the sum of the in-plane components. In elastic-plastic problems, the out-of-plane stress created by loading is altered by the out-of-plane plastic flow. Thus, the mean stresses obtained for the two problems will be different.

2.2.4 Gas Generation

This section outlines the approach used for incorporating the effect of gas pressures into simulations of backfilled and sealed WIPP rooms using **SPECTROM-32**. The assumptions are discussed first followed by the modeling approach and the specific equations of state considered.

2.2.4.1 GAS GENERATION ASSUMPTIONS

WIPP disposal rooms are modeled as sealed regions filled with compressible, consolidating porous media in which gas is being generated. The following assumptions are made:

- The surface of the region is perfectly impermeable, so that the gas within the porous region cannot leak through the surface.

- The hydraulic diffusivity (ratio of hydraulic conductivity to specific storage) of the porous media is extremely large, so that pressure gradients within the porous region are negligible and the total pressure is essentially uniform throughout the region.

- The apparent diffusion coefficients (Fickian diffusion coefficients modified to account for the interference of the solid phase) of the gas constituents are large enough that the composition of the gas is essentially uniform throughout the region.

- In lieu of the last two assumptions, it can be assumed that each gas constituent is being generated uniformly throughout the porous region, so that pressure and concentration gradients cannot develop.

- The temperature is constant and uniform throughout the porous region.

- The compressibility of the solid grains within the porous media is negligible compared to the compressibility of the voids and the gas occupying them, so that the change in the porous region's volume is essentially equivalent to the change in the void (and gas) volume within the region.

- The gas pressure can be calculated according to an equation of state that is defined in terms of the gas composition, mass, volume, and temperature.

- The change in gas pressure across a time step in the simulation is relatively small, so that the gas pressure can be treated as a constant across the time step.

2.2.4.2 MODELING APPROACH

Based upon the preceding assumptions, **SPECTROM-32** models the effect of gas generation on the closure of a WIPP disposal room by calculating the resultant gas pressure in the room and applying that pressure as a normal traction boundary condition acting on the surfaces of the room. Consequently, a portion of the surface load normally transmitted to and carried by the backfill in the disposal room will be supported by the gas pressure. This results in smaller mean stresses in the backfill, which in turn cause a reduction in the backfill consolidation rate since the consolidation rate is a function of the mean stress.

If the gas pressure becomes large enough, some or all of the room's surface will be supported entirely by the gas. In these areas, the backfill stress perpendicular to the surface will become zero because the backfill is not carrying any of the surface load. Further, if the pressure continues to increase, the surfaces entirely supported by the gas will actually open. In this case, the stress in the backfill should remain zero and should not become tensile. In **SPECTROM-32**, the creep-consolidation model that has been used to represent the backfill in WIPP disposal rooms contains a "no-tension" algorithm that enforces the latter condition.

To model the effect of gas generation, **SPECTROM-32** requires the following information to specify the gas-generation conditions:

- List of elements that defines the porous region in which the gas is confined.

- List of element sides that defines the impermeable surface surrounding the porous region.

- Initial porosity of the porous region.

- Absolute temperature of the gas.

- Equation of state that will be used to calculate the gas pressure as a function of the gas temperature, mass of its constituents, and the volume that it occupies.

- Tabulation of the mass of each gas constituent as a function of time.

- Universal gas constant and equation-of-state constants for each gas constituent.

The initial porosity specified in the gas-generation region needs to be consistent with the properties specified for the materials in the porous region. For example, if the initial and the grain (solid) densities of the porous materials are specified (as in the creep-consolidation constitutive model), the equivalent initial porosity is

$$\phi_o = 1 - \frac{\rho_o}{\rho_s} \qquad (2\text{-}78)$$

where

ϕ_0 = initial porosity

ρ_0 = initial density of the porous material

ρ_s = grain (solid phase) density of the porous material.

The initial porosity is used to calculate the initial void volume in the porous region according to the following equations:

$$V_0 = \sum^{R} V_i'(0) \qquad (2\text{-}79)$$

$$V_{vO} = \phi_0 V_0 \qquad (2\text{-}80)$$

where

$$V_0 = \text{initial volume of the porous region}$$

$$V_i^e(0) = \text{undeformed (t=0) volume of the i}^{th} \text{ element in the porous region}$$

$$V_{v0} = \text{initial void volume of the porous region.}$$

and the summation is over all of the elements in the porous region R. Gaussian quadrature is used to calculate the elemental volumes by integration. The initial volume V_o of the porous region is calculated in the initialization module of **SPECTROM-32** and is saved for subsequent calculations of the void volume.

2.2.4.3 EQUATIONS OF STATE

As stated in the assumptions, the gas pressure is calculated according to an equation of state that is defined in terms of the gas composition, volume, and temperature. Several equations of state are included in **SPECTROM-32**, including the ideal gas equation, the Redlich-Kwong equation, and the Beattie-Bridgeman equation. These three equations of state are incorporated because they have been used in past analyses of WIPP rooms and/or because they are fairly accurate within their applicable ranges.

2.2.4.3.1 Ideal Gas Equation of State

Weatherby et al. (1991) used the ideal gas equation of state to calculate the gas pressure in their analyses of the structural response of a WIPP disposal room with internal gas generation. The ideal gas equation leads to the following expression for the pressure of a pure gas:

$$P = \frac{nRT}{V} \tag{2-81}$$

where

$$P = \text{gas pressure}$$

$$n = \text{moles of gas (mass of gas divided by its molecular weight)}$$

$$R = \text{universal gas constant } (8.314 \times 10^{-6} \text{ MJ/mol K})$$

$$T = \text{absolute temperature of gas}$$

$$V = \text{volume occupied by gas.}$$

The pressure of a mixture of gases is calculated according to the Gibbs-Dalton Law, as follows:

$$P = \sum_{i=1}^{N_{mix}} P_i \qquad (2\text{-}82)$$

where

P = total pressure of gas mixture

N_{mix} = number of constituents in mixture

P_i = partial pressure of ith constituent.

The partial pressure of each gas constituent in the mixture is calculated using the ideal gas equation (Equation 2-81 with n replaced by n_i, the number of moles of the ith constituent).

Substituting partial pressures calculated according to the ideal gas equation into the Gibbs-Dalton Law produces Equation 2-81 with n replaced by $n_{mix} = \sum_{i=1}^{N} n_i$, the total moles of gas in the mixture. Consequently, only the total moles of gas needs to be known to calculate the pressure with this approach; the composition of the mixture is not needed.

Ideal gas behavior can be assumed with good accuracy at very low pressures regardless of the temperature. Further, at temperatures greater than twice the critical temperature of the gas, ideal gas behavior can be assumed with good accuracy to pressures of about 7 MPa. When the temperature is less than twice the critical temperature and the pressure is above a very low value (e.g., greater than atmospheric pressure), then the deviation from ideal gas behavior may be considerable (Van Wylen and Sonntag, 1973). At low pressures relative to the critical pressure, the Gibbs-Dalton Law usually yields total pressures to a precision approximating that of the constituent data (i.e., the partial pressures calculated using the ideal gas equation of state). However, at higher pressures, the Gibbs-Dalton Law becomes quite unreliable (Keenan, 1941).

2.2.4.3.2 Redlich-Kwong Equation of State

Lappin and Hunter (1989) used the Redlich-Kwong equation of state (Redlich and Kwong, 1949) to estimate the gas pressure in WIPP disposal rooms. This equation of state leads to the following expression for the pressure of a pure gas:

$$P = \frac{nRT}{V - nb} - \frac{n^2 a}{V\sqrt{T}(V + nb)} \qquad (2\text{-}83)$$

where

$$a = \Omega_a R^2 T_c^{2.5}/P_c \qquad (2\text{-}84)$$

$$b = \Omega_b RT_c/P_c \qquad (2\text{-}85)$$

$$\Omega_a = 0.4278$$

$$\Omega_b = 0.0867$$

$$T_c = \text{critical temperature}$$

$$P_c = \text{critical pressure.}$$

For application to gas mixtures, Redlich proposed that constants a and b in Equation 2-83 be calculated as follows:

$$a = \left(\sum_{i=1}^{N_{mix}} y_i \sqrt{a_i} \right)^2 \qquad (2\text{-}86)$$

$$b = \sum_{i=1}^{N_{mix}} y_i b_i \qquad (2\text{-}87)$$

where

a_i = constant a for the ith constituent
(calculated according to Equation 2-84)

b_i = constant b for the ith constituent
(calculated according to Equation 2-85)

y_i = mole fraction of the ith constituent (n_i/n_{mix}).

For mixtures, n in Equation 2-83 is replaced by n_{mix}, the total moles of gas in the mixture.

The Redlich-Kwong equation is a generalized equation of state. Constants a and b have an approximate physical significance: a provides a rough measure of the attractive intermolecular forces, and b gives an approximate indication of the molecular size. The values of coefficients Ω_a and Ω_b in Equations 2-84 and 2-85 were derived by equating to zero the first two derivatives of pressure with respect to volume at the critical point. This derivation leads to a compressibility

factor Z (where $Z = PV/nRT$) that is too large at the critical point. Nonetheless, the Redlich-Kwong equation of state is fairly accurate for pure gases at densities that are moderate relative to the critical density. For some mixtures, the mixing rules given by Equations 2-86 and 2-87 are very good. However, it appears that whenever two constituents are appreciably different from one another in chemical nature and/or molecular size, the proposed mixing rules are not reliable (Prausnitz, 1969).

2.2.4.3.3 Beattie-Bridgeman Equation of State

The Beattie-Bridgeman equation (Beattie and Bridgeman, 1928) is an empirical equation of state that is widely used and has proven to be of great utility in formulating the properties of the vapor phase of many substances. According to this equation of state, the pressure is calculated using the following equation:

$$P = \frac{RT(1 - \varepsilon)}{v^2}(v + B) - \frac{A}{v^2} \qquad (2\text{-}88)$$

where

$$A = A_0 (1 - a/v) \qquad (2\text{-}89)$$

$$B = B_0 (1 - b/v) \qquad (2\text{-}90)$$

$$\varepsilon = c/(vT^3) \qquad (2\text{-}91)$$

$$v = V/n \text{ (molal volume)}. \qquad (2\text{-}92)$$

For a pure gas, A_0, a, B_0, b, and c are constants that have been determined empirically for that specific gas. For a mixture of gases, Beattie (1929) proposed that the mixture constants be calculated from the constituent constants (denoted by subscript i) according to the following equations:

$$A_0 = \left(\sum_{i=1}^{N_{mix}} y_i \sqrt{A_{0i}} \right)^2 \tag{2-93}$$

$$a = \sum_{i=1}^{N_{mix}} y_i a_i \tag{2-94}$$

$$B_0 = \sum_{i=1}^{N_{mix}} y_i B_{0i} \tag{2-95}$$

$$b = \sum_{i=1}^{N_{mix}} y_i b_i \tag{2-96}$$

$$c = \sum_{i=1}^{N_{mix}} y_i c_i \tag{2-97}$$

and n in Equation 2-92 is replaced by n_{mix}, the total moles of gas in the mixture.

The Beattie-Bridgeman equation is quite accurate (within 2 percent) for pure gases at densities less than 0.8 of their critical density (Holman, 1974; Van Wylen and Sonntag, 1973). Further, when applied to mixtures, the Beattie-Bridgeman equation generally yields a good representation of the pressure over the range of conditions for which each pure constituent is well represented by the Beattie-Bridgeman equation (when the mass of each constituent divided by the total volume is less than half of that constituent's critical density, according to Keenan, 1941).

2.3 Description of the Disposal Room Problem

The specifications for the room geometry and contents in the disposal room simulations were defined by the WIPP baseline design (Bechtel, 1986). Note that this baseline design was adopted by the Engineered Alternatives Task Force (EATF). The baseline case was the most appropriate model of the disposal room system; the specifications for the baseline case were taken from Stone (1992).

2.3.1 Geometry, Boundary and Initial Conditions

In the baseline case, each disposal room is 3.96 m high by 10.06 m wide by 91.44 m in length, resulting in an initial room volume of 3,644 m^3. The disposal rooms are separated by 30.48-m thick pillars. The rooms are assumed to be located in a homogeneous layer of bedded salt thus eliminating the need to model the numerous stratigraphic layers present at the WIPP. Uniformly distributed throughout each room are 6,804 drums of unprocessed waste. The corresponding volume occupied by the drums of waste is 1,663 m^3. With the specified headspace of 0.71 m between the backfill and the roof, the total volume of crushed salt backfill in each room is approximately 1,328 m^3. The emplaced density of the crushed salt backfill is assumed to be 1300 kg/m^3, which corresponds to an initial porosity of approximately 0.4.

Combining the assumption of a homogeneous salt stratigraphy with the assumption that gravitational forces do not greatly affect material response near the room permits the introduction of a horizontal symmetry plane through the room and waste. The problem can thereby be reduced to a quarter-symmetry model. The model boundaries are vertical symmetry planes at the room and pillar centerlines, producing a model width of 20.27 m (66.5 ft), and a symmetry boundary at the bottom of the model and a traction boundary 54 m (177.2 ft) above the centerline of the room. The initial stress field throughout the modeled region was prescribed to be hydrostatic and equal to −14.8 MPa.

The gas generation rate in the baseline case is assumed to be 2 mol/drum/yr during the first 550 years and 1 mol/drum/yr during the next 500 years. Gas generation is assumed to cease after 1,050 years.

2.3.2 Material Properties

This section presents the material properties associated with the constitutive relations discussed in Section 2.2 for intact salt, crushed salt, TRU waste, and generated gas pressures that are pertinent to WIPP disposal room analyses. These properties are used for the verification and WIPP disposal room problems included in Chapter 3. Any exceptions from use of these material parameter values are indicated with the specific problem discussion.

2.3.2.1 INTACT SALT

The linear elastic parameter values for the constitutive relation given in Equation 2-3 and the parameter values for the Munson-Dawson constitutive equation represented by Equation 2-7 are presented in Table 2-1. Density of the intact salt is 2,140 kg $\cdot$ m^{-3}. The intact salt material parameters were taken from Munson (1989) for pure halite. Material parameters for the WIPP secondary creep law are given in Table 2-2 as reported by Krieg (1984). Note that analyses performed using the WIPP secondary creep model typically include a modulus reduced by a factor of 12.5 (Morgan and Krieg, 1988). Thus, the value for Young's modulus in Table 2-2 reflects the reduced value.

2.3.2.2 CRUSHED SALT

The nonlinear elastic parameter values describing the nonlinear moduli for crushed salt defined in Equation 2-41 are given in Table 2-3. The values labeled *Reduced Modulus Value* represent the parameter values used when the WIPP secondary creep law is used with the modulus reduced by 12.5. Thus, the crushed salt stiffness is also reduced so that the crushed salt consolidates to the reduced modulus value of intact salt. Table 2-3 also gives the initial and final (intact) densities for the crushed salt. Table 2-4 presents the parameter values for the creep consolidation constitutive equation represented by Equation 2-50. The crushed salt material parameters are taken from Sjaardema and Krieg (1987). When either the Munson-Dawson or WIPP secondary creep models are used to describe the deviatoric response in the crushed salt material model, as described for Equations 2-61 and 2-62, the creep parameter values given in Tables 2-1 and 2-2 are used in addition to the parameter values for the creep consolidation model.

2.3.2.3 TRU WASTE

The material parameters for the *crushable foam* TRU waste model described by Equations 2-64 and 2-67 are given in Tables 2-5 and 2-6. Table 2-5 includes the elastic material parameters, initial characteristics, and the parameters for the deviatoric portion of the plasticity model. Table 2-6 includes the pressure-volumetric strain relation used to describe the volumetric hardening behavior of the TRU waste.

Table 2-1. Munson-Dawson parameter values for intact salt

Parameter	Units	Value
	Elastic Parameter Values	
E	MPa	31,000
ν	—	0.25
	Munson-Dawson Creep Parameter Values	
A_1	yr^{-1}	2.645E+30
	s^{-1}	8.386E+22
A_2	yr^{-1}	3.050E+20
	s^{-1}	9.672E+12
Q_1/R	K	12,581
Q_1	cal/mol	25,000
Q_2/R	K	5,032
Q_2	cal/mol	10,000
n_1	—	5.5
n_2	—	5.0
B_1	yr^{-1}	1.919E+14
	s^{-1}	6.0856E+06
B_2	yr^{-1}	9.568E+05
	s^{-1}	3.034E−02
q	—	5.335E+03
σ_o	MPa	20.57
μ	MPa	12,400
m	—	3
K	—	6.275E+5
c	K^{-1}	9.198E-3
α	—	−17.37
β	—	−7.738
δ	—	0.58

Table 2-2. WIPP steady-state creep law parameters for salt

Parameter	Units	Value
Elastic Parameter Values		
E	MPa	2,480
ν	—	0.25
Creep Parameter Values		
A_1	$MPa^{-n_1} \cdot yr^{-1}$	1.4544×10^{-6}
	$MPa^{-n_1} \cdot yr^{-1}$	$4.5866 \times 10^{+1}$
n_1	—	4.9
Q_1	cal/mol	12,000
Q_1/R	K	6,039
μ	MPa	1.0

Table 2-3. Nonlinear elastic material parameters for crushed salt

Parameter	Units	Value	Reduced Modulus Value
K_0	MPa	0.01760	0.001408
K_1	m^3/kg	0.00653	0.006530
G_0	MPa	0.01060	0.000846
G_1	m^3/kg	0.00653	0.006530
K_f	MPa	20,626	1,656
G_f	MPa	12,423	992
ρ_0	kg/m^3	1,300	1,300
ρ_f	kg/m^3	2,140	2,140

2.3.2.4 GAS GENERATION

Gas generation potential and gas production rate within the disposal room are composed of gas resulting from anoxic corrosion and microbial activity. The pressure within the disposal room caused by the gas generation is assumed to be governed by the ideal gas law discussed in

Section 2.2.4.3. Therefore, the only parameter value needed to prescribe the pressure resulting from the gas generation is the number of moles of gas production. Stone (1992) reports that the estimated gas production from anoxic corrosion is 1,050 mol/drum with a production rate of 1 mol/drum/yr and the estimated gas production from microbial activity is 550 mol/drum with a production rate of 1 mol/drum/yr. This means that the microbial activity ceases after 550 years while the anoxic corrosion ceases after 1,050 years. The number of drums within a disposal room is assumed to be 6,804.

Table 2-4. Creep consolidation material parameters for crushed salt

Parameter	Units	Value
B_0	$kg/m^3 \cdot s^{-1}$	$1.3 \times 10^{+8}$
	$kg/m^3 \cdot yr^{-1}$	$4.10 \times 10^{+15}$
B_1	MPa^{-1}	0.82
A	m^3/kg	-1.73×10^{-2}

Table 2-5. Material parameters values for TRU waste

Parameter	Units	Value
ρ_0	kg/m^3	790.4
ϕ_0		0.74
K	MPa	222
G	MPa	333
a_0	MPa^2	0
a_1	MPa	0
a_2		3

Table 2-6. Crushable foam pressure — volumetric relation for TRU waste

Point	Volumetric Strain, ε_{kk} (Natural)	Volumetric Strain, ε_{kk} (Engineering)	Mean Stress, σ_m (MPa)
1	0.032	0.0315	0.028
2	0.741	0.5234	0.733
3	0.898	0.5926	1.133
4	1.029	0.6426	1.667
5	1.180	0.6927	2.800
6	1.536	0.7848	10.170

3.0 SIMULATION RESULTS

This chapter compares the results of numerical simulations performed with **SANCHO** (RE/SPEC Version 1.06) and **SPECTROM-32** (Versions 4.03 and 4.04) and discusses observed differences. However, since this report is a summary of the current status of studies conducted to explain the cause of simulation differences, a brief history up to and including the analyses presented later in this chapter is included. Presentation and discussion of the verification problems and the disposal room simulation results follow the history.

3.1 Brief History of Recent Disposal Room Modeling Efforts

Butcher and Mendenhall (in preparation) discuss the results of analyses performed with **SPECTROM-32** and **SANCHO** on empty rooms, backfilled rooms, rooms with waste and backfill, and rooms with gas-generating waste and backfill. Differences between the calculated results are noted in their report. Plausible explanations for these differences include: (1) infinitesimal strain theory used in **SPECTROM-32** versus finite strain theory used in **SANCHO**, (2) different models of the intact salt (an empirically scaled secondary creep model in **SANCHO** versus an experimentally based fundamental creep model in **SPECTROM-32**), and (3) different waste compaction models (a volumetric plasticity model in **SANCHO** versus an empirically based nonlinear elastic model in **SPECTROM-32**). The objective of the work reported herein was to eliminate the last two factors from consideration and to identify the magnitude of finite strain effects that could be expected for a representative disposal room problem. Elimination of differences in constitutive models was accomplished through modifications to **SPECTROM-32**.

Initially, **SPECTROM-32** contained a nonlinear elastic model for the TRU waste as described in Callahan and DeVries (1991). Discrepancies in the amount of compaction computed by **SANCHO** and **SPECTROM-32** for the TRU waste prompted a more detailed examination of the model included in the two codes (see Appendix A). The differences in the results produced by the **SPECTROM-32** nonlinear elastic model and the **SANCHO** plastic compaction model were found to be largely attributable to different assumptions used to derive each of the models' parameters from TRU waste compaction experiments (Butcher et al., 1991). The compaction experiments were conducted on simulated waste in rigid steel sleeves and only the axial stress component was measured. To evaluate parameter values for the TRU waste models, assumptions were required regarding the magnitude of the lateral stress components. Two bounding assumptions are available to infer values for the lateral stress components in the experiments: (1) the lateral

components are zero (i.e., $\sigma_a = 3\sigma_m$) and (2) the lateral stress components are equal to the axial stress component (i.e., $\sigma_a = \sigma_m$), where σ_a and σ_m represent the axial and mean stress, respectively. The first assumption was used to derive the nonlinear elastic model for the TRU waste and the second assumption was used to derive the pressure-volumetric strain relation for the plastic compaction model of the TRU waste. When the second assumption was used for development of the nonlinear elastic model, the average void fractions in the TRU waste (Appendix A) computed using **SPECTROM-32** increased substantially and were similar in magnitude to those computed using **SANCHO** with the plastic compaction TRU waste model. Subsequent efforts (Appendix B) showed that the volumetric behavior predicted by the nonlinear elastic model and the plastic compaction model are equivalent except in plane strain problems (cf. Section 2.2.3). Therefore, to eliminate model differences entirely as an issue, the **SANCHO** plastic compaction model used for TRU waste was incorporated into **SPECTROM-32**. A description of this volumetric plasticity model (also called the crushable foam model) is included in Section 2.2.3 and may also be found in the **SANCHO** manual (Stone et al., 1985).

A specific documented verification problem was not available for this model within the **SANCHO** manual so Verification Problem 29, or simply VP29, was created to test implementation of the plastic compaction TRU waste model in **SPECTROM-32**. VP29 and six other simple verification problems were run to examine the correctness of the model implementation. A secondary objective for these verification problems was to provide a set of simple problems that could be analyzed with both **SANCHO** and **SPECTROM-32** to assist the general understanding of other potential code differences.

A substantial effort was also required to develop a version of **SANCHO** that could be used for comparative analyses with **SPECTROM-32**. This was required because **SANCHO** was not installed on the open computer systems (the Sandia National Laboratories Cray X-MP system at Livermore and VAX Cluster in Building 823) being used for analyses. Therefore, a version of **SANCHO** obtained in 1987 and installed on RE/SPEC's MicroVAX was used. The major modification to this version of **SANCHO** included incorporation of the creep consolidation model used for crushed salt.

3.2 Verification Problem Analyses

Two of the seven simple verification problems were analyzed with **SPECTROM-32** and **SANCHO** to examine the TRU waste and crushed salt constitutive model behavior. The first problem is Verification Problem 29 (VP29), a standard verification problem used for **SPECTROM-32**. VP29

consists of volumetric compaction of a material that behaves according to the plastic compaction TRU waste model (crushable foam plasticity model). The second verification problem examines the time-dependent compaction of a cylindrical (axisymmetric) material that behaves according to the crushed salt creep consolidation model. Descriptions of these two problems and comparison of the results obtained with **SPECTROM-32** and **SANCHO** are discussed separately in the next two subsections.

3.2.1 Hydrostatic Compaction of TRU Waste (VP29)

Verification Problem 29 simulates a body that is loaded hydrostatically in 1 MPa increments up to 5 MPa. Two geometrical configurations are considered — axisymmetric and plane strain. Unload-reload cycles occur at 2 and 4 MPa for the problem with axisymmetric geometry; however, no unload cycles were included for the plane strain geometry problem. Other than these differences in loading and geometry, the two problems were identical. The volumetric strain calculated by the crushable foam plasticity model is the output of interest.

VP29 is a uniform stress and strain problem; thus, arbitrary specimen dimensions can be chosen. **SPECTROM-32** and **SANCHO** both modeled a one unit wide by one unit high problem domain. The left boundary represents the axis of symmetry for the axisymmetric problem and a plane of symmetry for the plane strain problem, and the lower boundary is fixed against displacement normal to the boundary (i.e., rollered) for both geometries. Tractions were applied to the top and right boundaries and scaled by a history function to simulate the increments in loading and unloading. The unloading cycle in the **SANCHO** simulations did not totally remove the load but instead reduced the applied traction to a nominally low value (0.025 MPa) to prevent nonconvergence of the solution; whereas, the load was reduced to zero in the **SPECTROM-32** simulations. The input files for the **SANCHO** and **SPECTROM-32** simulations are given in Appendix C. Additional information regarding the **SPECTROM-32** simulation may be found in Appendix **B**.

SPECTROM-32 has two options for specification of the compaction function — pressure-volumetric strain data pairs or a mean stress-porosity functional form from which the volumetric hardening can be evaluated. Both options were exercised in obtaining the solution to VP29 with **SPECTROM-32**. The pressure-volumetric strain pairs used in **SPECTROM-32** are given in Appendix B; the parameter values for the functional form given by Equation 5 in Appendix B were $\kappa = 0.06784$ MPa and $\phi_0 = 0.65$. **SANCHO** has only the pressure-volumetric strain tabular form of input, with the maximum number of data pairs being six. Since the number of data pairs **SANCHO** accepts is smaller than the number of pairs used in the **SPECTROM-32** pressure-volumetric

strain input, the parameters for the functional form were used to calculate the **SANCHO** input pairs, where the six input pairs were chosen to give a reasonable approximation to the function through the stress magnitudes of interest. This procedure was also used to calculate the **SPECTROM-32** data pairs. To generate the **SANCHO** pressure-volumetric strain data pairs, Equation 5 in Appendix B is combined with the definition of porosity, $\phi = 1 - \rho/\rho_f$, which leads to the calculation of volumetric strain (ε_v) as defined by the finite strain code **SANCHO** (noting that here compaction is positive):

$$\varepsilon_v = \ln\left(\frac{\rho}{\rho_0}\right) = \ln\left(\frac{\rho_f}{\rho_0}(1 - \phi)\right) \qquad (3\text{-}1)$$

The material parameters used for the TRU waste compaction problem are given in Table 3-1. The large value assigned to a_2 suppresses the deviatoric response portion of the model and enables examination of the volumetric response only. The pressure-volumetric strain pairs listed in Table 3-2 define the compaction function for the (waste) medium used in the **SANCHO** simulation of VP29. Note that these values, which differ from the pressure-volumetric strain input for **SPECTROM-32** (Appendix B), represent the only compensation that can be made for the small/finite strain differences. However, the conversion of the bulk (volumetric) material properties from finite strain in **SANCHO** to engineering strain in **SPECTROM-32** only partially compensates for the differences. As shown in the discussion of the results, differences still appear in the computed volumetric strains for the two codes because of the inherent differences caused by the small strain versus the finite strain structure of the codes.

Table 3-1. Material parameter values for TRU waste verification problem

Parameter	Units	Value
ρ_0	kg/m^3	978.1
ϕ_0		0.65
K	MPa	100
G	MPa	60
a_0	MPa^2	0
a_1	MPa	0
a_2		50

Table 3-2. Pressure — volumetric relation for TRU waste problem

Point	Volumetric Strain, ε_{kk} (Natural)	Mean Stress, σ_m (MPa)
1	3.21E-5	0.0001
2	0.0223	0.0600
3	0.1651	0.5000
4	0.4335	1.7000
5	0.6140	3.0000
6	0.8365	6.0000

Simulation Results. Three figures summarize the results of **SPECTROM-32** and **SANCHO** simulations of VP29. Figure 3-1 compares the mean stress versus volumetric strain that develops during loading and unloading of the cylinder (axisymmetric geometry problem). Figures 3-2 and 3-3 plot mean stress versus volumetric strain (Figure 3-2) and the out-of-plane stress versus volumetric strain (Figure 3-3) that develop during an assumed plane strain problem geometry of the loading portion of the problem. In these figures, volumetric strain from the **SANCHO** simulations has been converted from the natural or true strain (e_v) to the engineering strain (ε_v) by the following equation:

$$\varepsilon_v = \exp(e_v) - 1 \qquad (3\text{-}2)$$

The volumetric response results (Figure 3-1) from the two codes for the crushable foam model compare reasonably well for the axisymmetric problem. However, several observations are worth noting. First, the stepped configuration of the **SPECTROM-32** results appears simply because each loading step (elastic response) is plotted before the plastic flow occurs. The viscoplastic solution algorithm used in **SPECTROM-32** enables recovery of this information. The **SANCHO** results appear at the end of a load step. Second, since this is a stress-controlled problem, the stress results are exactly the same for the two codes; differences appear in the resulting strain magnitudes. However, the magnitude of the forces have to be different because the finite strain code updates the geometry, and the forces must change to maintain the required boundary tractions. The small strain code's basis is always the original configuration; thus, changes in material stiffness and boundary forces caused by deformation are not required. Third,
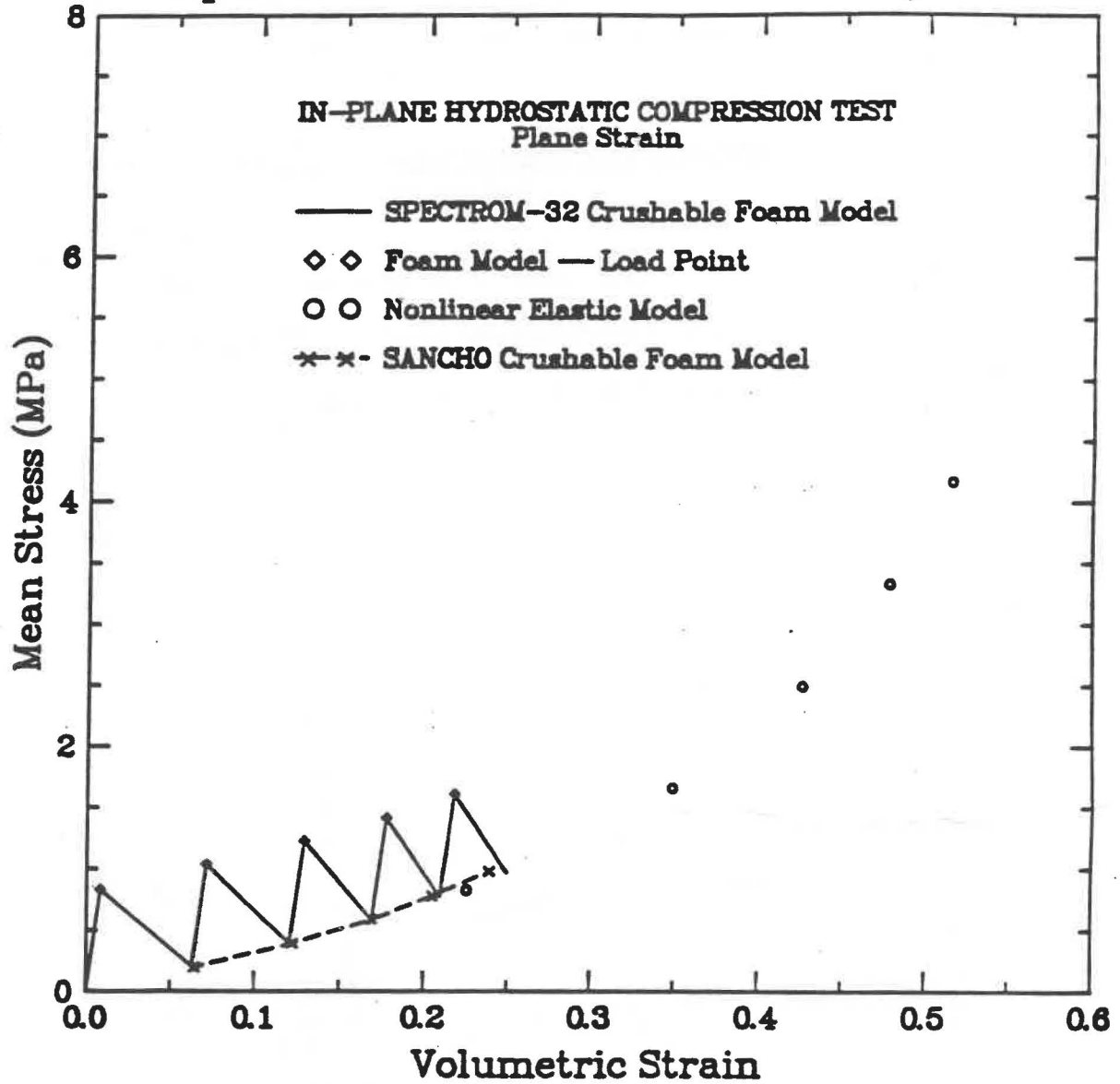
VP29: Response of Crushable Foam Plasticity Model

HYDROSTATIC COMPRESSION LOAD–UNLOAD TEST
Axisymmetric

——— SPECTROM–32 Crushable Foam Model

o o SPECTROM–32 Nonlinear Elastic Model

✳–✳– SANCHO Crushable Foam Model
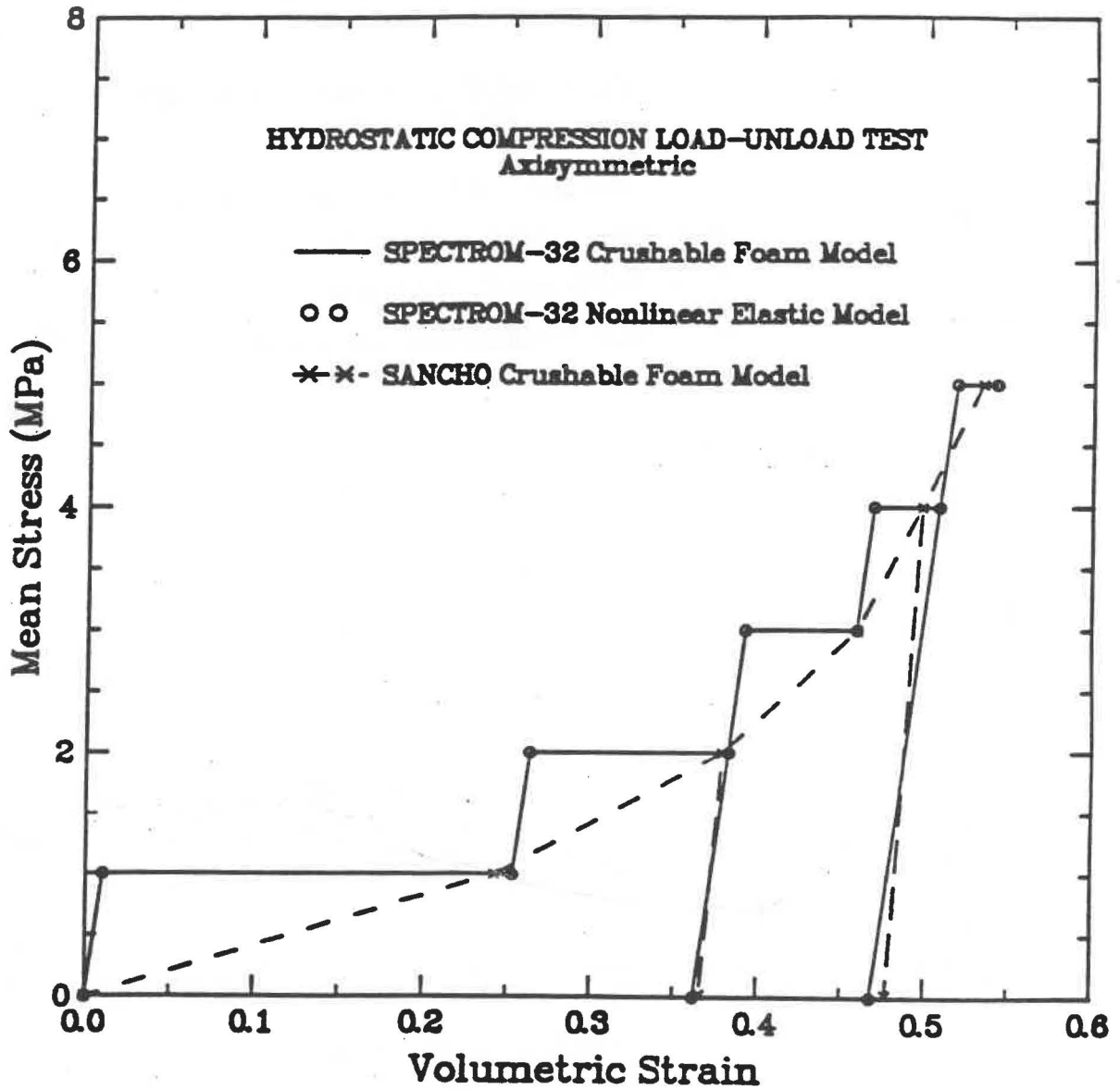
RSI-217-93-001

Figure 3-1. Comparison of volumetric response of crushable foam model in **SANCHO** and **SPECTROM-32.**

Response of Crushable Foam Plasticity Model

IN—PLANE HYDROSTATIC COMPRESSION TEST
Plane Strain

——— SPECTROM-32 Crushable Foam Model
◇ ◇ Foam Model — Load Point
O O Nonlinear Elastic Model
✳-✳- SANCHO Crushable Foam Model

Mean Stress (MPa) vs Volumetric Strain

Figure 3-2. Comparison of volumetric response of crushable foam model in **SANCHO** and **SPECTROM-32** for a plane strain problem.
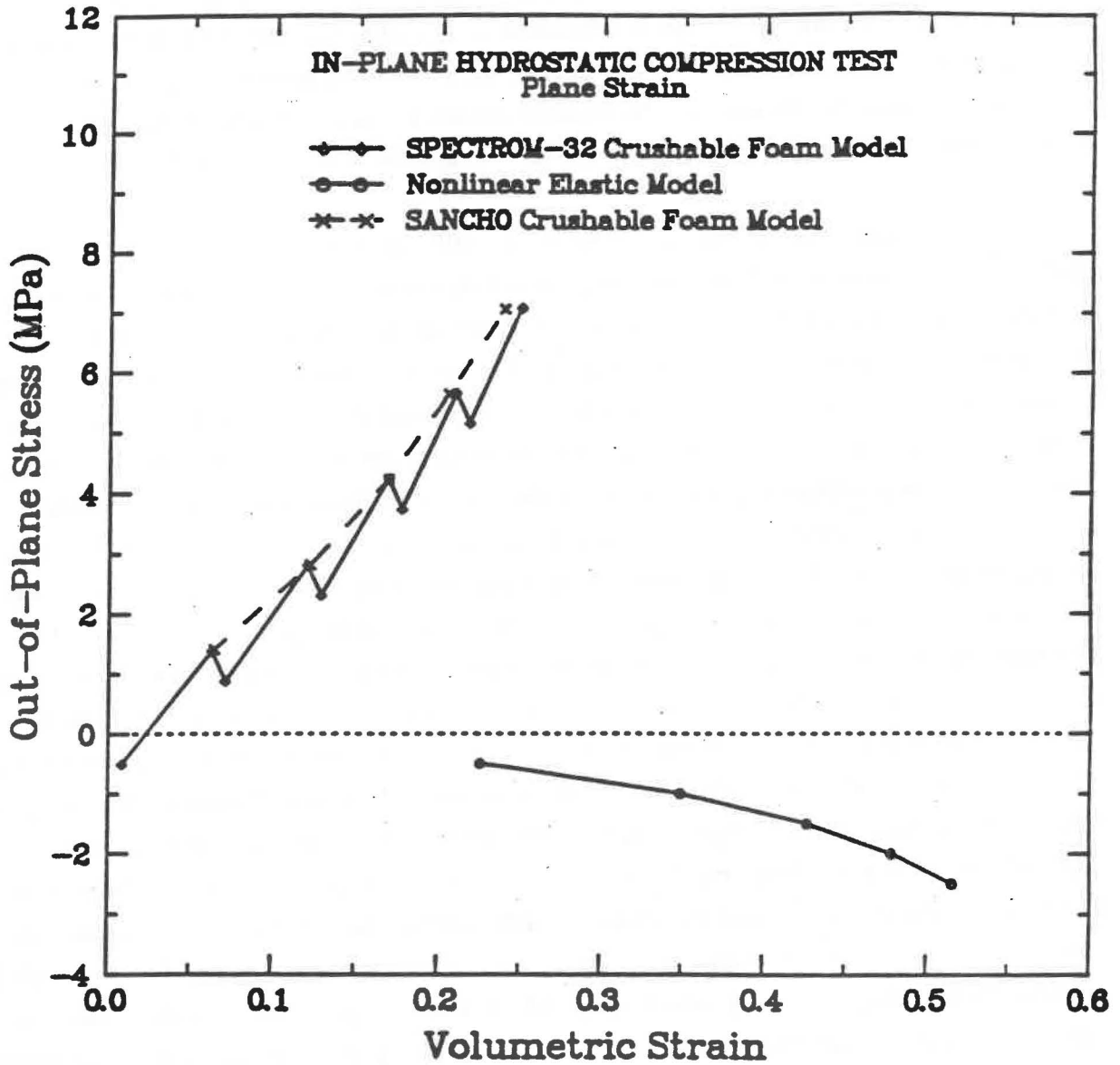
Figure 3-3.   Comparison of out-of-plane stresses from the crushable foam model in **SANCHO** and **SPECTROM-32** for a plane strain problem.

comparison of the results for the two codes at the end of the load steps appears to be random rather than a gradually increasing difference in the volumetric strain with increased deformation as expected. This is a consequence of the approximation used in the two codes to represent the pressure-volumetric strain relation. The six data pairs given in Table 3-2 for **SANCHO** provide a much coarser representation of the relation than the eleven points (Appendix C) used in **SPECTROM-32**. Finally, the bulk modulus of the crushable foam material is evident from the load-unload cycles in Figure 3-1. The **SPECTROM-32** results illustrate the constant bulk modulus of the material; whereas, the bulk modulus appears variable in the **SANCHO** analysis. The apparent variable bulk modulus appears in the **SANCHO** results because the **SANCHO** natural volumetric strains were converted to engineering volumetric strains for comparison in Figure 3-1.

Figures 3-2 and 3-3 illustrate the volumetric strain and out-of-plane stress response for the TRU waste compaction problem assuming plane strain geometry. The results obtained for this problem show trends similar to those obtained for the axisymmetric problem (Figure 3-1). The volumetric strain behavior in the plane strain simulation shows essentially identical mean stresses for the two codes but differences in the accompanying volumetric strains. These differences are of the same magnitude as observed for the axisymmetric problem and are attributable to the same force and stiffness differences that occur for the small and finite strain implementations. For comparison, the nonlinear elastic model results are included on Figures 3-2 and 3-3. Although not shown on Figure 3-1, the nonlinear elastic model produces results identical to the crushable foam model for the axisymmetric geometry. However, under plane strain conditions, the nonlinear elastic model produces significantly different results from the crushable foam model. This occurs because of the out-of-plane behavior in elastic and plastic types of problems. In plane strain problems, the requirement is that the total out-of-plane strain be zero. In plastic or other types of inelastic problems, the out-of-plane inelastic flow is balanced by the elastic behavior to maintain zero total out-of-plane strain. Therefore, the inelastic behavior reduces the magnitude of the out-of-plane stress. However, for the elastic problems, no mechanism exists to change out-of-plane stress, and the Poisson effect increases the component for increases in the in-plane loading. Therefore, some of the differences observed in past comparisons of **SANCHO** and **SPECTROM-32** disposal room simulations (which included plane strain geometries) can be explained by these waste model differences. Beyond this, even with the same waste model, differences can still be expected because of the inherent differences included in the small and finite strain formulations.

3.2.2 Uniaxial Compression of a Crushed-Salt Cylinder

The uniaxial compression verification problem simulates a cylindrical specimen (axisymmetric geometry) of crushed salt subjected to a constant 10 MPa axial stress. The individual strain components and the volumetric strain that develops as the specimen compacts are the output variables of interest. This problem has been solved previously using **SPECTROM-32** and is documented by Callahan (1990).

The problem was modeled with a vertical axis of symmetry through the center of the cylinder (left boundary), and the lower boundary was fixed against normal displacements (rollered boundary condition). The right boundary is free of kinematic and traction boundary conditions, and the top boundary has a normal traction of 10 MPa applied. In the **SPECTROM-32** simulation, this traction is constant throughout the simulation time of 10^6 seconds. In the **SANCHO** simulation, the boundary traction was applied gradually. No traction was applied at time zero, the traction was ramped to 1 MPa at 1,000 seconds and then ramped to 10 MPa at 2,000 seconds, and held constant from that time to the end of the simulation. The effect of ramping the load (traction), which was necessary to maintain numerical stability when first applying a load to the loose crushed salt material, is evident only in the very early-time strains; ramping the load did not noticeably effect late-time strain values even though the material is highly nonlinear.

The nonlinear elastic and volumetric creep consolidation parameter values used in the simulations of this problem are given in Tables 2-3 (full modulus values) and 2-4 with the following exceptions: $K_f = 20,700$ MPa, $G_f = 12,425$ MPa, and $\rho_0 = 1,700$ kg/m^3. The deviatoric portion of the creep consolidation equation was prescribed in **SPECTROM-32** using the steady-state creep law option, which is the only option in **SANCHO**. The creep parameter values for the deviatoric portion of the model are given in Table 2-2 with the exception that $Q_1/R = 5979$; however, reduced modulus values were not used. Other than being in units of Pa instead MPa for the **SANCHO** input, the material parameters used in the simulations for both codes are identical. The primary difference between the two codes and their simulations of the uniaxial problem are the models of deviatoric response. As described in Section 2.2.2.2, **SPECTROM-32** uses two components to describe the deviatoric response of the crushed salt material; whereas, **SANCHO** uses one. However, other than the one deviatoric component that **SANCHO** does not include, the constitutive model adopted in the two codes are the same. Two other less significant differences exist between the two codes:

1. The **SPECTROM-32** version of the creep consolidation model has a switch to change from the creep consolidation model to a model of intact salt once the final density is reached. In this case, that model was the steady-state creep model for intact salt.

2. **SPECTROM-32** provides for the specification of limiting values of the bulk and shear moduli but **SANCHO** does not. Although **SANCHO** does not explicitly have either of these features in the code, it effectively models both behaviors by virtue of the way the algorithms are constructed.

Neither of these differences should have any impact on the results of the uniaxial compression problem because over the time period simulated the material does not approach full consolidation.

Simulation Results. The results of the uniaxial compression of a crushed salt material are given in Figure 3-4. The individual strain components and the volumetric strain from the **SANCHO** simulations have been converted from natural strains to engineering strains as provided in Equation 3-2.

The volumetric strain components calculated by **SANCHO** and **SPECTROM-32** compare reasonably well. However, the individual tensorial strain components are significantly different. The discrepancies that are apparent in Figure 3-4 are a result of the difference in the deviatoric creep consolidation models. **SANCHO** does not contain the deviatoric component implemented by Callahan (1990) in **SPECTROM-32** (see Section 2.2.2.2) which serves to eliminate lateral compaction of a uniaxially loaded body. This correction to the creep consolidation model is appealing intuitively since one would not expect a significant amount of lateral compaction on a body when there is no loading in that direction. This corrective deviatoric component also serves to eliminate large out-of-plane tensile stresses when plane strain geometries are involved. Figure 3-4 shows that the **SANCHO** radial, tangential, and vertical strains differ from their **SPECTROM-32** counterparts. In fact, the **SANCHO** lateral strains are opposite in sign from the **SPECTROM-32** lateral strains. However, when **SPECTROM-32** is run with the volumetric creep consolidation model only, results similar to those produced by **SANCHO** are obtained (e.g., see Figure 4-3; Callahan, 1990).

3.3 Disposal Room Simulation

The creep closure of WIPP disposal rooms is simulated in this problem. The objective of this problem is to compare **SANCHO** and **SPECTROM-32** simulations of average void volume, room

Response of Creep Consolidation Model
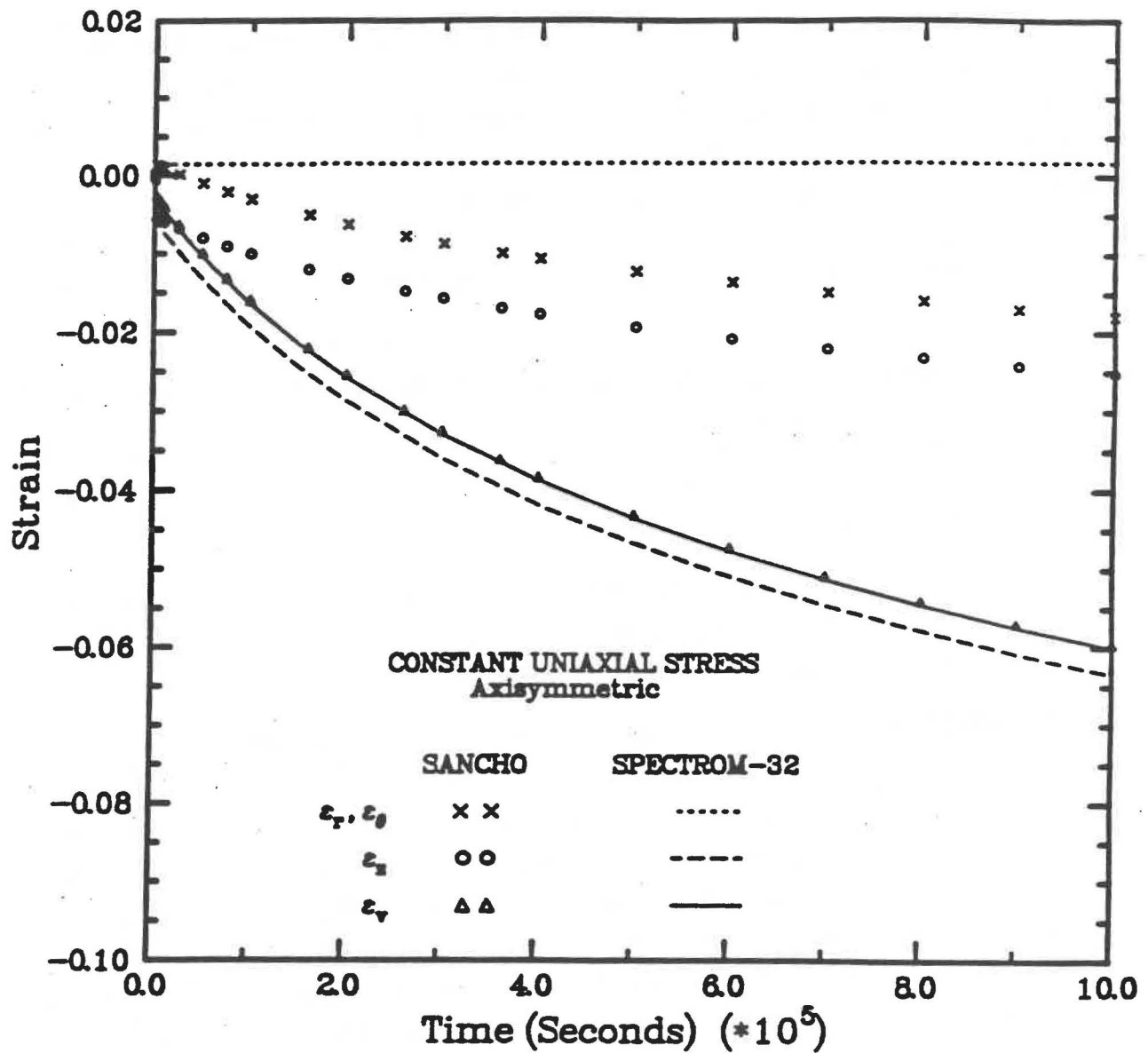
Figure 3-4.   Comparison of strain components from the creep consolidation model in **SANCHO** and **SPECTROM-32** for a constant uniaxial stress test.

closure, and gas pressure. This simulation involves the three components of a disposal room (as currently envisioned): (1) intact salt, (2) crushed salt (backfill), and (3) TRU waste. The specifications for the geometry and contents of the disposal rooms were defined by the WIPP baseline design (Bechtel, 1986) and are the same as those described in Section 2.3; the material properties are presented in Section 2.3.2.

The **SANCHO** simulation for the disposal room problem was completed earlier and has been documented by Stone (1992). In so far as possible, the same modeling approach and features were used in defining the **SPECTROM-32** model as were used in the **SANCHO** model. Consequently, the description of the **SPECTROM-32** model in this section is equally applicable to the **SANCHO** model except where differences are specifically noted.

The geometric simplifications made for the two analyses were:

1. The rooms are assumed to be located in a homogeneous layer of bedded salt eliminating the need to model the numerous stratigraphic layers present at the WIPP.

2. The deformation is assumed to be symmetric about a horizontal plane that passes through the center of the rib. Hence, the modeled region consists of the material above the symmetry plane.

3. The vertical extent of the region modeled is limited to 54 m above the room centerline. This boundary placement is identical to Stone (1992) and is far enough removed to eliminate significant boundary influence.

The **SPECTROM-32** finite element representation used for this two-dimensional, plane strain problem is shown in Figure 3-5. The finite element model consists of 776 four-noded quadrilateral elements. Although the geometrical details of the **SANCHO** model are essentially the same, the discretization is somewhat different resulting in 618 four-noded quadrilateral elements. The finite element mesh is composed of four distinct regions which are used to represent the material regions in the baseline case. The room detail given in Figure 3-5 shows the regions used to represent the TRU waste, the backfill material, and the air gap. The TRU waste region is 4.5 m wide by 1.01 m high in the lower left corner of the mesh. The crushed salt region surrounds the TRU waste and extends to the rib (i.e., the vertical boundary of the room surface). The crushed salt region extends vertically to the boundary of the air gap region, which is 0.355 m below the upper boundary of the room. These three regions comprise the disposal room and its contents with the remaining portion of the model representing the intact salt in the vicinity of the disposal room. The corners of the disposal room were assumed to be round (0.355 m radius). The cross-sectional area of the waste, backfill, and air gap regions are approximately
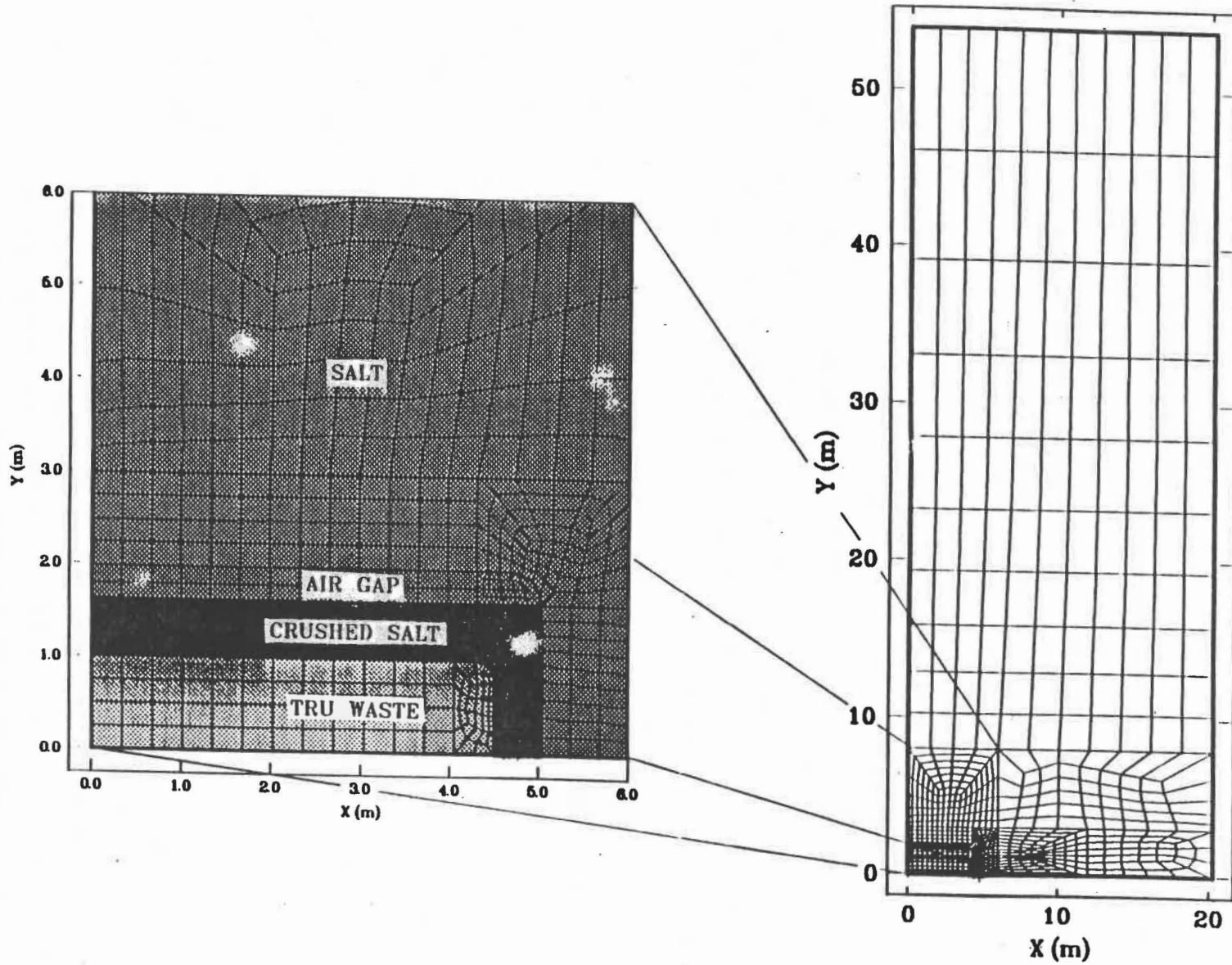
Figure 3-5. Finite element model of the WIPP disposal room.

RSI-217-93-005

4.54 m², 3.64 m², and 1.76 m², respectively, yielding a total cross-sectional area for the modeled disposal room quarter-section of approximately 9.94 m². Symmetry conditions require no displacements normal to the boundary along the bottom, left, and right edges of mesh. These kinematic constraints were prescribed as the boundary conditions for the mesh. The temperature throughout the modeled region was specified as 27°C.

As indicated in Section 3.1, the issue of differences in constitutive models was almost entirely eliminated. Some differences still remain and are discussed in our description of the constitutive models for intact salt, crushed salt, and waste (Section 2.2). The WIPP secondary (steady-state) creep law was assumed to describe the creep component of the intact salt model and the deviatoric portion of the creep component of the crushed salt model. The reduced modulus values corresponding to the WIPP secondary creep law were assumed for the intact salt and crushed salt. The only difference between the material parameter values used to simulate this problem and those reported by Stone (1992) occurred for G_0 given in Table 2-3. Stone (1992) reported a value of 0.000864; however, this value is believed to be a typographical error because 0.000846 is the value consistent with the nonlinear elastic crushed salt parameter values reported by Sjaardema and Krieg (1987).

The initial stress field before excavation was assumed to be a homogeneous, lithostatic state of stress. The magnitude of the initial stress field was defined by prescribing a superincumbent overburden traction of 14.8 MPa. Gravitational forces were neglected with lateral earth pressure coefficients equal to one. Therefore, the initial state of stress everywhere in the defined problem region was −14.8 MPa. The initial stress condition for the analysis was established by simulating excavation of the disposal room into the host medium under the assumed lithostatic stress condition. Subsequently, the TRU waste and backfill were emplaced under stress free conditions (i.e., body forces were neglected in the TRU waste and crushed salt backfill). As a consequence of the assumed symmetry condition about the bottom boundary, the waste in the finite element model is located in the center of the room and is surrounded on all four sides by the backfill material. The air gap isolates the TRU waste and backfill from the room roof and floor until sufficient deformation is attained to provide contact. The air gap is simulated in **SPECTROM-32** by a special gap element in which the deformation is continuously monitored. When the deformation of the gap element reaches its prescribed value, the material is changed to another material (i.e., intact salt in this case). Thus, the gap element provides unrestrained deformation through a predetermined magnitude. In the actual configuration, the waste will rest on the floor of the room and be surrounded by the backfill material on three sides with the headspace located between the crushed salt and disposal room roof.

The modeling procedure for the air gap is believed to be a source of discrepancy between the **SPECTROM-32** and **SANCHO** solutions. Stone (1992) states that the air gap was discretized as though it was crushed salt and remained a low modulus material until the **disposal room** volume had decreased by the requisite air gap volume. Then the air gap material assumed characteristics of the crushed salt backfill. This implies a difference from the **SPECTROM-32** simulation because the requisite air gap volume was only absorbed by the air gap region shown in Figure 3-5; whereas, the **SANCHO** analysis apparently assumed the air gap was gone when an equivalent room volumetric closure had occurred.

Another specific difference in modeling procedures between the two codes involves the treatment of the room contents when the gas pressure becomes large enough to cause closure of the room to cease and create an increase in room volume. If room expansion occurs, it is believed that the room surface would separate from the room contents. This separation would occur with the room contents providing no resistance to the expansion of the room. Since the material boundaries of the room and room contents are in intimate contact and cannot separate, the room contents would become tensile upon expansion of the room without special treatment. The material models for the crushed salt and TRU waste in **SPECTROM-32** include tensile limits. Therefore, as the room expands and attempts to create tensile loads in the room contents, the loads are transferred back to the intact salt and the room contents provide no resistance to the room expansion. In **SANCHO**, the elements representing the waste and room contents were deleted at the point where the room begins to expand. Stone (1992) found that the process of deleting the room contents was a sensitive modeling parameter and several analyses were usually performed to establish the appropriate deletion time. If the full room contents became tensile in the **SPECTROM-32** analysis at the same instant as the room contents were deleted in the **SANCHO** analysis, the two processes should produce equivalent results. However, the full impact of this difference in modeling procedure on the results is difficult to judge.

Simulation Results. The baseline case with full gas generation rate (i.e., $f = 1$ as stated by Stone, 1992) was simulated for a 2,000-year period. In the **SPECTROM-32** analysis, the air gap is essentially gone after approximately 20 years, and the disposal room roof comes in intimate contact with the backfill. The crushed salt backfill was changed to a creeping material obeying the WIPP steady-state constitutive model when the volume of the crushed salt was sufficiently reduced such that all of the voids were removed and the density reached the density of intact salt. Thus, following complete consolidation, the crushed salt becomes intact salt. Initially the stiffnesses of the crushed salt and TRU waste are very low compared to the host salt formation. Therefore, even after the air gap has disappeared very little resistance to room closure is provided by the backfill and waste. However, while these processes are occurring, gas is also being

generated. The gas pressure increases as long as mass is being generated and also because the pore space is decreasing in the crushed salt and TRU waste. The gas pressure resists room closure and continues to increase until generation ceases. As the crushed salt and TRU waste compact, they become stiffer and provide stabilizing forces for the underground structure and reduce the room closure rate. However, the stiffness of the TRU waste remains quite low until it is compacted to within about 80 percent of its fully compacted density. Because the stiffness of the TRU waste is so low, little support is provided for the crushed salt backfill, and the rate of consolidation of the crushed salt is slower than if the room was completely filled with crushed salt. When the gas pressure becomes large enough, closure of the room ceases and the room volume increases with increasing gas pressure.

Figure 3-6 shows the average void fractions in the room, backfill, and waste for the two codes. The **SANCHO** results were obtained by digitizing the room results presented by Stone (1992) and the waste and backfill results presented by Stone (1993). The initial porosities in the crushed salt (0.4) and TRU waste (0.74) are evident in the figure at time zero. In the **SANCHO** results, the backfill and air gap porosities are combined; the combined initial porosity of these two components is 0.60. In **SPECTROM-32**, the backfill porosity curve includes only the backfill material region illustrated as crushed salt in Figure 3-5. The **SANCHO** waste and backfill-and-air-gap porosity histories end at 300 years because the room elements were eliminated after room expansion started. The void fractions decrease until the gas pressure is sufficient to halt room closure and initiate room expansion. The minimum room void fraction is obtained between 150 and 200 years (**SPECTROM-32** at 150 years and **SANCHO** at 200 years). The results obtained by **SANCHO** and **SPECTROM-32** are quite close through the first 100 years. After that time, the **SPECTROM-32** results show a slightly larger decrease in room void fraction than the **SANCHO** results. This offset is fairly constant through 2,000 years where the difference is about 5 percent.

Consideration of these results in light of the behavior observed in the verification problems will help understand these differences. The average void fraction curves in Figure 3-6 show that at maximum compaction, the crushed salt (alone) and the waste have porosities of approximately 3 percent and 50 percent, respectively. The volumetric strain associated with these porosities is greater than 40 percent. Typically, at a volumetric strain exceeding 20 percent, finite strain effects become important, which gives rise to the growing differences between the **SANCHO** and **SPECTROM-32** results, as was seen for the verification problems. In general, the corresponding strain levels are higher in the **SPECTROM-32** simulations, producing greater densities and lower porosities. As gas generation leads to pressurization of the room, the room contents essentially do not affect the calculation; this occurs in the 300- to 500-year time frame. After this time, porosity changes are solely a result of room expansion.

EATF Baseline Case for f = 1.0
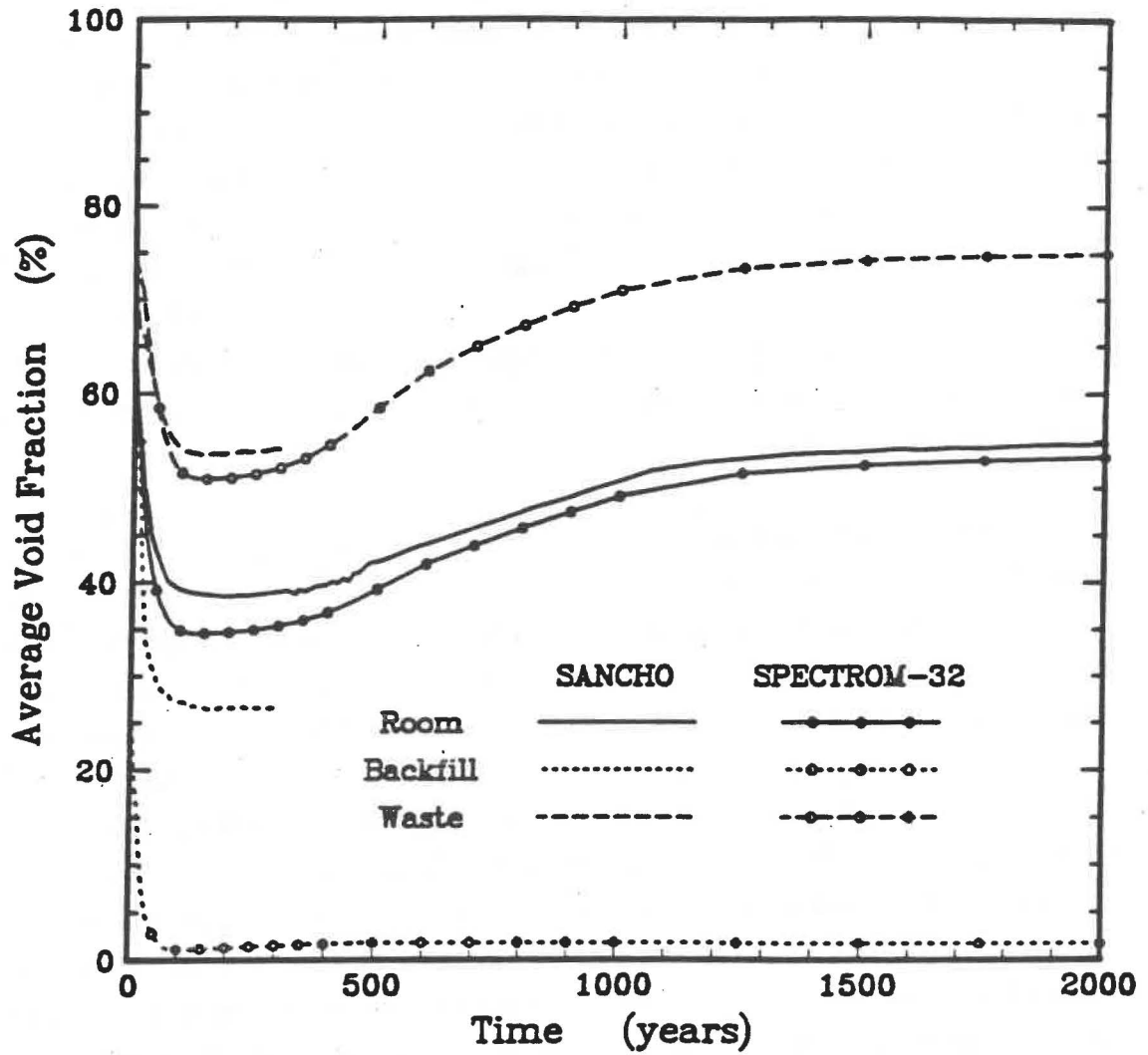
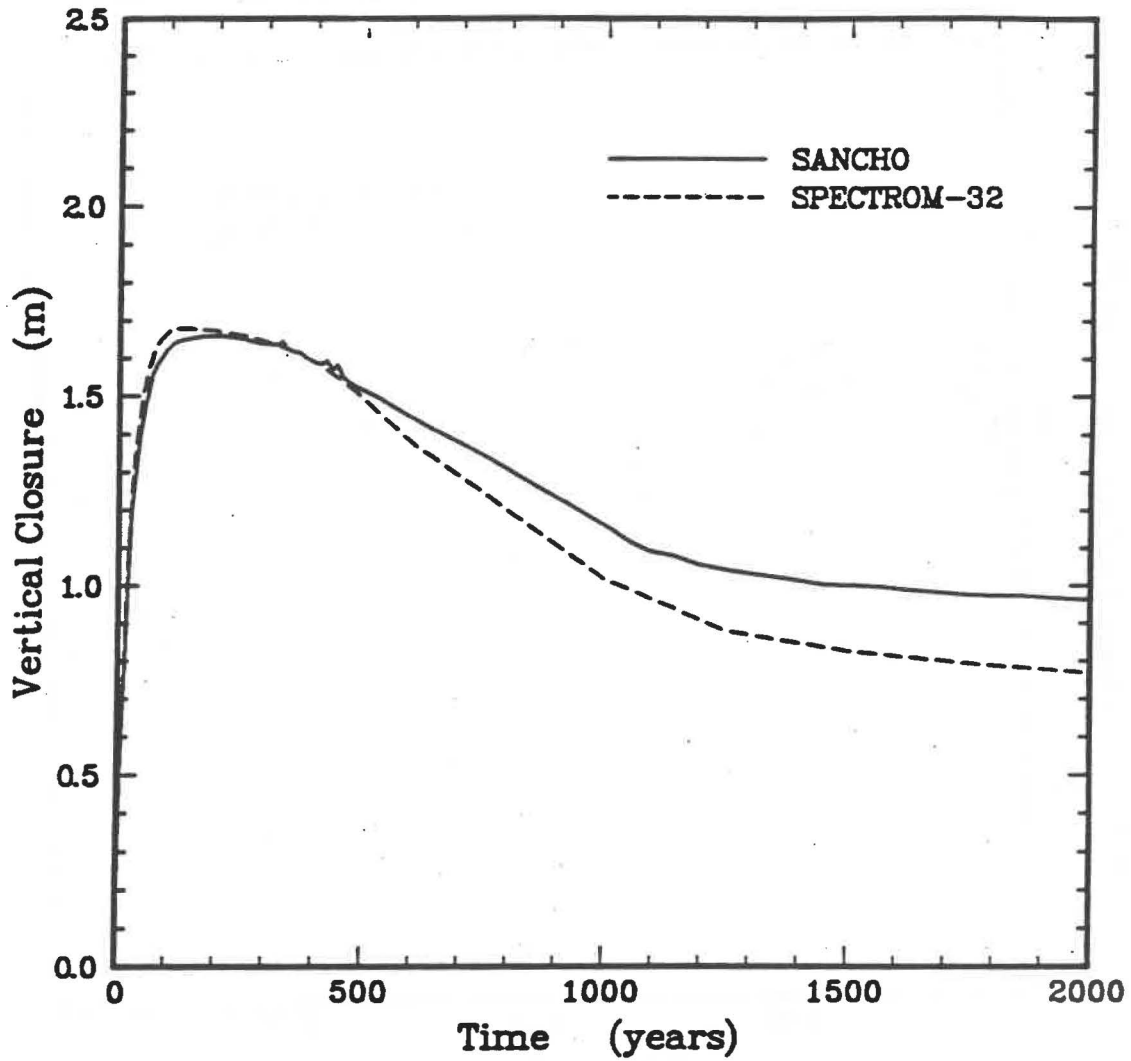Figure 3-6. Comparison of disposal room void fraction histories.

RSI-217-93-006

Evaluation of the backfill response is more difficult because a direct comparison cannot be made between the **SANCHO** and **SPECTROM-32** results. The **SPECTROM-32** backfill porosity plot starts at an initial value of 0.4 compared to the **SANCHO** backfill-and-air-gap porosity of 0.6. However, since the air gap has essentially disappeared in the **SPECTROM-32** simulation after 20 years, the backfill porosity curve of **SPECTROM-32** is also representative of the backfill-and-air-gap porosity results after 20 years. Thus, there is a large discrepancy between the **SANCHO** and **SPECTROM-32** backfill porosity results. Two potential sources for this large difference include the air gap model and the crushed salt model. The response observed in the uniaxial verification problem for crushed salt consolidation presented in Section 3.2.2 would lead one to believe that the crushed salt model is probably responsible for the discrepancy. However, the uniaxial compression problem contains a large deviatoric loading which creates the large differences between codes; whereas, the deviatoric loading on the backfill in a disposal room is typically much smaller. In fact, previous comparisons of the crushed salt backfill behavior in WIPP disposal rooms for the two codes (e.g., Callahan and DeVries, 1991) have shown much closer agreement. The previous code comparisons indicate that the crushed salt constitutive model differences cannot create the observed discrepancies in the backfill porosities. Therefore, the backfill porosity differences observed between the two codes have to be attributable to the air gap modeling procedures.

The vertical and horizontal closures of the disposal room are shown in Figures 3-7 and 3-8. These closure values are nodal displacement values at the centerline of the roof and midheight of the pillar multiplied by a factor of two to reflect the total room closure. **SPECTROM-32** attains a maximum horizontal closure of about 1.74 m at 150 years and a maximum vertical closure of about 1.68 m at 140 years. After 50 years, the **SPECTROM-32** horizontal closures are consistently about 10 percent greater than those predicted by **SANCHO**. However, comparison of the vertical closure results shows fairly good agreement between the **SANCHO** and **SPECTROM-32** results through the first 500 years. After this time, the **SPECTROM-32** vertical closures become less than those predicted by **SANCHO** and are about 20 percent less at 2,000 years. The greater amount of vertical room opening shown in the **SPECTROM-32** results seems consistent with the greater gas pressures illustrated in Figure 3-9. However, one would expect the greater volume to yield a reduction in pressure. Apparently, the increased horizontal closure and overall reduced room volume produced in the **SPECTROM-32** analysis are sufficient to maintain the higher pressure. As shown in Figure 3-9, the **SPECTROM-32** gas pressures are consistently about 5 percent higher than those predicted by **SANCHO** after 500 years.

Less can be said in a direct way about the closure results because the deformations produced are a result of combined volumetric compaction (and expansion) and deviatoric strains. However,
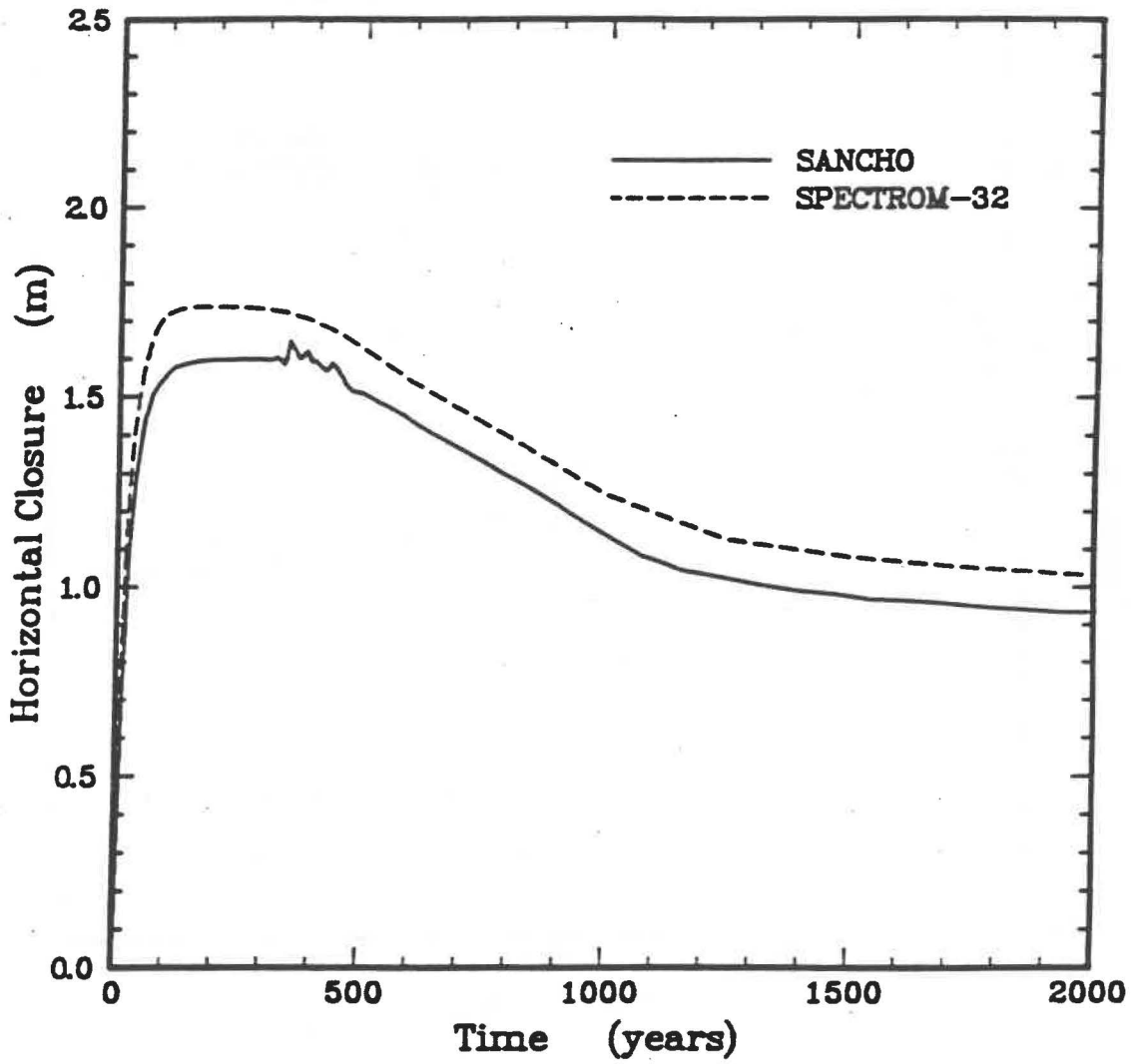
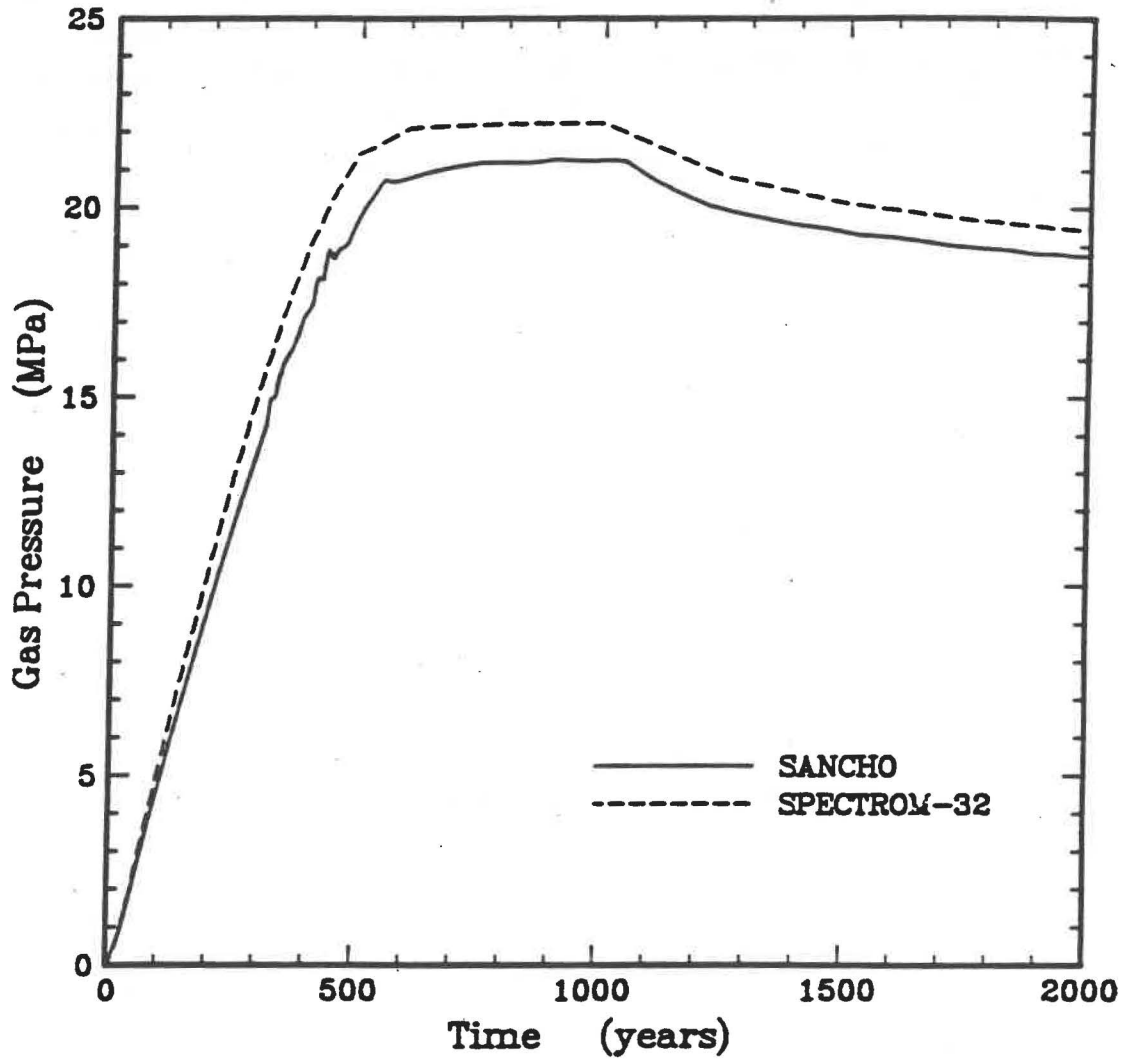Figure 3-7. Comparison of disposal room vertical closure histories.

EATF Baseline Case for f = 1.0

Figure 3-8. Comparison of disposal room horizontal closure histories.

RSI-217-83-008

EATF Baseline Case for f = 1.0

Figure 3-9. Comparison of disposal room gas pressure histories.

RSI-217-93-008

two additional factors (since all previous comments made relative to the porosity also apply to the closure histories) should be considered. First, the deviatoric strain correction factor in the crushed salt model for **SPECTROM-32**, discussed in Section 2.2.2, impacts all of the strain components. Second, the plane strain analysis of VP29 showed that the out-of-plane response differs between the two codes. The contribution of these factors to the differences in closure apparent in Figures 3-7 and 3-8 cannot be ascertained because the influence of these factors is not directly quantifiable. The primary consequence of the differences between the two codes is that greater waste compaction and room closure develop in the **SPECTROM-32** simulation. Likewise, higher gas pressures develop in the room. Although higher gas pressures (22+ MPa in **SPECTROM-32** versus 21+ MPa in **SANCHO**) induce greater room expansion, as was indicated above, the 1 MPa difference in pressure does not produce noticeably different room expansion rates.

4.0 CONCLUSIONS

The purpose of this chapter is to summarize the results of comparisons between numerical simulations performed by **SANCHO** and those performed by **SPECTROM-32** and to present recommendations for further activities which would place **SPECTROM-32** and **SANCHO** (or its successor **SANTOS**) on essentially identical foundations for future room modeling efforts.

Simulations of two idealized and simplified uniaxial stress (in axisymmetric and plane strain geometry) and hydrostatic stress tests with both **SPECTROM-32** and **SANCHO** have provided valuable insight into the actual and relative behavior of two constitutive models in the two codes. The closure of an idealized disposal room in intact salt at the center of a waste panel with crushed salt backfill and gas-generating TRU waste in the room was also simulated for a period of 2,000 years. This simulation also provides valuable insight into the issues surrounding the use of **SANCHO** and **SPECTROM-32** for WIPP disposal room simulations. As a result of the numerical studies documented in this report, several conclusions can be made regarding the future use of either of these codes, or similar codes, for WIPP disposal room modeling studies. These are listed below along with recommendations that will reduce questions of code differences, that always manifest themselves in important results, to a minimum.

1. Significant strain magnitudes can develop in materials within the disposal room, frequently greater than 50 percent. Since **SPECTROM-32** is an infinitesimal strain code, deficiencies can be expected at these large strains. **SPECTROM-32** could be modified to include finite strain to improve future disposal room simulations.

2. Ostensibly, the same constitutive models are available in both **SANCHO** and **SPECTROM-32** for WIPP room disposal simulations. However, specific differences between each of the disposal room component models exist.

   2a. The secondary creep power law model and the Munson-Dawson model are utilized as models of intact salt. The former is used in **SANCHO/SANTOS** with empirical corrections to some of the input parameters. **SPECTROM-32** can simulate problems using either model, but the Munson-Dawson model is the preferred option because it has a more sound theoretical and experimental basis.

   2b. The creep consolidation model used for crushed salt is implemented in both families of codes although there is a difference in an inelastic shear strain component (identified in Equation 2-52 of this report). This component is

present in the **SPECTROM-32** implementation but not in the **SANCHO/SANTOS** implementation. This deviatoric component is a correction factor for lateral strains; it does not effect volumetric strain magnitudes, but it significantly affects normal and shear strain components.

2c. The question of what should be the assumption regarding the lateral stress components for the TRU waste tests was raised. This was not an issue in the analyses reported herein; however, the choice of which of two assumptions is made ($\sigma_a = 3\sigma_m$ or $\sigma_a = \sigma_m$) has a significant impact on waste compaction and room porosity.

3. Several bookkeeping issues must be given attention when comparing results of simulations from two codes. First, problem definitions must be checked to insure that identical problems are being simulated as closely as possible; several instances were encountered where different problems were modeled and results were compared. Second, material parameter input values should be verified and made consistent between codes; when different units are used in different codes, calculation of input parameters should be based on a common set of values. A document containing all relevant physical and mechanical properties required for room disposal modeling should be assembled for use by WIPP project analysts. Third, consistent definition of variables must be used when comparing results (e.g., room porosity). Finally, when stress and strain measures calculated by different codes are graphically compared, the same definitions must be used.

4. Gas pressurization of disposal rooms reverses the loading direction from the creep closure phase of the simulation. Care must be taken to insure that this less frequently exercised portion of constitutive models be checked for consistency as well.

5.0 REFERENCES

Beattie, J.A. 1929. *J. Am. Chem. Soc.* Vol. 51, 19–30.

Beattie, J.A. and O.C. Bridgeman. 1928. "A New Equation of State for Fluids," *Proc. Am. Acad. Arts Sci.* Vol. 63, 229–308.

Bechtel, Inc., 1986. *WIPP Design Validation Final Report.* DOE/WIPP-86-010. San Francisco, CA: US Department of Energy.

Butcher, B.M., and F.T. Mendenhall. In Preparation. *A Summary of the Models Used for Predictions of the Mechanical Response of Disposal Rooms in the Waste Isolation Pilot Plant.* SAND92-0427. Albuquerque, NM: Sandia National Laboratories.

Butcher, B.M., T.W. Thompson, R.G. VanBuskirk, and N.C. Patti. 1991. *Mechanical Compaction of Waste Isolation Pilot Plan Simulated Waste.* SAND90-1206. Albuquerque, NM: Sandia National Laboratories.

Callahan, G.D., and K.L. DeVries. 1991. *Analyses of Backfilled Transuranic Waste Storage Rooms.* SAND91-7052. Albuquerque, NM: Sandia National Laboratories.

Callahan, G.D. 1990. *Crushed Salt Consolidation Model Adopted for SPECTROM-32.* RSI-0358. Rapid City, SD: RE/SPEC Inc.

Callahan, G.D., A.F. Fossum, and D.K. Svalstad. 1990. *Documentation of SPECTROM-32: A Finite Element Thermomechanical Stress Analysis Program.* DOE/CH/10378-2. Chicago, IL: US Department of Energy. Vol. 1 and 2.

Callahan, G.D. 1982. "A Plasticity Approach for Rock Containing Planes of Weakness." PhD thesis. Minneapolis, MN: University of Minnesota.

Chen, W.F., and D.J. Han. 1988. *Plasticity for Structural Engineers.* New York, NY: Springer-Verlag.

Fossum, A.F., G.D. Callahan, L.L. Van Sambeek, and P.E. Senseny. 1988. "How Should One-Dimensional Laboratory Equations be Cast Into Three-Dimensional Form?," *Proceedings: 29th U.S. Symposium: Rock Mechanics,* Minneapolis, MN: University of Minnesota.

Holman, J.P. 1974. *Thermodynamics.* New York, NY: McGraw-Hill Book Company.

Keenan, J.H. 1941. *Thermodynamics.* Cambridge, MA: M.I.T. Press.

Krieg, R.D. 1984. *Reference Stratigraphy and Rock Properties for the Waste Isolation Pilot Plant (WIPP) Project.* SAND83-1908. Albuquerque, NM: Sandia National Laboratories.

Lappin, A.R., and R.L. Hunter, eds. 1989. *Systems Analysis, Long-Term Radionuclide Transport, and Dose Assessments.* SAND89-0462. Albuquerque, NM: Sandia National Laboratories.

Morgan, H.S., and R.D. Krieg. 1988. *A Comparison of Unified Creep-Plasticity and Conventional Creep Models for Rock Salt Based on Predictions of Creep Behavior Measured in Several In Situ and Bench-Scale Experiments.* SAND87-1867. Albuquerque, NM: Sandia National Laboratories.

Munson, D.E. 1989. *Proposed New Structural Reference Stratigraphy, Law, and Properties,* Internal Memorandum. Albuquerque, NM: Sandia National Laboratories.

Munson, D.E., A.F. Fossum, and P.E. Senseny. 1989. *Advances in Resolution of Discrepancies Between Predicted and Measured In Situ WIPP Room Closures.* SAND88-2948. Albuquerque, NM: Sandia National Laboratories.

Prausnitz, J.M. 1969. *Molecular Thermodynamics of Fluid-Phase Equilibria.* Englewood Cliffs, NJ: Prentice-Hall, Inc.

Redlich, O., and J.N.S. Kwong. 1949. *Chem. Rev.* Vol. 44, no. 233.

Sandler, I.S., F.L. DiMaggio, and G.Y. Baladi. 1976. "Generalized Cap Model for Geological Materials," *Journal of the Geotechnical Engineering Division.* ASCE, Vol. 102, no. GT7, 683-699.

Sjaardema, G.D., and R.D. Krieg. 1987. *A Constitutive Model for the Consolidation of Crushed Salt and Its Use in Analyses of Backfilled Shaft and Drift Configurations.* SAND87-1977. Albuquerque, NM: Sandia National Laboratories.

Stone, C.M. 1993. *SANCHO Results for EATF Baseline f=1, Comparison of Porosities to 300 Years.* Personal Communication to D.A. Labreche, RE/SPEC Inc., Albuqueruqe, NM.

Stone, C.M. 1992. *Creep Closure of Waste Disposal Rooms in Bedded Salt Due to Gas Generation Produced by Several Alternatives of the Engineered Alternatives Task Force,* Internal Memorandum to B.M. Butcher, Sandia National Laboratories, Albuquerque, NM.

Stone, C.M., R.D. Krieg, and Z.E. Beisinger. 1985. *SANCHO A Finite Element Computer Program for the Quasistatic, Large Deformation, Inelastic Response of Two-Dimensional Solids.* SAND84-2618. Albuquerque, NM: Sandia National Laboratories.

Timoshenko, S.P., and J.N. Goodier. 1970. *Theory of Elasticity.* Third Edition, New York, NY: McGraw-Hill Book Company.

Van Wylen, G.J., and R.E. Sonntag. 1973. *Fundamentals of Classical Thermodynamics, Second Edition.* New York, NY: John Wiley and Sons, Inc.

Weatherby, J.R., J.G. Argüello, B.M. Butcher, and C.M. Stone. 1991. "The Structural Response of a WIPP Disposal Room with Internal Gas Generation." *Proceedings: 32nd U.S. Symposium: Rock Mechanics as a Multidisciplinary Science.* Ed. J.-C. Roegiers. Rotterdam, Netherlands: A. A. Balkema. 929–937.

Zeuch, D.H. 1990. "Isostatic Hot-Pressing Mechanisms Maps for Pure and Natural Sodium Cloride—Applications to Nuclear Waste Isolation in Bedded and Domal Salt Formations," *International Journal of Rock Mechanics and Mining Science & Geomechanics Abstracts.* Vol. 27, no. 6, 505-524.

Zeuch, D.H. 1988. *Isostatic Hot-Pressing Mechanisms Maps for Pure and Natural Sodium Cloride: Applications to Nuclear Waste Isolation in Bedded and Domal Salt Formations.* SAND88-2207. Albuquerque, NM: Sandia National Laboratories.

F-76

APPENDIX A: DISCUSSION OF THE TRU WASTE MODEL

RE/SPEC Inc.
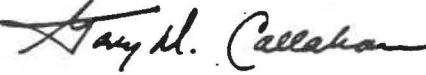### RESEARCH/SPECIALISTS

Rapid City. South Dakota • Albuquerque. New Mexico

External Memorandum

To: Dr. Fred T. Mendenhall
              Sandia National Laboratories
              Organization 6345
              P.O. Box 5800
              Albuquerque, NM 87185–5800
              cc: Dr. Barry M. Butcher (Sandia Division 6345)
                   Mr. C. A. Madole (Sandia Division 3716)
                   Mr. Duane A. Labreche (RE/SPEC)
                   Project Records File 217/GR10

From: Dr. Gary D. Callahan
              RE/SPEC Inc.
              P.O. Box 725
              Rapid City, SD 57709

Date: March 13, 1992

Subject: Further Discussion of the TRU Waste Model
              (Sandia Contract No. 78-7829)

Introduction

The purpose of this memorandum is to present additional discussion on the TRU waste model discussed in Callahan and DeVries [1991] and hopefully clarify some of the *inconsistencies* discussed by Dr. Butcher in his memorandum dated March 4, 1992.

TRU Waste Model Discussion

The basic equation used to describe the TRU waste behavior is

$$\sigma_e = \frac{1}{\kappa} \ln\left(\frac{\phi}{\phi_0}\right) \tag{1}$$

3824 Jet Drive. P.O. Box 725, Rapid City, South Dakota 57709 • (605) 394-6400 • TLX 3791625 RESPEC • FAX (605) 394-6456

where

$$\sigma_a = \text{axial stress, } \sigma_a = 3\sigma_m$$
$$\sigma_m = \text{mean stress}$$
$$\kappa = \text{material parameter}$$
$$\phi = \text{porosity}$$
$$\phi_0 = \text{initial porosity.}$$

A key assumption associated with the above equation concerns specifying the mean stress when only one stress component was measured during the experiments. The following discussion was given by Callahan and DeVries [1991] starting on Page 29:

> The assumption stated above (i.e., $\sigma_a = 3\sigma_m$) is significant. The need for this assumption stems from the fact that the experiments were conducted on the compaction of simulated waste in a rigid steel sleeve [Butcher et al., 1991] and only the axial stress component was measured. To evaluate the parameter values for the TRU waste model, all three stress components need to be known. Two bounding assumptions to infer values for the lateral stress components are (1) the lateral stress components are zero (i.e., $\sigma_a = 3\sigma_m$) and (2) the lateral stress components are equal to the axial stress (i.e., $\sigma_a = \sigma_m/3$). Assumption (1) represents an unconfined test, and Assumption (2) represents a hydrostatic test. Neither assumption is correct in the sense that it represents the conditions in the experiment; however, the two assumptions bound the true stress conditions. The first assumption was adopted because it provides the less stiff representation of the TRU waste. The less stiff representation is felt to be more conservative because it provides less resistance to room closure and lower back pressure on the surrounding backfill, which increases the time required to obtain lower porosities in the backfill surrounding the TRU waste.

Under Assumption (2) above, the statement $\sigma_a = \sigma_m/3$ is incorrect and should read $\sigma_a = \sigma_m$. When Assumption (1) above was adopted, the thinking was that it would be the more conservative of the two assumptions with regard to the porosities in backfill surrounding the waste and not necessarily in the TRU waste itself. However, as Dr. Butcher stated in his memorandum, porosity (void fraction) is the variable of interest since it is used to estimate permeability. With this in mind, Assumption (2) would be the more conservative of the two assumptions in that it would tend to produce the largest porosities (i.e., least compaction) for the same stress states in the TRU waste. However, Assumption (2) will not necessarily produce the more conservative results for the backfill material since the expectation is that the stiffer TRU waste will enhance the reduction of porosity in the backfill.

Then, the questions are: what is the impact of Assumption (2) on the waste parameters, and what is the impact of these different parameter values on the results?

To answer these questions, we will first examine the tangent bulk modulus, which is defined as

$$K = \frac{d\sigma_m}{d\epsilon_v} = \frac{d\sigma_m}{d\phi}\frac{d\phi}{d\rho}\frac{d\rho}{d\epsilon_v} \tag{2}$$

Mean stress is substituted into Equation 1 for the two different assumptions. First, substituting $\sigma_m = \sigma_a/3$ and performing the differentiation indicated in Equation 2 on Equation 1 results in

$$K(\rho) = \frac{\rho^2}{3\kappa\rho_0(\rho_f - \rho)} \tag{3}$$

For the second assumption, substituting $\sigma_m = \sigma_a$ and performing the differentiation indicated in Equation 2 on Equation 1 results in

$$K(\rho) = \frac{\rho^2}{\kappa\rho_0(\rho_f - \rho)} \tag{4}$$

With the second assumption, we see that the TRU waste is three times stiffer than that obtained using the first assumption. This is also shown in Figure 1, which is a reproduction of Figure 2-7 in Callahan and DeVries [1991] for the series model. In Figure 1, the ordinate has been changed from *axial stress* to *mean stress*, and the series model representation (squares) for the second assumption has been added. The ordinate was changed to mean stress to avoid confusion. The confusion is apparent because Dr. Butcher states in his memorandum that Callahan's Figure 2-7 supports a porosity of 24 percent at lithostatic pressure (15 MPa). A lithostatic pressure of 15 MPa implies that $\sigma_{xx} = \sigma_{yy} = \sigma_{zz} = 15$ MPa. However, the inherent assumption in Figure 2-7 was that the lateral components were zero. Thus, to achieve a mean stress of 15 MPa (under Assumption (1)), the axial stress would have to be 45 MPa. Also, we see from Figure 1 that at a lithostatic value of 15 MPa, the curve (circles) generated for Assumption (1) yields a porosity value of about 4 percent.

Although there is a significant difference between the curves obtained using the two assumptions, the procedure for adopting Assumption (2) to produce the stiffer TRU waste model is simple. To obtain TRU stiffnesses according to Assumption (2), material parameter κ is divided by 3. Therefore, the same material model adopted for the TRU waste and included in SPECTROM-32 can be used to represent the stiffer TRU waste and obtain the higher values of porosity.
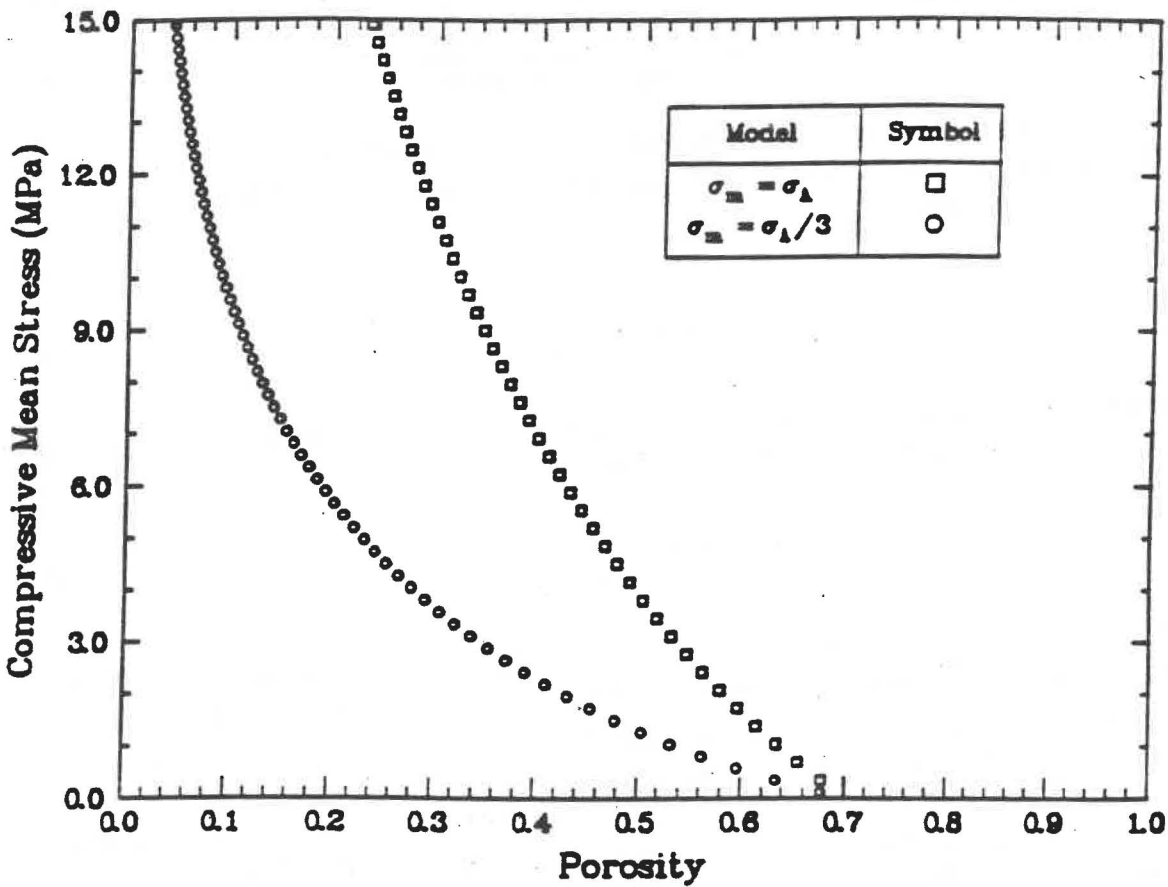
Figure 1. Comparison of Two Different TRU Waste Model Assumptions.

New Crushed Salt TRU Waste Model Analysis

To illustrate the influence of Assumption (2) on the room scale results, the problem representing the room filled with TRU waste and covered with crushed salt as reported by Callahan and DeVries [1991] was run with TRU waste properties dictated by Assumption (2). The results of this analysis (labelled $\sigma_m = \sigma_a$) are compared with the results (labelled $\sigma_m = \sigma_a/3$) generated via Assumption (1) as reported by Callahan and DeVries [1991] in Figures 2 through 4. Figure 2 compares the vertical and horizontal room closures from the two analyses, and as expected, the stiffer TRU waste model produced the least amount of room closure. Figure 3 compares the mean stress histories at different locations. Figure 4 shows the average void fraction results obtained for the two different TRU waste representations. Figure 4 is comparable to Figure B-6 given in Callahan and DeVries [1991]. The SANCHO results were removed, and the SPECTROM-32 results obtained by replacing material parameter κ by $\kappa/3$ are included. The results show that the stiffer TRU waste model indeed causes the crushed salt backfill to consolidate more rapidly, although the change is moderate. The TRU waste exhibits an average void fraction of about 36 percent after 200 years for the stiffer model, which is a substantial increase from the previous result (about 3 percent). The average void fraction in the room is about 18 percent after 200 years for the stiffer model compared to the previous result of about 1 percent.

Conclusions

Two different methods were used to generalize the TRU waste functional form (Equation 1) to three-dimensional states of stress. The two methods produce TRU waste stiffnesses that vary by a factor of 3. The results produced by these two generalizations can be substantially different. The first generalization (Assumption (1)) produces conservative results with respect to the backfill material; whereas, the second generalization (Assumption (2)) produces conservative results with respect to the TRU waste when porosity is the variable being considered in a typical disposal room environment.

References

Butcher, B. M., T. W. Thompson, R. G. VanBuskirk, and N. C. Pattie, 1991. *Mechanical Compaction of Waste Isolation Pilot Plant Simulated Waste*, SAND90-1206, prepared by Sandia National Laboratories, Albuquerque, NM, June.

Callahan, G. D., and K. L. DeVries, 1991. *Analyses of Backfilled Transuranic Waste Storage Rooms*, SAND91-7052, prepared by RE/SPEC Inc., Rapid City, SD, RSI-384, for Sandia National Laboratories, Albuquerque, NM.
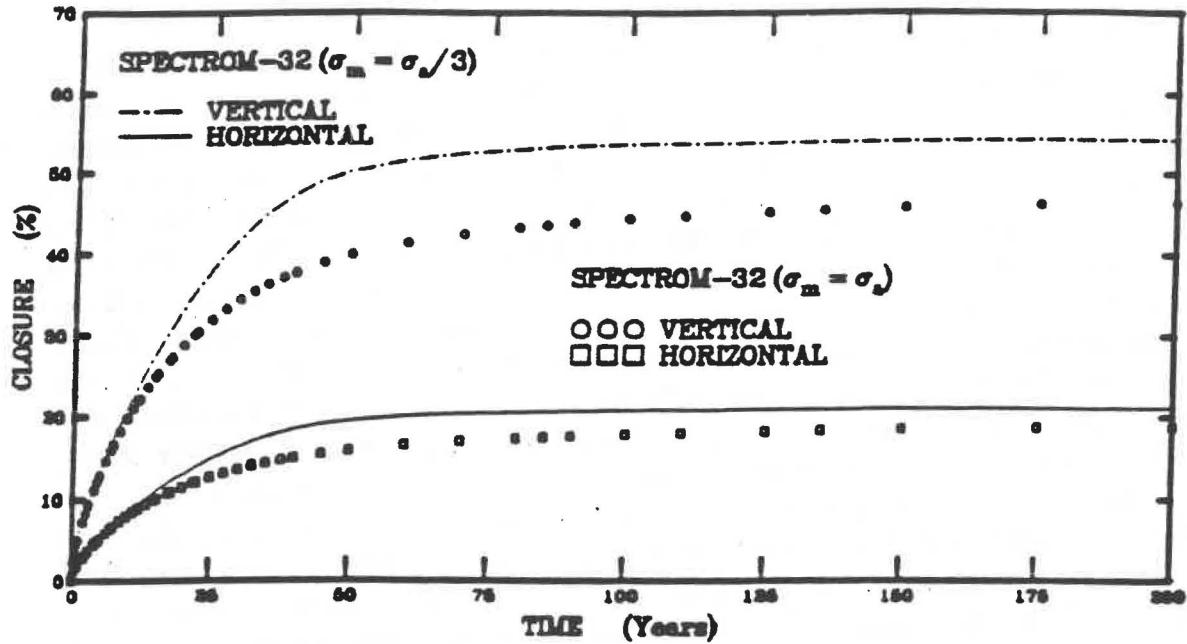
Figure 2. Room Closure History of a Disposal Room Filled with TRU Waste and Crushed Salt.
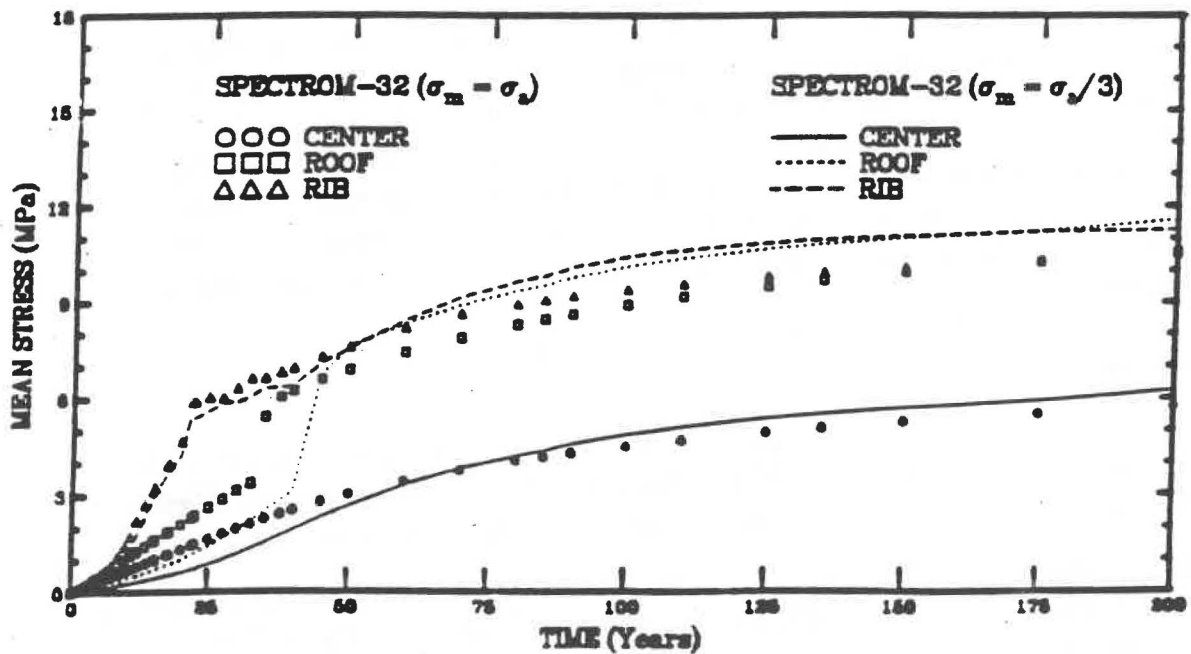
RSI-217-92-006

Figure 3. Mean Stress History of a Disposal Room Filled with TRU Waste and Crushed Salt.
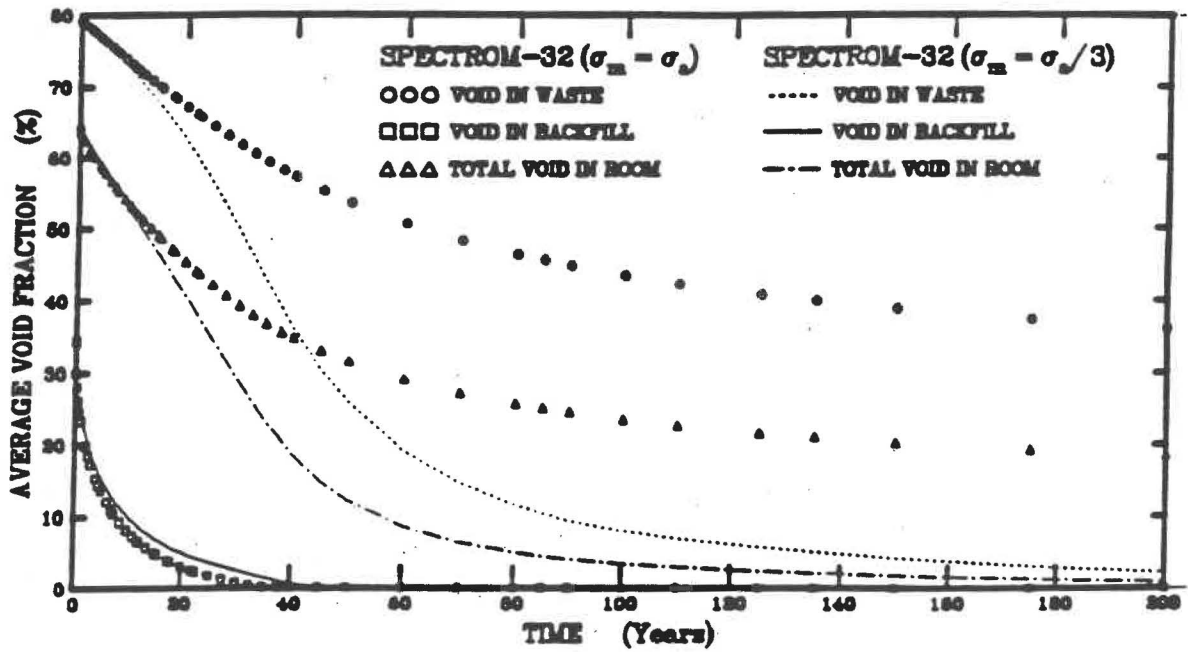
RSI-217-92-007

Figure 4. Average Void Fractions in a Room Containing TRU Waste and Crushed Salt (Current Volume).

F-86

APPENDIX B: DOCUMENTATION OF SPECTROM-32 ANALYSIS OF VERIFICATION PROBLEM 29

F-88

RE/SPEC INC.
RESEARCH / SPECIALISTS

Rapid City. South Dakota • Albuquerque. New Mexico

External Memorandum

To: Dr. Barry M. Butcher
Sandia National Laboratories
Organization 6345
P.O. Box 5800
Albuquerque, NM 87185-5800

   cc: Mr. Duane A. Labreche (RE/SPEC Inc.)
Project Records File 217-GR10

From: Dr. Gary D. Callahan
Vice President of Operations
RE/SPEC Inc.
P.O. Box 725
Rapid City, SD 57709

Date: October 15, 1992

Subject: Incorporation of the Crushable Foam Model Into SPECTROM-32 (Sandia Contract No. 78-7829)

INTRODUCTION

The purpose of this memorandum is to document the incorporation of the SANCHO crushable foam model, which is used to model compaction of the TRU waste, into SPECTROM-32. In addition, a secondary effort is documented that includes implementation and testing to ensure that the WIPP secondary creep model used in SANCHO can be executed using SPECTROM-32.

Results of simple verification problems are presented that demonstrate the crushable foam plasticity model and the WIPP secondary creep model. In addition, results from a WIPP disposal room containing TRU waste covered with crushed salt backfill (with the TRU waste simulated using the crushable foam model) are presented and compared with the previous SPECTROM-32 results [Callahan, 1992] obtained using a nonlinear elastic model. Before presenting the problems analyzed, the theoretical considerations for the constitutive models are presented.

3824 Jet Drive, P.O. Box 725, Rapid City, South Dakota 57709 • (605) 394-6400 • FAX (605) 394-6456

THEORETICAL CONSIDERATIONS FOR CRUSHABLE FOAM

The basic equations describing the SANCHO TRU waste model as given by Stone et al. [1985] are presented in this section. The SANCHO TRU waste model is an elastic-plastic model of the Drucker-Prager type with a flat volumetric cap coincident with the deviatoric plane in principal stress space. The deviatoric part of the model is elastic-perfectly plastic such that the surface of revolution in principal stress is stationary (i.e., neither kinematic nor isotropic hardening is allowed). The cap portion of the model hardens with volumetric straining such that the cap moves outward along the hydrostatic axis during volumetric yielding. The deviatoric and volumetric hardening parts of the model are uncoupled. The deviatoric yield function is given by

$$F_d = J_2 - \left(a_0 - a_1\sigma_m + a_2\sigma_m^2\right) \tag{1}$$

where

$$
\begin{aligned}
J_2 &= \frac{1}{2}S_{ij}S_{ij} \\
S_{ij} &= \sigma_{ij} - \sigma_m\delta_{ij}, \text{ deviatoric stress} \\
\sigma_m &= \frac{\sigma_{kk}}{3}, \text{ mean stress} \\
\delta_{ij} &= \text{Kronecker delta}
\end{aligned}
\tag{2}
$$

$$a_o, \ a_1, \ a_2 = \text{material constants.}$$

At yield, $F_d = 0$ and we may write Equation 1 as

$$F_d = \sqrt{J_2} - \sqrt{\left(a_o - a_1\sigma_m + a_2\sigma_m^2\right)} \tag{3}$$

which can more readily be compared to a Drucker-Prager type yield function. Note that Equation 1 differs from the SANCHO equation in that the a_1 term is opposite in sign. This sign change occurs because SANCHO assumes compression positive; whereas, in SPECTROM-32 tension is taken to be positive.

The volumetric yield function is simply

$$F_v = \sigma_m - f(\varepsilon_v) \tag{4}$$

where $\varepsilon_v = \varepsilon_{kk}$ is the volumetric strain and $f(\varepsilon_v)$ describes the volumetric hardening by a set of pressure-volumetric strain relations (i.e., data pairs entered in tabular form). As an option, we have also included a mean stress-porosity functional form by which the volumetric hardening can be evaluated. This function is written as

$$\sigma_m = \frac{1}{3\kappa} \ln\left(\frac{\phi}{\phi_0}\right) \tag{5}$$

where

κ = material parameter
ϕ_0 = initial porosity.

In addition to the deviatoric and volumetric parts of the plastic constitutive model, a tensile limit is also imposed. Tensile fracture does not occur as long as a particular tensile pressure is not large enough to produce a zero or imaginary deviatoric yield stress. Mathematically, fracture has not occurred if

$$\sigma_m < h \tag{6}$$

where h is the minimum root of the polynomial $a_0 - a_1\sigma_m + a_2\sigma_m^2 = 0$. If Equation 6 is not satisfied, the mean stress is set equal to h.

The plastic strain increment vector $d\varepsilon_{ij}^p$ is given by the flow rule

$$d\varepsilon_{ij}^p = d\lambda \frac{\partial G}{\partial \sigma_{ij}} \tag{7}$$

where G is the plastic potential function. If the yield function (F_d) is equal to the plastic potential function, F_d replaces G in Equation 7, and it is termed an associative flow rule; otherwise, the term nonassociative flow is used. For associative flow, the normality rule is satisfied which ensures a unique solution for boundary-value problems. For the deviatoric portion of the model, SANCHO uses a nonassociative flow rule so that deviatoric strains produce no volume change. This requires that the plastic potential function for the deviatoric model be

$$G = \sqrt{J_2} \tag{8}$$

and Equation 7 becomes

$$d\varepsilon_{ij}^p = d\lambda \frac{S_{ij}}{2\sqrt{J_2}} \tag{9}$$

For the volumetric portion of the model, Drucker's stability postulate for work-hardening materials (linearity requirement) is considered (e.g., see Chen and Han [1988]), which requires that

$$d\varepsilon_{ij}^{p} = \frac{1}{h}\partial F_v \frac{\partial F_v}{\partial \sigma_{ij}} = \frac{1}{h}\frac{\partial F_v}{\partial \sigma_{ij}}\frac{\partial F_v}{\partial \sigma_{mn}}d\sigma_{mn} \qquad (10)$$

where h is a scalar hardening function which may depend upon stress, strain, and loading history. Using Equation 4, $\frac{\partial F_v}{\partial \sigma_{ij}} = \frac{\delta_{ij}}{3}$, and $\partial F_v = d\sigma_m$, Equation 10 takes the form

$$d\varepsilon_{ij}^{p} = \frac{1}{h}\frac{\delta_{ij}}{3}d\sigma_m \qquad (11)$$

Rewriting Equation 11 for the plastic volumetric strain gives

$$d\varepsilon_{kk}^{p} = \frac{1}{h}d\sigma_m \qquad (12)$$

which may be rearranged to produce

$$h = \frac{d\sigma_m}{d\varepsilon_{kk}^{p}} \qquad (13)$$

Therefore, the hardening modulus describes the relationship between increments in mean stress (pressure) and increments in volumetric strain. Rather than prescribe a specific hardening function, SANCHO requires a pressure-volumetric strain relationship to describe the volumetric hardening behavior $f(\varepsilon_v)$, which is shown by Stone et al. [1985] plotted schematically as σ_m versus $\ln(\frac{\rho}{\rho_0})$ with an initial bulk modulus of K_0.

Recall that the tangent bulk modulus described by Callahan and DeVries [1991] used to model the TRU waste as a nonlinear elastic material is given by

$$K_t = \frac{d\sigma_m}{d\varepsilon_v} \qquad (14)$$

where the mean stress-volumetric strain is written in terms of the porosity ϕ as given in Equation 5. Therefore, from Equations 13 and 14, a basic equivalency exists between the nonlinear elastic tangent bulk modulus and the flat, volumetric, plastic-cap hardening modulus. Thus, the volumetric strain behavior produced by the nonlinear elastic and crushable foam plastic models should yield equivalent results as long as the same pressure-volumetric strain relationships are used to define the tangent bulk modulus and the plastic hardening modulus. This is also a conclusion of Sandler et al. [1976] who state that the behavior of a cap model with a vertical cap and a bulk modulus, K (which may be a constant or a function of pressure), which is the same for loading and unloading (i.e., $K_L = K_U$) is identical to the uncapped model with $K_L < K_U$. This is readily seen because with an associative flow rule applied to the vertical cap, only plastic volume changes occur. The crushable foam model uses the initial bulk modulus K_0 for loading and unloading. The SPECTROM-32 nonlinear elastic model uses the tangent bulk modulus for loading and unloading (loads and unloads along the same path). Therefore, if we

neglect unloading, the crushable foam plastic and nonlinear elastic models should produce equivalent volumetric behavior. This conclusion is basically true but is violated in plane strain types of problems because of the nature of the out-of-plane behavior in elastic and plastic types of problems. In elastic problems, the out-of-plane stress created by loading is equal to Poisson's ratio times the sum of the in-plane components. In elastic-plastic problems, the out-of-plane stress created by loading is altered by the out-of-plane plastic flow. Thus, the mean stresses obtained for the two problems will be different.

CONSIDERATIONS FOR WIPP SECONDARY CREEP MODEL

The purpose of the addition of the crushable foam was to eliminate differences in the material models between SPECTROM-32 and SANCHO. Therefore, we also need to be able to run the steady-state WIPP reference creep law. Krieg [1984] presents the secondary creep (steady-state) equation defining the creep strain rate $\dot{\varepsilon}_{ij}^c$ as

$$\dot{\varepsilon}_{ij}^c = \frac{3\dot{\varepsilon}_e^c}{2\sigma_e} S_{ij} \tag{15}$$

where

$$\dot{\varepsilon}_e^c = \sqrt{\frac{2}{3}\dot{\varepsilon}_{ij}\dot{\varepsilon}_{ij}}$$

$$\sigma_e = \sqrt{\frac{3}{2}S_{ij}S_{ij}}$$

As written, Equation 15 implies selection of the Mises flow potential. The effective creep strain rate $\dot{\varepsilon}_e$ is defined as

$$\dot{\varepsilon}_e = D\sigma_e^n \exp\left(-\frac{Q}{RT}\right) \tag{16}$$

where

Q = activation energy, $\dfrac{cal}{mol}$

R = universal gas constant, $1.987 \dfrac{cal}{mol \cdot K}$

T = temperature, K

D, n = material constants.

To implement the WIPP secondary creep law, the Munson-Dawson model is used with only one of the steady-state mechanisms active. The effective strain rate $\dot{\varepsilon}_{s_i}$ for the dislocation climb mechanism is written as (e.g., see Callahan and DeVries [1991])

F-93

$$\dot{\varepsilon}_{s_1} = A_1 \left(\frac{\sigma_e}{\mu}\right)^{n_1} \exp\left(-\frac{Q_1}{RT}\right) \tag{17}$$

where

Q_1 = activation energy, $\dfrac{cal}{mol}$

μ = normalizing parameter, 12,400 MPa

A_1, n_1 = material constants.

Equations 16 and 17 are equivalent if $D = \dfrac{A_1}{\mu^n}$. If we redefine μ as 1, then a one-to-one correspondence exists between Equations 16 and 17, and the WIPP secondary creep law implementation is complete. The only remaining requirement is that the Mises flow potential be specified for execution.

Material environment input for the WIPP reference creep law in **SPECTROM-32** will look approximately like the following example:

```
MATERIAL  1  "WIPP REF. CREEP"  2480..0.25,0.,0.,0.
    MUNDAW
      A1 = 45.86   Q1DIVR = 6039.   N1 = 4.9   MU = 1.0
    MISEQSTRESS
```

CRUSHABLE FOAM EXAMPLE PROBLEM

This verification problem consists of a specimen at a constant temperature of 297 K that is incrementally loaded with 1.0 MPa increments up to 5.0 MPa. Two geometric situations are investigated: axisymmetric and plane strain. For the cylindrical specimen, the loading is hydrostatic, and for the planar specimen the loading is equal in the plane. Unload-reload cycles occur at 2.0 and 4.0 MPa for the axisymmetric specimen, but the planar specimen is incrementally loaded without unloads. The volumetric strain produced by the crushable foam plasticity model is of interest. Thus, we use one eight-noded axisymmetric element (radius/width = 1m and height = 1m) with incremental vertical and lateral surface tractions of 1.0 MPa. Since the problem is one of constant stress, the dimensions are immaterial since the strain will also be constant throughout the element. The material properties for the crushable foam material (i.e., the volumetric hardening properties), where the negative signs on both volumetric strain and mean stress have been dropped for convenience, are

Point	Volumetric Strain, ε_{kk}	Mean Stress, σ_m
1	0.0001	0.0001
2	0.1525	0.5
3	0.2550	1.0
4	0.3283	1.5
5	0.3832	2.0
6	0.4255	2.5
7	0.4591	3.0
8	0.4862	3.5
9	0.5084	4.0
10	0.5269	4.5
11	0.5424	5.0

For the deviatoric portion of the crushable foam model (cf. Equations 1 and 2), a_0 and a_1 were assigned values of zero while a_2 was assigned a large value (50). This selection of deviatoric parameter values forces the deviatoric portion of the model to be inactive.

Additionally, we wish to compare the crushable foam plasticity model results to those obtained using the nonlinear elastic model described by Equation 5. Callahan and DeVries [1991] present the tangent stiffness for this model in terms of the initial (ρ_0), current (ρ), and final (ρ_f) densities as

$$K_t = \frac{d\sigma_m}{d\varepsilon_v} = \frac{d\sigma_m}{d\phi}\frac{d\phi}{d\rho}\frac{d\rho}{d\varepsilon_v} = \frac{\rho^2}{3\kappa\rho_0(\rho_f - \rho)} \tag{18}$$

For this example problem, $\rho_0 = 978.1\frac{kg}{m^3}$, $\rho_f = 2{,}792.8\frac{kg}{m^3}$, and $\kappa = 0.06784$ MPa. These density values correspond to an initial porosity of $\phi_0 = 0.65$. Using the values for κ and ρ_0 in Equation 5 with porosity defined as

$$\phi = 1 - \frac{\rho_0}{\rho_f(1 + \varepsilon_v)} \tag{19}$$

the tabular mean stress-volumetric strain data pairs used for the crushable foam model are reproduced. Thus, the nonlinear elastic and crushable foam volumetric compression properties were selected so that the two models produce the same mean stress-volumetric strain curves under hydrostatic compression.

Figure 1 shows the volumetric strain/mean stress results for the axisymmetric example problem. The solid line represents the results of the crushable foam model, and the circles represent the results of the nonlinear elastic analysis. The crushable foam results show the elastic load/unload cycles followed by plastic flow; whereas, the nonlinear elastic results show the result of the loading only (no unloading was performed). The volumetric strain and mean stress values were scaled by −1. to produce positive values for plotting. The crushable foam and nonlinear elastic results agree quite well for this axisymmetric problem.

Figure 2 shows the volumetric strain/mean stress results for the plane strain geometry. The solid line represents the crushable foam results with the diamond symbol showing the result of the elastic loading, which is followed by plastic flow. The nonlinear elastic results are represented by circles. Both the crushable foam and the nonlinear elastic results are created by five 1 MPa in-plane load increments. However, the plane strain condition produces different out-of-plane stresses (σ_z) in the elastic and plastic solutions creating different mean stresses. Elastically, $\sigma_z = \nu(\sigma_x + \sigma_y)$; whereas, for the plastic solution, the out-of-plane plastic flow is equal and opposite to the elastic strain, which decreases (reduction in the compressive magnitude) the out-of-plane stress. Figure 3 compares the out-of-plane stress components for the elastic and plastic analyses. The figure shows that the out-of-plane plastic flow drives the stress component into tension, which reduces the mean stress.

WIPP SECONDARY CREEP LAW EXAMPLE PROBLEM

This example problem consists of a cylindrical specimen at a constant temperature of 297 K under a constant axial load of 30.72 MPa. We use one eight-noded axisymmetric element (radius = 1m and height = 1m) with a surface traction of 30.72 MPa. Since the problem is one of constant stress, the dimensions are immaterial since the strain will also be constant throughout the element. The vertical creep deformation is compared for the WIPP secondary creep law with the modulus reduced by a factor of 12.5 and the Munson-Dawson model.

The material properties for the Munson-Dawson model are taken from Munson [1989] and are given in Table 1. The material properties for the WIPP reference creep law were taken from Krieg [1984] and Weatherby [1989] and are given in Table 2 (cf. Equation 17). The Young's modulus value used in conjunction with the WIPP reference creep law was reduced by a factor of 12.5 to be consistent with past analyses performed with SANCHO.

Axial strain results as a function of time for this simple example problem are show in Figure 4. The Munson-Dawson model exhibits a noticeable transient during early time, and the axial strain is substantially greater than the steady-state only model. At the end of the simulation, the Munson-Dawson model results are almost three times those of the WIPP secondary creep model.
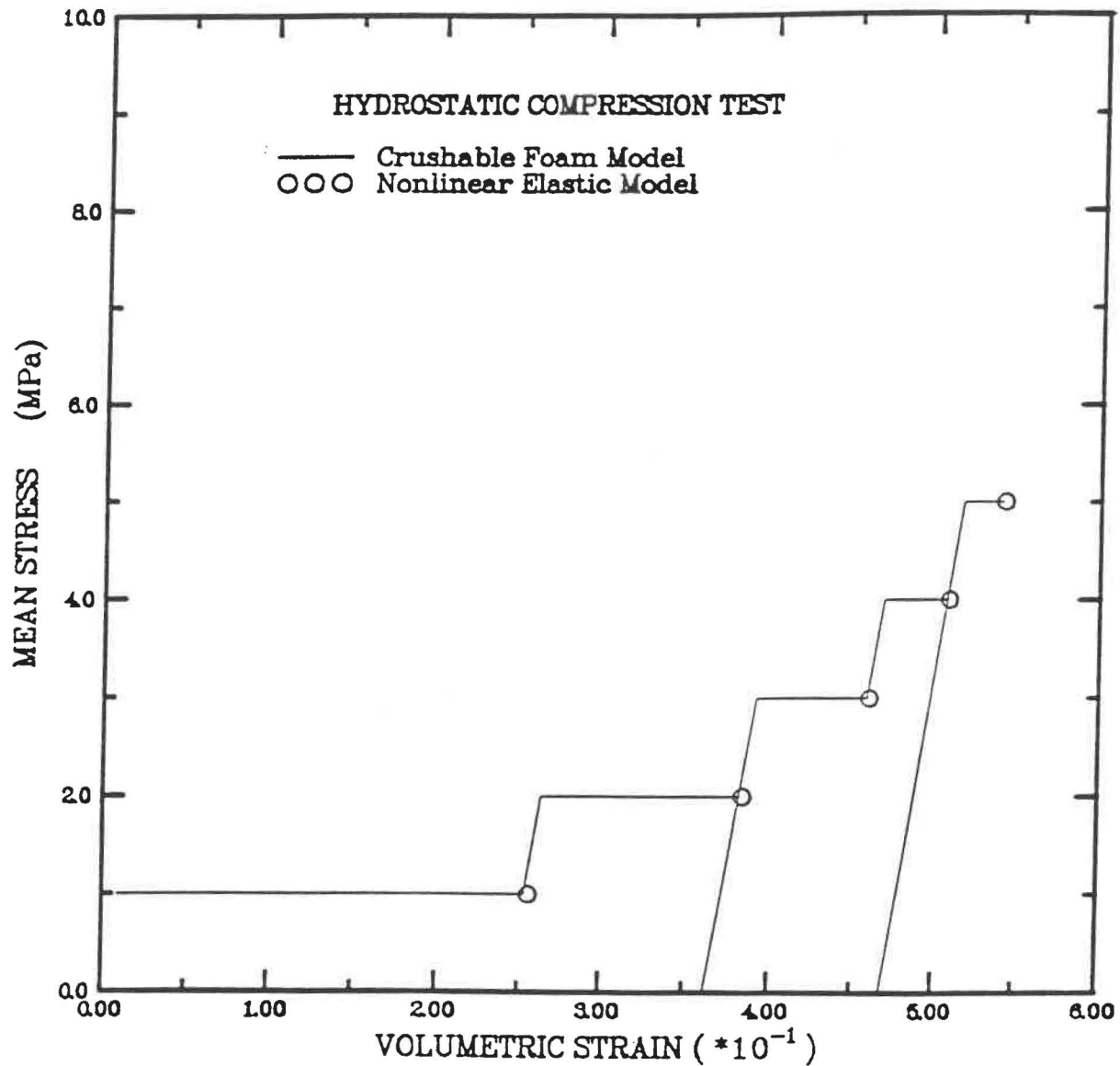
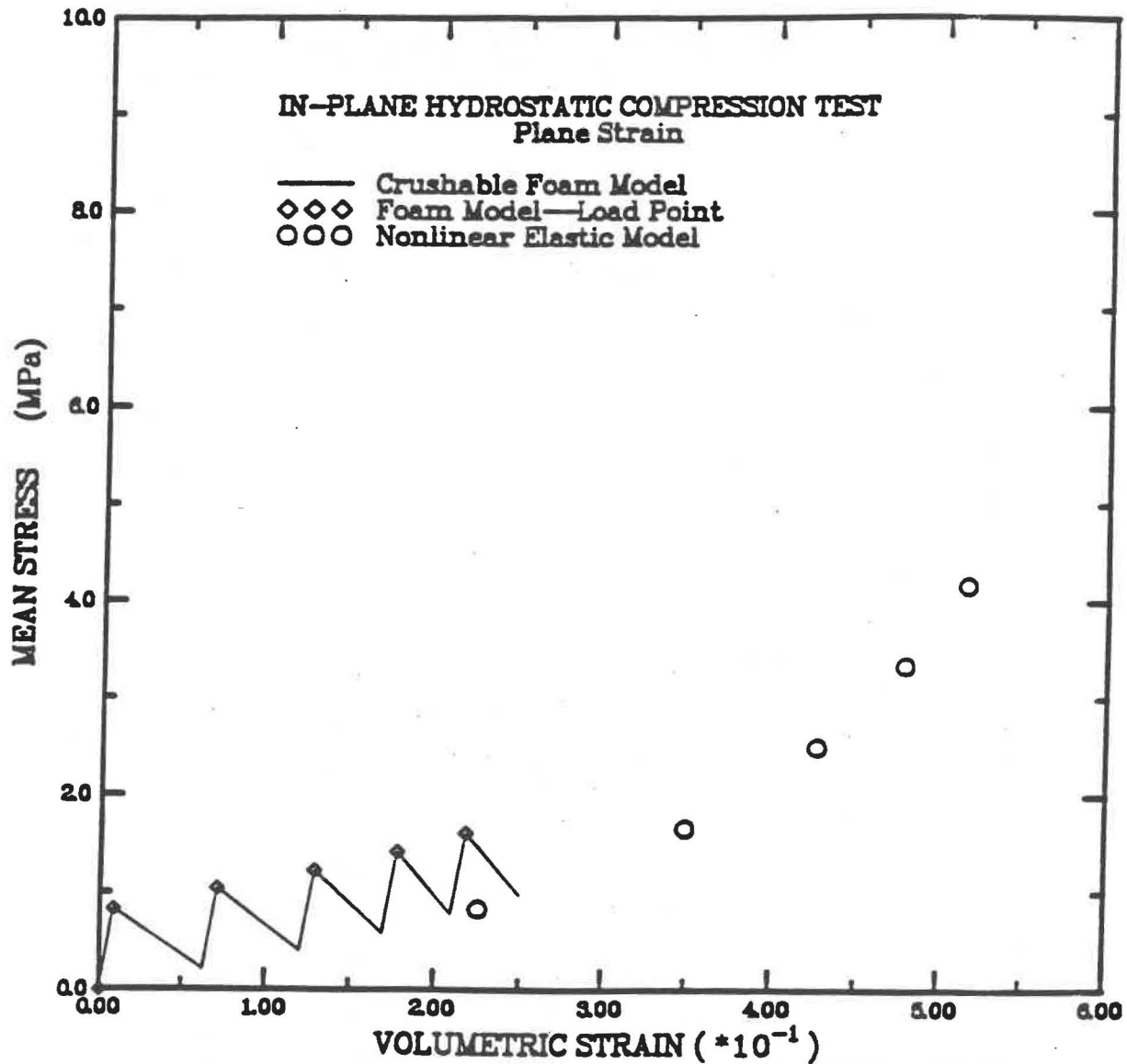**Figure 1.** Stress-Strain Behavior of the Crushable Foam Plasticity Model for an Axisymmetric Problem.

Figure 2. Stress-Strain Behavior of the Crushable Foam Plasticity Model for a Plane Strain Problem.
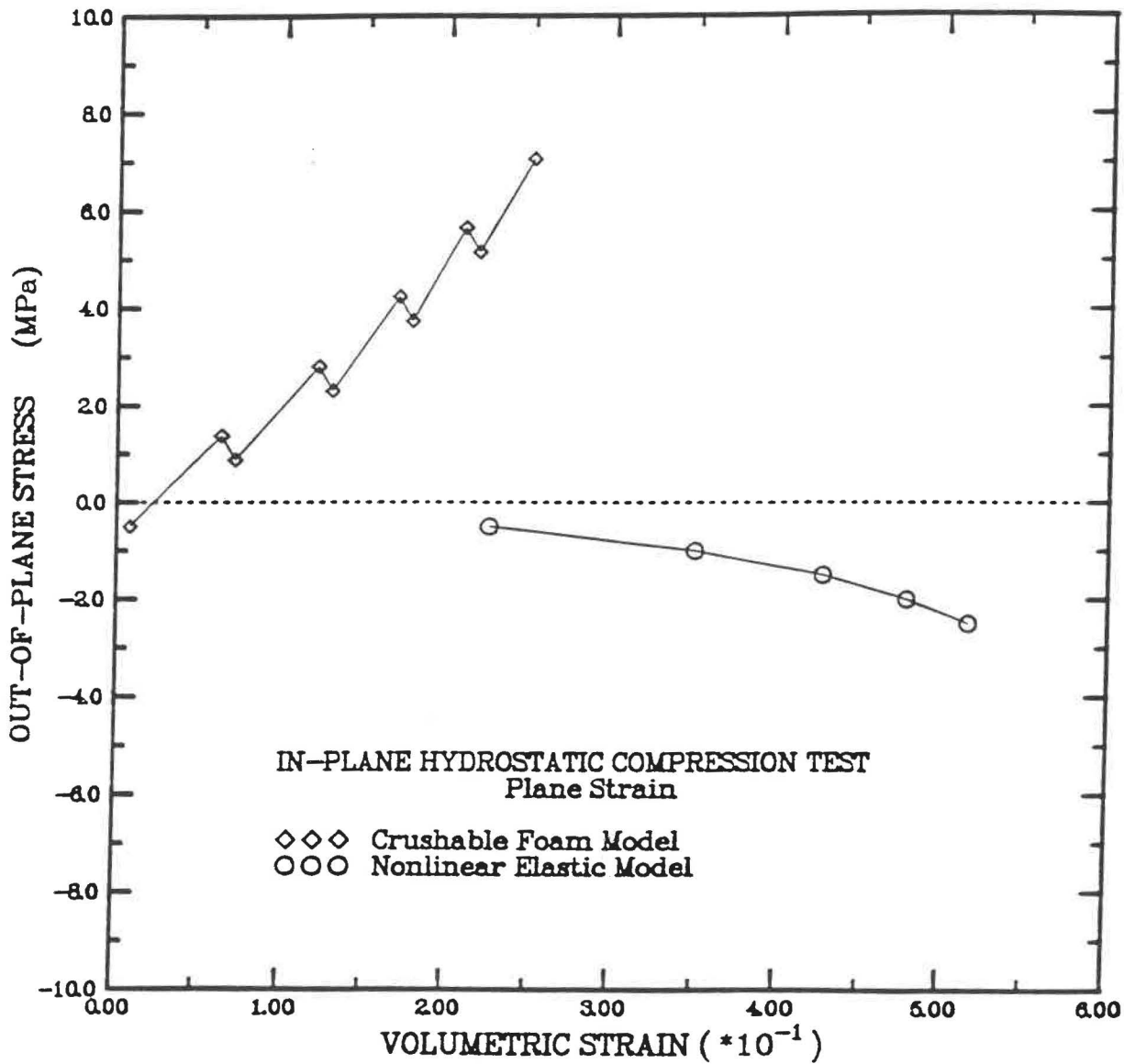
CRUSHABLE FOAM PLASTICITY

Figure 3. Out-Of-Plane Stress Behavior for the Crushable Foam Plasticity Model in a Plane Strain Problem.

Table 1. Munson-Dawson Parameter Values for Intact Salt

Parameter	Units	Value
Elastic Parameter Values		
E	MPa	31,000
ν	—	0.25
Munson-Dawson Creep Parameter Values		
A_1	yr^{-1} s^{-1}	2.645E+30 8.386E+22
A_2	yr^{-1} s^{-1}	3.050E+20 9.672E+12
Q_1/R Q_1	K cal/mol	12,581 25,000
Q_2/R Q_2	K cal/mol	5,032 10,000
n_1	—	5.5
n_2	—	5.0
B_1	yr^{-1} s^{-1}	1.919E+14 6.0856E+06
B_2	yr^{-1} s^{-1}	9.568E+05 3.034E–02
q	—	5.335E+03
σ_0	MPa	20.57
μ	MPa	12,400
m	—	3
K	—	6.275E+5
c	—	9.198E–3
α	—	–17.37
β	—	–7.738
δ	—	0.58

WIPP SECONDARY CREEP LAW EXAMPLE

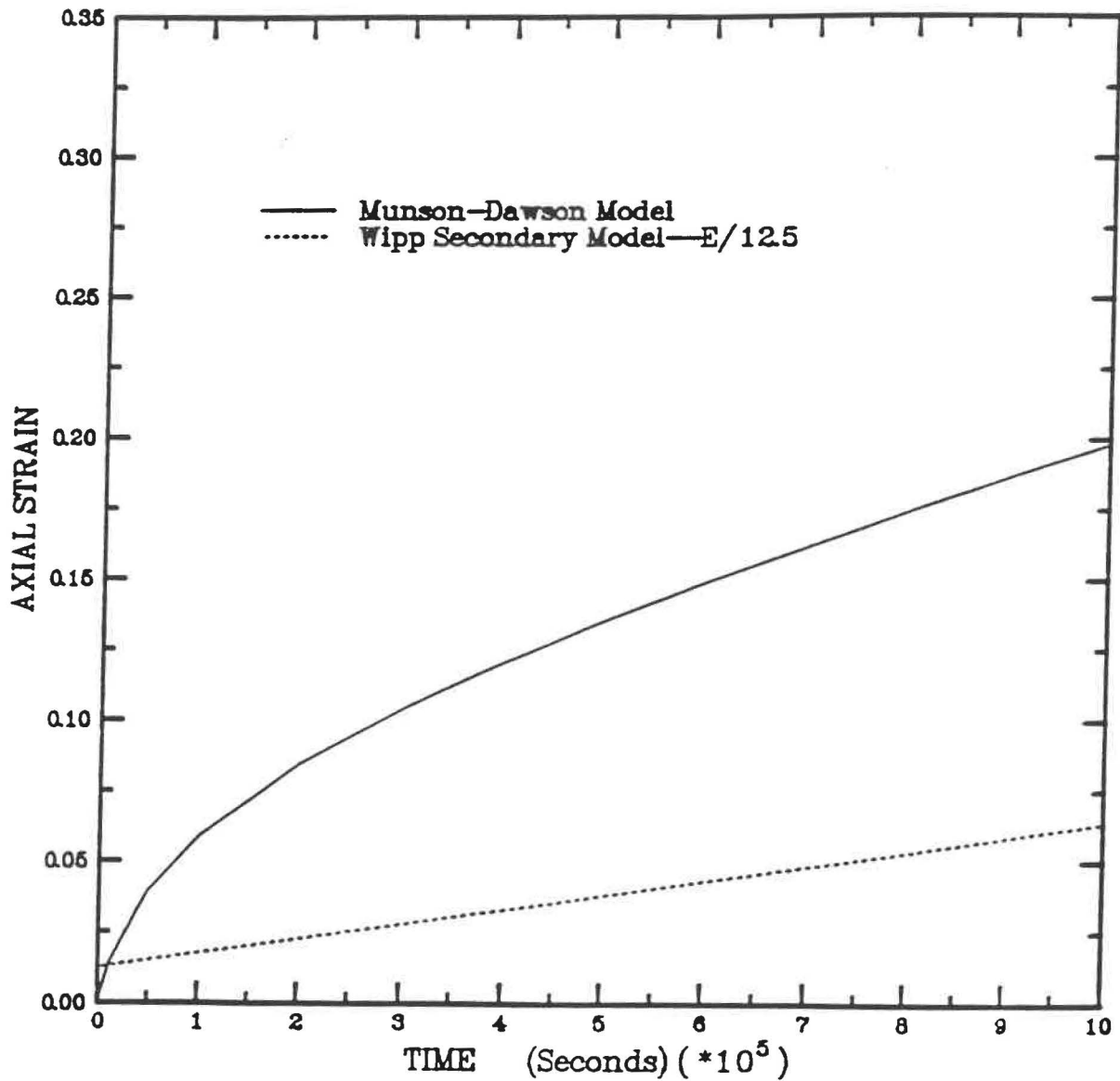**Figure 4.** Axial Strain for the WIPP Secondary Creep Law Example Problem.

Table 2. WIPP Reference Creep Law Parameters for Salt

Parameter	Units	Value
Elastic Parameter Values		
E	MPa	2,480
ν	—	0.25
Creep Parameter Values		
A_1	MPa$^{-n_1}$ s^{-1} MPa$^{-n_1}$ yr^{-1}	1.4544×10^{-6} $4.5866 \times 10^{+1}$
n_1	—	4.9
Q_1 Q_1/R	cal/mol K	12,000 6,039
μ	MPa	1.0

TRU WASTE/CRUSHED SALT BACKFILL DISPOSAL ROOM PROBLEMS

In this section, results are presented for a room containing TRU waste covered with crushed salt backfill. The geometry, initial conditions, and finite element representation for this problem are identical to those presented by Callahan and DeVries [1991]. To describe the different analyses performed, we first present the constitutive model parameters used in the analyses since the only difference in the three analyses performed was the constitutive model used to describe the salt, waste, or backfill.

Description of Analyses

The elastic and creep consolidation parameter values for the crushed salt model used in conjunction with the Munson-Dawson creep model for intact salt were taken from Callahan and DeVries [1991] and are given in Tables 3 and 4. When the WIPP reference creep law was used, the nonlinear elastic parameter values for the crushed salt were reduced by the 12.5 factor to be consistent with the modulus reduction in the intact salt and past analyses performed using SANCHO. These modified nonlinear elastic crushed salt parameter values are given in Table 5.

The TRU waste was modeled using both the nonlinear elastic description and the crushable foam plasticity model. The nonlinear elastic TRU waste description used (Equation 5) is detailed by Callahan [1992]. The TRU waste properties are given in Table 6.

The pressure-volumetric strain data used for the crushable foam model were taken from Weatherby et al. [1991]. The natural strain values of Weatherby (i.e., $\varepsilon_v = \ln(\frac{\rho}{\rho_o})$ were

Table 3.   Nonlinear Elastic Material Parameters for Crushed Salt
Used With the Munson-Dawson Intact Salt Model

Parameter	Units	Value
K_0	MPa	0.01760
K_1	m^3/kg	0.00653
G_0	MPa	0.01060
G_1	m^3/kg	0.00653
K_f	MPa	20,626
G_f	MPa	12,423
ρ^s_0	kg/m^3	1,400
ρ_f	kg/m^3	2,140

Table 4.   Creep Consolidation Material Parameters for Crushed Salt

Parameter	Units	Value
B_0	$kg/m^3 s^{-1}$ $kg/m^3 yr^{-1}$	$1.3 \times 10^{+8}$ $4.10 \times 10^{+15}$
B_1	MPa^{-1}	0.82
A	m^3/kg	-1.73×10^{-2}

converted to engineering strain values. The pressure-volumetric strain relation is given in Table 7 where the negative signs for stress and strain (compression and compaction) have been dropped for convenience. The material properties for the deviatoric portion of the model are $a_0 = 0.0$, $a_1 = 0.0$, and $a_2 = 3.0$ (Weatherby et al. [1991]). The nonlinear elastic TRU waste description is compared with the crushable foam TRU waste description in Figure 5. The nonlinear elastic description shown by the solid line is moderately stiffer than the crushable foam description.

Three different analyses were performed for comparison with the following constitutive model variations:

Table 5. Nonlinear Elastic Material Parameters for Crushed Salt Used With the WIPP Reference Creep Law for Intact Salt

Parameter	Units	Value
K_0	MPa	0.001408
K_1	m^3/kg	0.00653
G_0	MPa	0.000848
G_1	m^3/kg	0.00653
K_f	MPa	1,656
G_f	MPa	992
ρ_0^s	kg/m^3	1,400
ρ_f	kg/m^3	2.140

Table 6. Nonlinear Elastic Material Parameters for TRU Waste

Parameter	Units	Value
ρ_0	kg/m^3	542
ρ_f	kg/m^3	2,599
ϕ_0		0.79
κ	MPa^{-1}	0.0408
ν		0.25
K_f	MPa	10,282
G_f	MPa	6,169

1. Analysis 1

- Intact Salt-Munson-Dawson Model (Table 1)

- Crushed Salt-Nonlinear Elastic (Table 2), Creep Consolidation (Table 4)

- TRU Waste-Nonlinear Elastic (Table 6)

Table 7. Crushable Foam Pressure — Volumetric Relation for TRU Waste

Point	Volumetric Strain, ε_{kk} (Natural)	Volumetric Strain, ε_{kk} (Engineering)	Mean Stress, σ_m (MPa)
1	0.032	0.0315	0.028
2	0.741	0.5234	0.733
3	0.898	0.5926	1.133
4	1.029	0.6426	1.667
5	1.180	0.6927	2.800
6	1.536	0.7848	10.170

2. Analysis 2

- Intact Salt-Munson-Dawson Model (Table 1)

- Crushed Salt-Nonlinear Elastic (Table 2), Creep Consolidation (Table 4)

- TRU Waste-Crushable Foam (Table 7)

3. Analysis 3

- Intact Salt-WIPP Reference Creep (Table 2)

- Crushed Salt-Nonlinear Elastic (Table 5), Creep Consolidation (Table 4)

- TRU Waste-Crushable Foam (Table 7)

The results or each of these analyses and their comparison is included in the next section. Comparison of Analyses 1 and 2 provides basic differences between the nonlinear elastic and crushable foam plastic TRU waste models. Comparison of Analyses 2 and 3 provides differences expected between use of the Munson-Dawson and WIPP reference creep models.

Disposal Room Results

Each of the three analyses were simulated using SPECTROM-32 for a period of 200 years. The vertical and horizontal room closures are compared for Analyses 1 and 2 in Figure 6. The only difference between these two analyses is the characterization of the TRU waste (i.e., 1–nonlinear elastic and 2–crushable foam). The closure results are nearly identical through the first 20 years of the simulation. After 20 years, Analysis 2 closures (crushable foam) are greater than those obtained with the nonlinear elastic TRU waste characterization. This is partially a result of the nonlinear elastic model being slightly stiffer as shown in Figure 5. Mean stress results
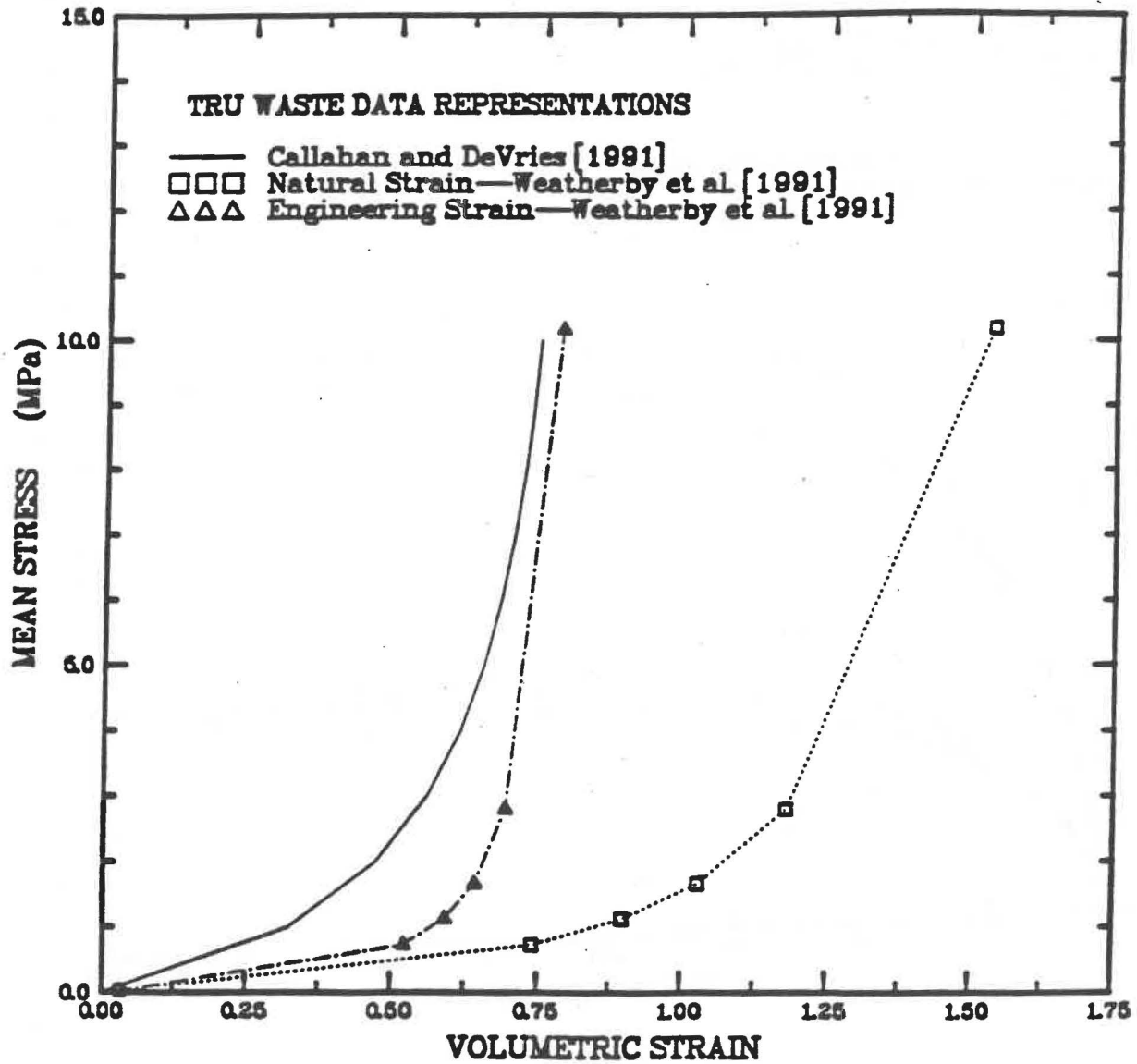
TRU WASTE DESCRIPTIONS

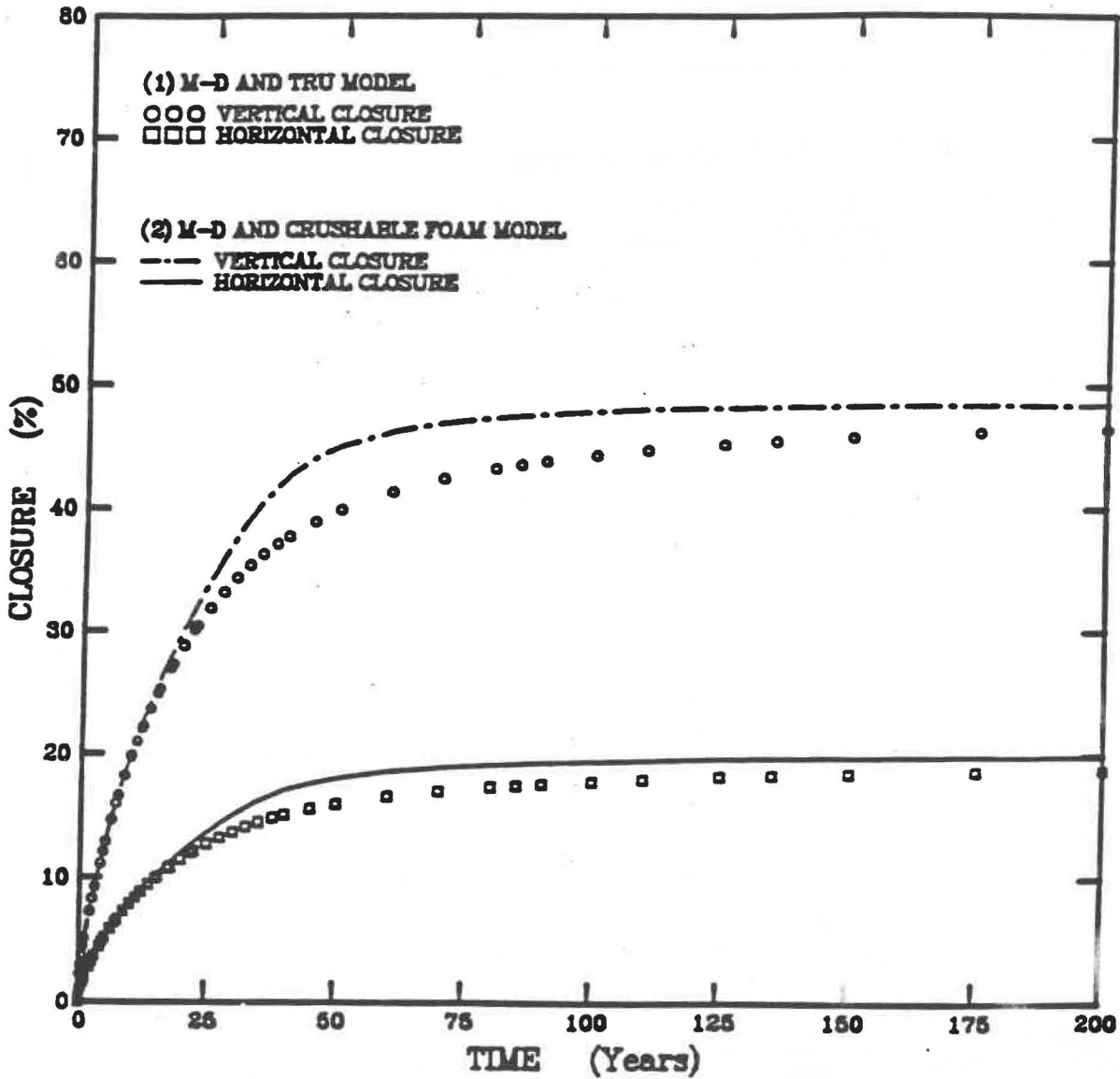Figure 5. Comparison of TRU Waste Model Descriptions.

Figure 6. Comparison of Room Closures for Different TRU Waste Models Using the Munson-Dawson Model.

F-104

at three locations in the room (center–center of the room within the TRU, roof–centerline of room near the roof within the backfill, and rib–midheight of the room near the rib within the backfill) are presented for Analyses 1 and 2 in Figure 7. As one would expect from the closure results, the mean stress values for the nonlinear elastic TRU waste description (Analysis 1) are generally greater than those obtained with the crushable foam description. This is partially a result of the out-of-plane plastic flow demonstrated in the crushable foam example problem (Figures 2 and 3). The average void fractions in the room, waste, and backfill for Analyses 1 and 2 are shown in Figure 8. The nonlinear elastic TRU waste description void fractions are generally higher than the crushable foam TRU waste characterization results indicating that the nonlinear elastic description is slightly stiffer than the crushable foam description, which is consistent with the mean stress results.

The vertical and horizontal room closures are compared for Analyses 2 and 3 in Figure 9. Differences between these two analyses include the characterization of the intact salt (i.e., 2–Munson-Dawson material with Tresca flow potential and 3–WIPP reference creep law with Mises flow potential and modulus reduced by 12.5) and the crushed salt consolidation model. The deviatoric portion of the crushed salt consolidation models is different; however, the crushed salt behavior is governed primarily by the volumetric consolidation portion of model, which is the same for the two analyses. In addition, as shown in Tables 3 and 5, the nonlinear elastic properties for the crushed salt are different. The closure results agree reasonably well during the last 100 years of the simulation; however, during the initial 100-year period, the WIPP reference law results are substantially less than those produced with the Munson-Dawson model. Mean stress results at three locations in the room are presented for Analyses 2 and 3 in Figure 10. As one would expect from the closure results, the mean stress values for the Munson-Dawson model results (Analysis 2) are generally greater than those obtained for the WIPP reference law. In addition, as shown in Figure 11, the overall compaction represented by the void fraction obtained with the Munson-Dawson model is greater than those obtained using the WIPP reference law. This is true for the average void fractions in the room, waste, and backfill as shown in Figure 11.

For ease in comparing the results of all three analyses, Figures 12 through 14 contain the results for the room closures, mean stresses, and average void fractions for all three analyses, respectively. These three different combinations of the constitutive models produce a range in average void fractions in the waste as large as 10 percent.

SUMMARY

The crushable foam plasticity model used to model TRU waste compaction and the WIPP reference creep law are presented as they were incorporated into SPECTROM-32. A simple example problem is included, which compares the nonlinear elastic and crushable foam plasticity models used to model TRU waste. The WIPP reference creep model is compared to the Munson-Dawson model for a simple simulated creep experiment. Three WIPP disposal room analyses are compared to examine the differences in results produced by different combinations of the constitutive models for the intact salt, backfill, and waste. The range in results obtained shows the importance of using the most appropriate models.
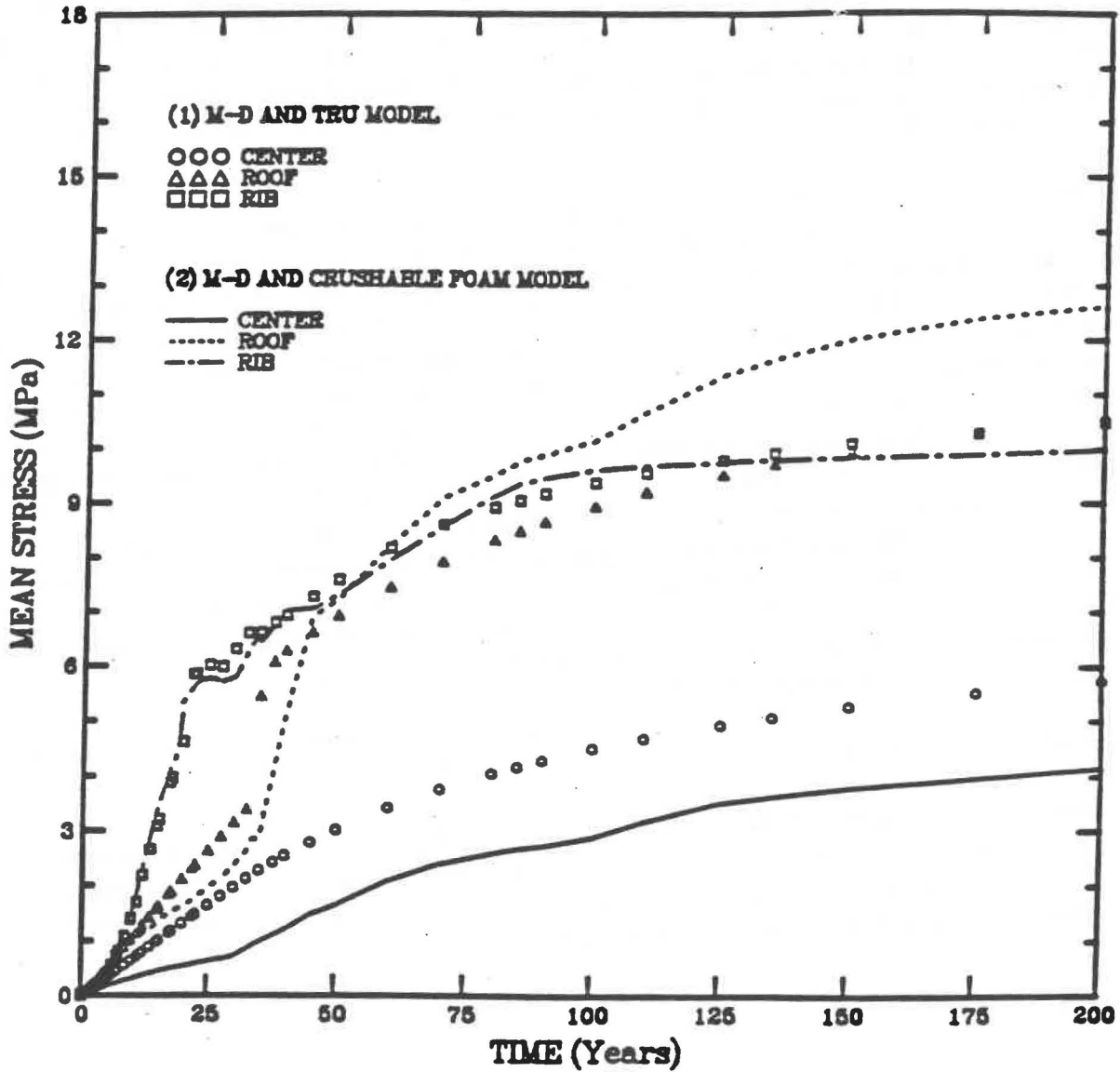
Figure 7. Comparison of mean Stresses for Different TRU Waste Models Using the Munson-Dawson Model.

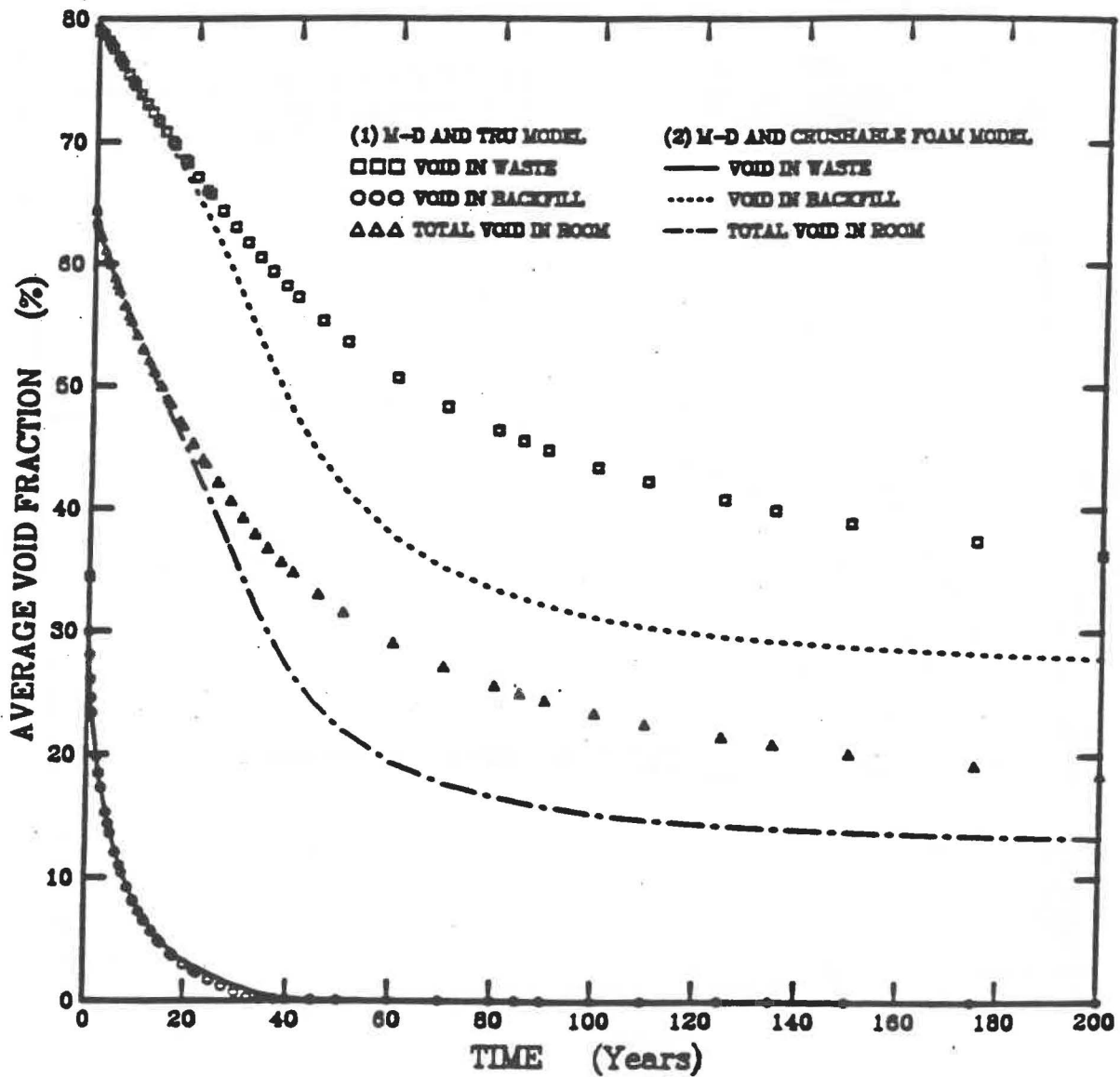**Figure 8.** Comparison of Average Void Fractions for Different TRU Waste Models Using the Munson-Dawson Model.

Figure 9. Comparison of Room Closures With the TRU Crushable Foam Model Using the Munson-Dawson and WIPP Reference Creep Models.

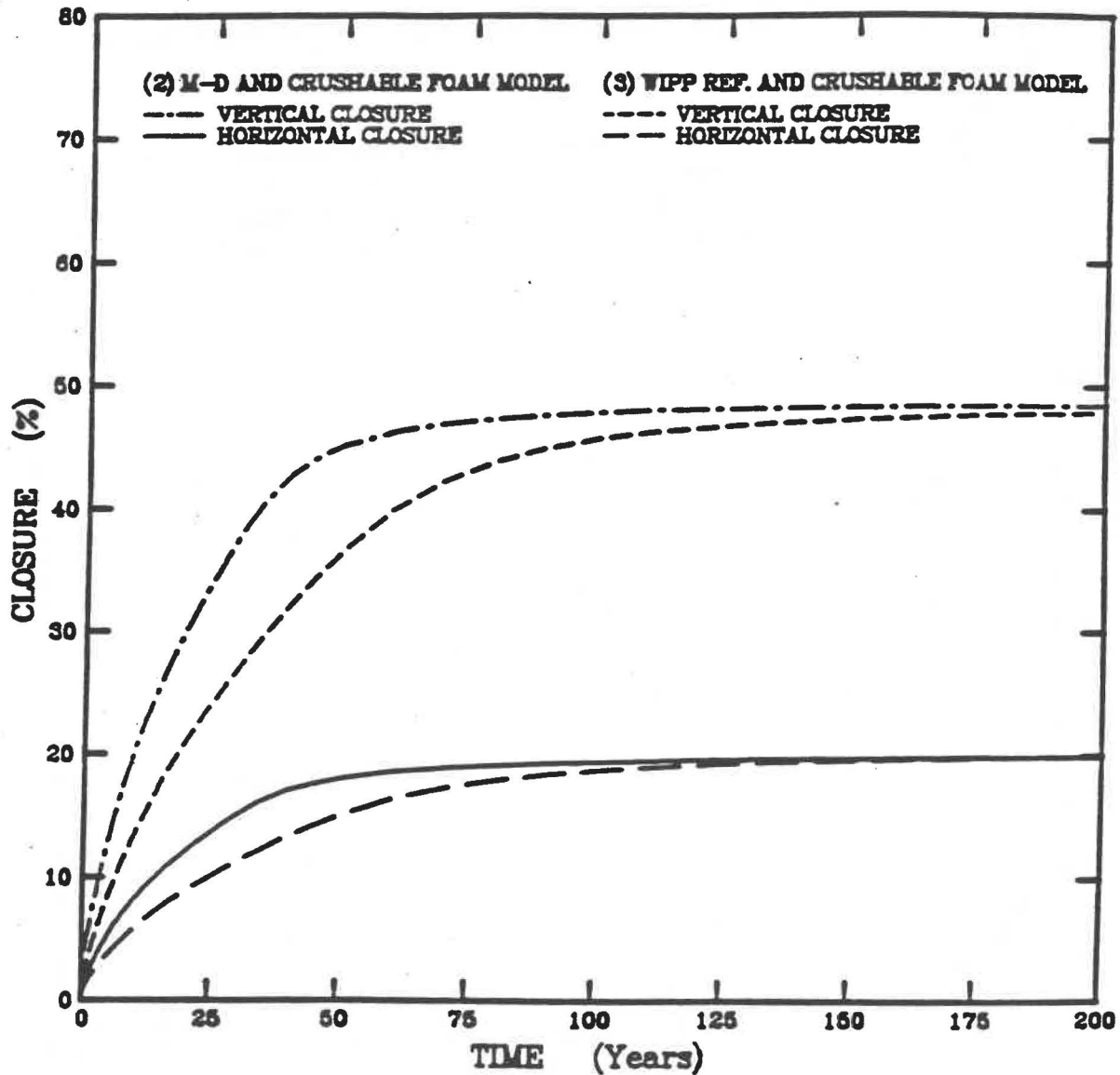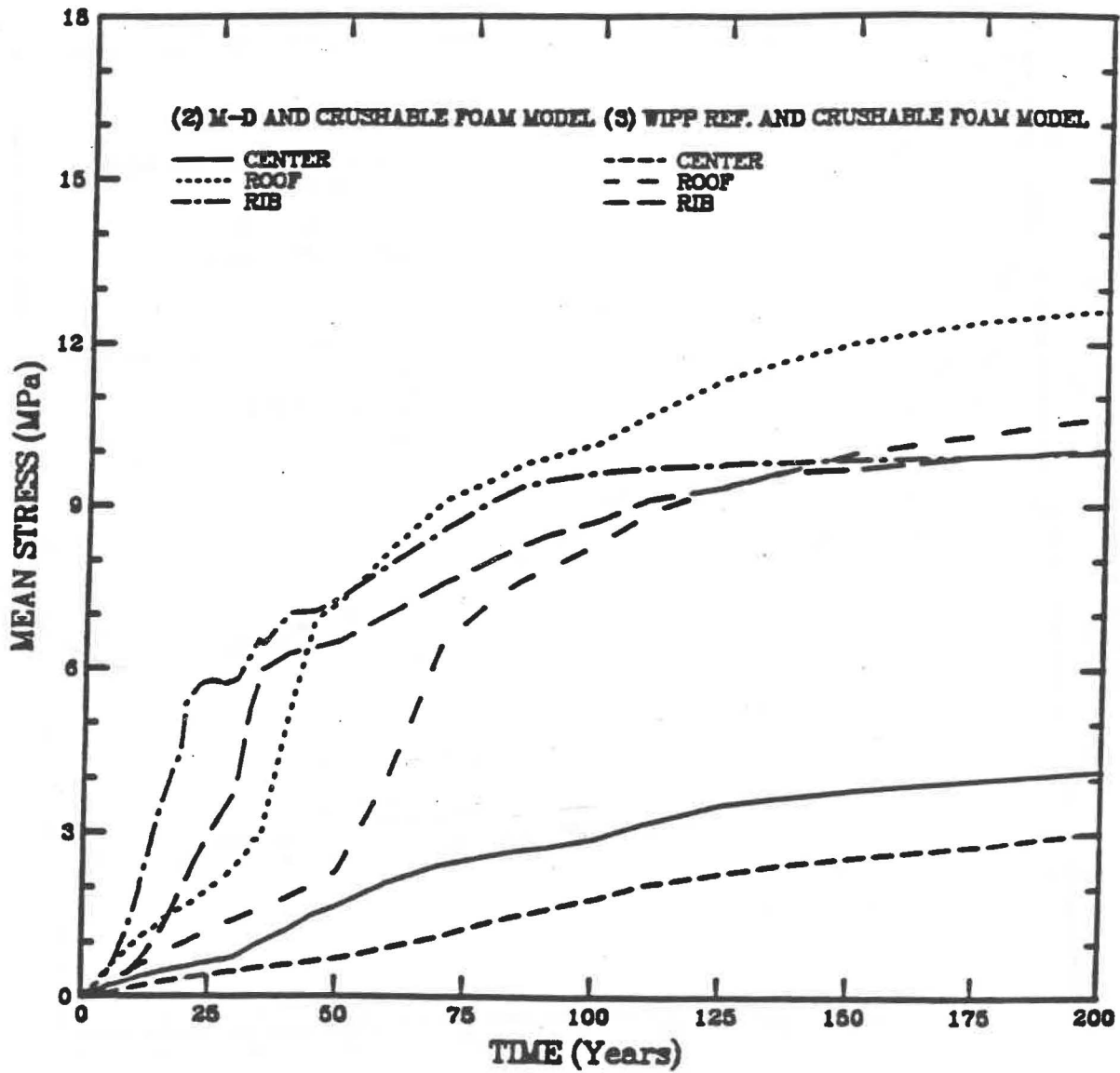**Figure 10.** Comparison of Mean Stresses With the TRU Crushable Foam Model Using the Munson-Dawson and WIPP Reference Creep Models.

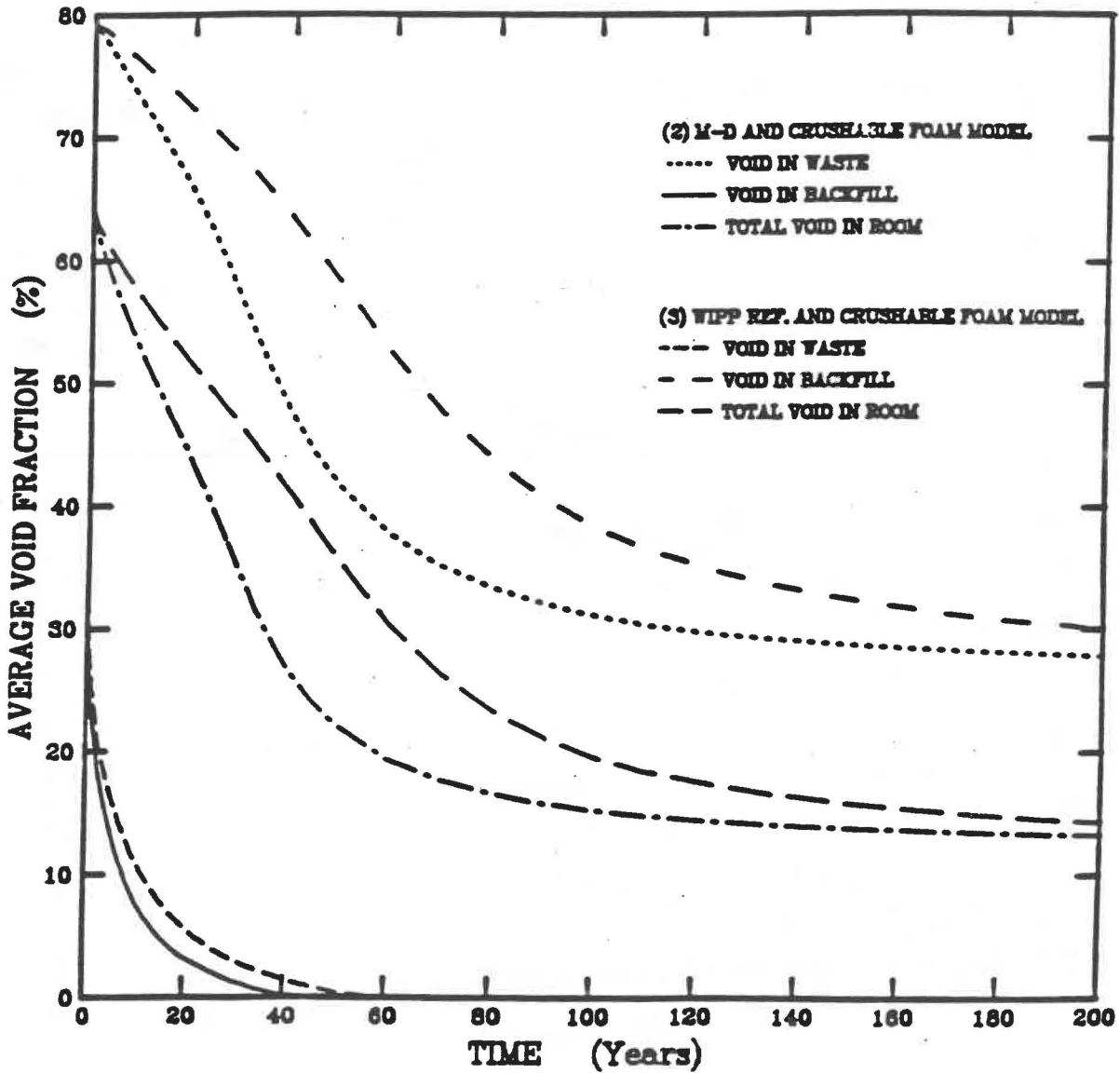**Figure 11.** Comparison of Average Void Fractions With the TRU Crushable Foam Model Using the Munson-Dawson and WIPP Reference Creep Models.

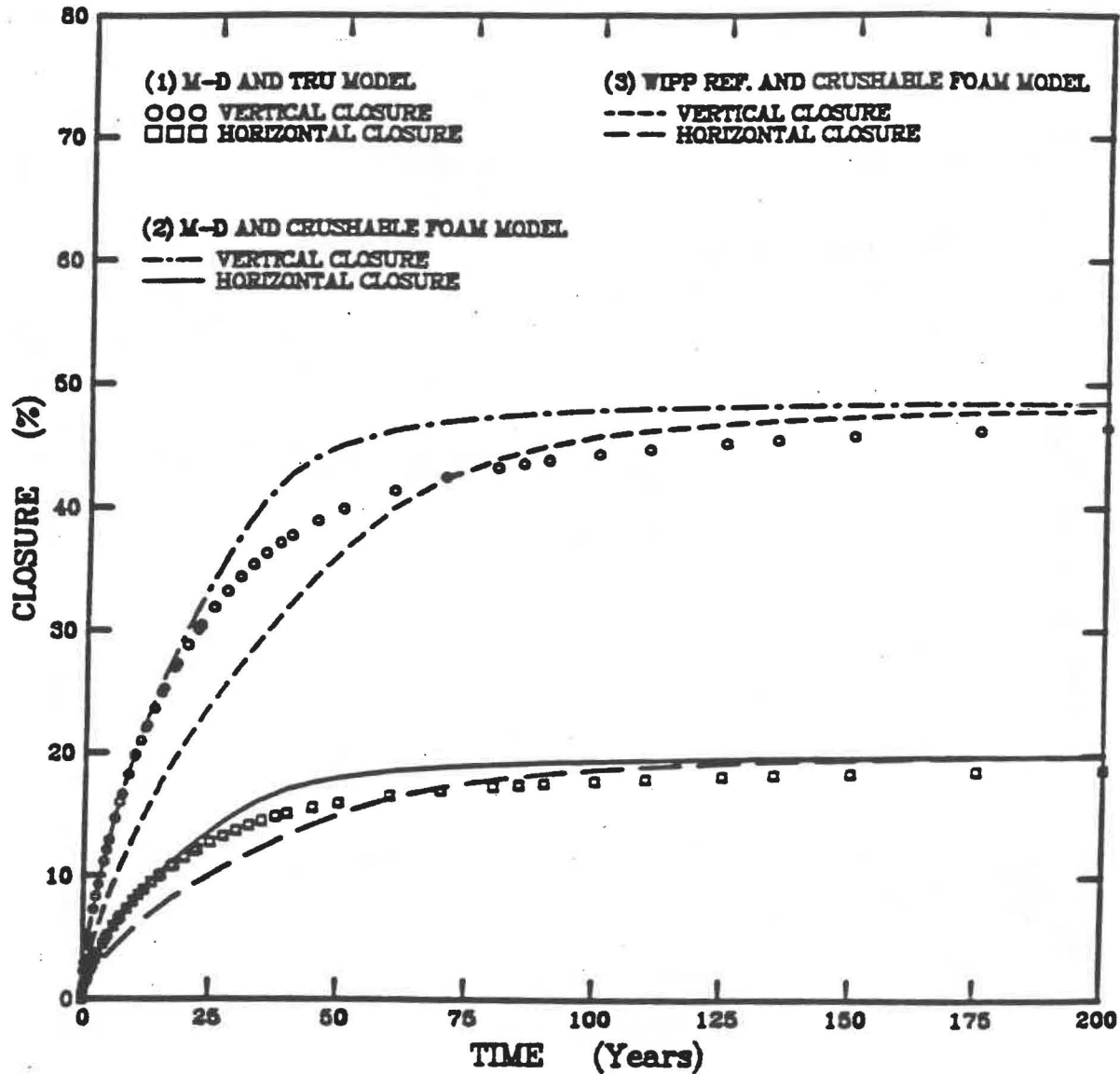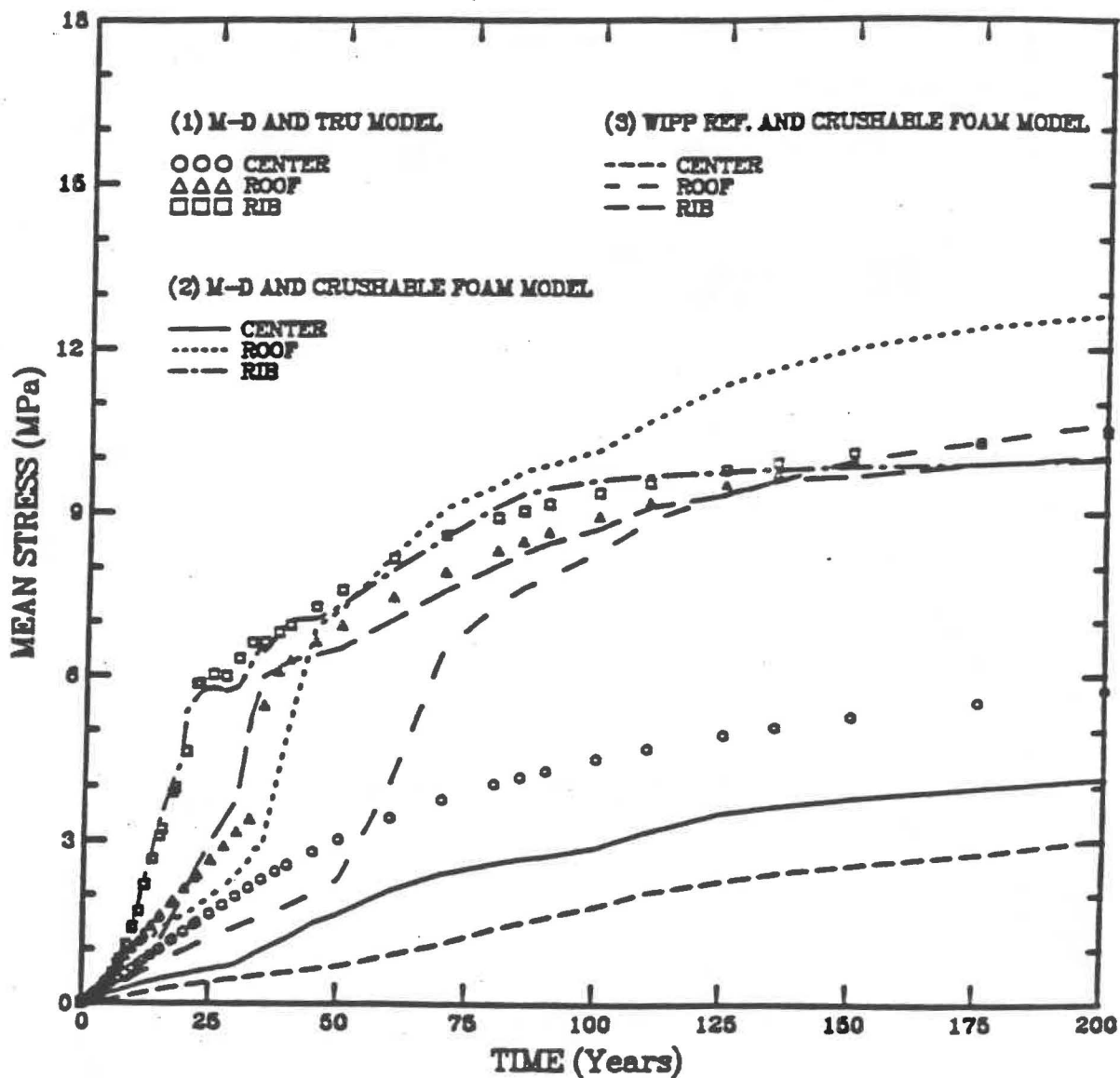**Figure 12. Comparison of Room Closures for all Three WIPP Disposal Room Analyses.**

F-111

Figure 13. Comparison of Mean Stresses for all Three WIPP Disposal Room Analyses.
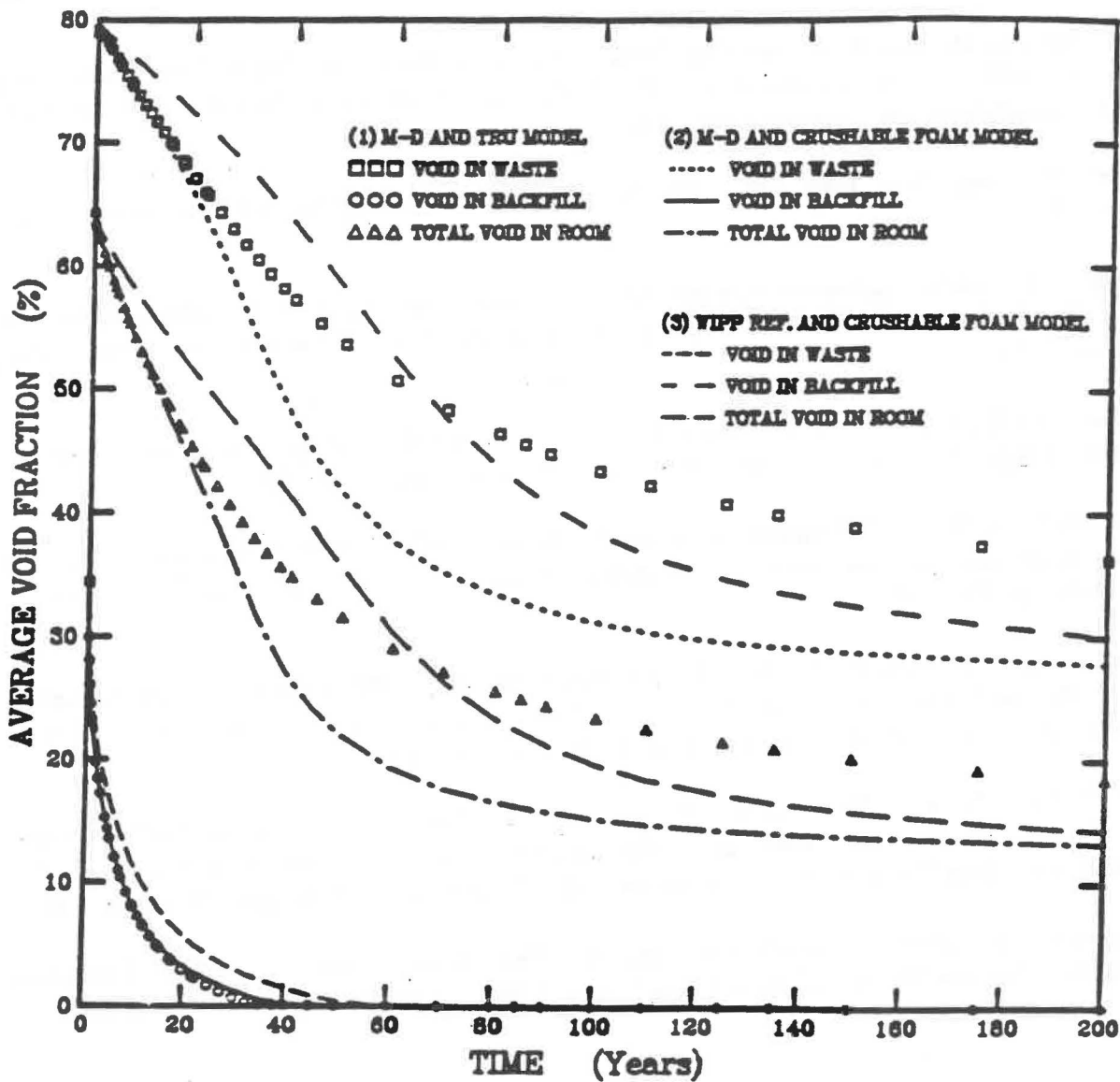
Figure 14. Comparison of Average Void Fractions for all Three WIPP Disposal Room Analyses.

REFERENCES

Callahan, G. D., 1992. *Further Discussion of the TRU Waste Model*, External Memorandum prepared by RE/SPEC Inc., Rapid City, SD, for F. T. Mendenhall, Sandia National Laboratories, Albuquerque, NM, March 13.

Callahan, G. D., and K. L. DeVries, 1991. *Analyses of Backfilled Transuranic Waste Storage Rooms*, SAND91-7052, prepared by RE/SPEC Inc., Rapid City, SD, RSI-0384, for Sandia National Laboratories, Albuquerque, NM.

Chen, W. F. and D. J. Han, 1988. *Plasticity for Structural Engineers*, Springer-Verlag, New York, NY.

Krieg, R. D., 1984. *Reference Stratigraphy and Rock Properties for the Waste Isolation Pilot Plant (WIPP) Project*, SAND83-1908, prepared by Sandia National Laboratories, Albuquerque, NM, January.

Munson, D. E., 1989. *Proposed New Structural Reference Stratigraphy, Law, and Properties*, Sandia National Laboratories Internal Memorandum, Albuquerque, NM.

Sandler, I. S., F. L. DiMaggio, and G. Y. Baladi, 1976. "Generalized Cap Model for Geological Materials," *Journal of the Geotechnical Engineering Division*, ASCE, Vol. 102, No. GT7, July, pp. 683-699.

Stone, C. M., R. D. Krieg, and Z. E. Beisinger, 1985. *SANCHO A Finite Element Computer Program for the Quasistatic, Large Deformation, Inelastic Response of Two-Dimensional Solids*, Prepared by Sandia National Laboratories, SAND84-2618, April.

Weatherby, J. R., W. T. Brown, and B. M. Butcher, 1991. "The Closure of WIPP Disposal Rooms Filled with Various Waste and Backfill Combinations," *Proceedings of the 32nd U.S. Symposium on Rock Mechanics*, J.-C. Roegiers (ed.), University of Oklahoma, Norman, OK.

Weatherby, J. R., 1989. *Finite Element Analysis of TRU Storage Rooms Filled With Waste and Crushed Salt*, Sandia National Laboratories Internal Memorandum to B. M. Butcher, Division 6332, Albuquerque, NM.

GDC:krl

APPENDIX C: INPUT FILES FOR SANCHO AND SPECTROM-32

SANCHO Input File for the Hydrostatic Compaction of TRU Waste Problem (VP29-Axisymmetric)

```
SANCHO Solution of Verification Problem 29 (SPECTROM-32): Part 1
CONTROL, 1, 14, 0, 3          $1 material; 14 press BC pts; 0 displ pts; Cauchy
DXSCALE.0.70                  $crit time step mltplr to insure stability
SOLUTION. 0.0005, 50, 2000, 0.015 $toler=.0005; soln prntd evry 50; 2000 maxiter; maxtoler=.01
AXISYM                       $axisymmetric
TIMESTEP, 0., 13, 13.        $start time; nsteps; final time...
TIMEPRNT, 0., 1, 13.         $print time; increm; final time...
TIMEPLOT, 0., 1, 13.         $plot time; increm; final time...
PLOT.GLOBAL.RMAG.ITER
PLOT.ELEMENT.STRESS.STRAIN.STATE
PLOT.NODAL.DISP.RESIDUAL.TEMP
NODES                        $data written to print file for all nodes
ELEMENTS                     $data written to print file for all elements
ENDSET                       $end of problem definition set
MATERIAL, 2, 978.1, 0.,0.,0. $Mat type 2; density (kg/m^3); gravx.gravy.omega
   Crushable Foam/TRU Waste
   60.0, 100.0, 0., 0., 50.  $G, Ku, a0, a1, a2
   3.20499E-5.0.0001, 0.0222628.0.0600, 0.165095,0.5000, 0.433493,1.7000*
   0.613994,3.00, 0.836465,6.00  $volume strain-pressure pairs
ENDSET                       $end of material definition set
DISPZ, 111,                  $lower boundary restrained vertically
PRESSURE.222,1,0,0.          $right boundary traction
PRESSURE.333,1,0,0.          $top boundary traction
DISPR, 444,                  $left vertical boundary is axis of symmetry
DISPRZ.999,                  $center node on-axis pinned
PHISTORY, 0..1., 1..1., 2..2., 3..2., 4...025, 5..2., 6..3., 7..3..*
8..4., 9..4., 10...025, 11..4., 12..5., 99..5.
END
```

SANCHO Input File for the Hydrostatic Compaction of TRU Waste Problem (VP29-Plane Strain)

```
SANCHO Solution of Verification Problem 29 (SPECTROM-32): Plane Strain
CONTROL. 1. 14. 0. 3          $1 material; 14 press BC pts; 0 displ pts; Cauchy
DXSCALE.0.50                  $crit time step mltplr to insure stability
SOLUTION. 0.0005. 50. 2000. 0.015  $toler=.0005; soln prntd evry 50; 2000 maxiter; maxtoler=.01
.PLANE                        $plane strain
TIMESTEP. 0.. 13. 13.         $start time; nsteps; final time...
TIMEPRNT. 0.. 1. 13.          $print time; increm; final time...
TIMEPLOT. 0.. 1. 13.          $plot time; increm; final time...
PLOT.GLOBAL.RMAG.ITER
PLOT.ELEMENT.STRESS.STRAIN.STATE
PLOT.NODAL.DISP.RESIDUAL.TEMP
NODES                         $data written to print file for all nodes
ELEMENTS                      $data written to print file for all elements
ENDSET                        $end of problem definition set
MATERIAL. 2. 978.1. 0..0..0.  $Mat type 2: density (kg/m^3); gravx.gravy.omega
   Crushable Foam/TRU Waste
   60.0. 100.0. 0.. 0.. 50.   $G. Ku. a0. a1. a2
   3.20499E-5.0.0001. 0.0222628.0.0600. 0.165095.0.5000. 0.433493.1.7000*
   0.613994.3.00. 0.836465.6.00  $volume strain-pressure pairs
ENDSET                        $end of material definition set
DISPZ. 111.                   $lower boundary restrained vertically
PRESSURE.222.1.0.0.           $right boundary traction
PRESSURE..333.1.0.0.          $top boundary traction
DISPR. 444.                   $left vertical boundary is axis of symmetry
DISPRZ.999.                   $center node on-axis pinned
PHISTORY. 0..1.. 1..1.. 2..2.. 3..2.. 4..2.. 5..2.. 6..3.. 7..3..*
8..4.. 9..4.. 10..4.. 11..4.. 12..5.. 99..5.
END
```

SPECTROM-32 Input File for the Hydrostatic Compaction of TRU Waste Problem (VP29-Axisymmetric)

VERIFICATION PROBLEM 29 - CRUSHABLE FOAM MODEL (TRU WASTE)

PROBTYPE 2   AXISYMMETRIC   ELEMTYPE 8   INTORD 2

MAXSTEPS 22   MAXTIME 13.0   LOCONVERGENCE = YES

MAXITER = 100   CONVERGENCE = 0.005   MAXFAIL = 0

TIMESTEP 1..1..0.0.1.   STEPRFAC 1.0

MATERIAL 1 "CRUSHABLE FOAM/TRU WASTE"

   BULKMODULUS 100.0 SHRMODULUS 60.0   DENSITY 542.

   CRFOAM   1 0.0 0.0 50.0 0.0 0.00 0.01

FUNCTION 1

0.0001	0.0001
0.1525	0.5
0.255	1.0
0.3283	1.5
0.3832	2.0
0.4255	2.5
0.4591	3.0
0.4862	3.5
0.5084	4.0
0.5269	4.5
0.5424	5.0

TEMP0 23.85 CENTIGRADE

NODES

1	0.0	0.0
2	0.5	0.0
3	1.0	0.0
4	0.0	0.5
5	1.0	0.5
6	0.0	1.0
7	0.5	1.0
8	1.0	1.0

ELEMENTS

 1   1   2   3   5   8   7   6   4   1

KINBC 0.0

 FIXDISP 0..

  NODELIST 1.4.6

 FIXDISP ..0.

  NODELIST 1.2.3

TRACTION 0.0

```
     SURFTRACTION 1.0 1.0 1.0  SURFACE 1  3  5  8
     SURFTRACTION 1.0 1.0 1.0  SURFACE 1  8  7  6

   TRACTION 2.0
     SURFTRACTION 1.0 1.0 1.0  SURFACE 1  3  5  8
     SURFTRACTION 1.0 1.0 1.0  SURFACE 1  8  7  6

   TRACTION 4.0
     SURFTRACTION -2.0 -2.0 -2.0  SURFACE 1  3  5  8
     SURFTRACTION -2.0 -2.0 -2.0  SURFACE 1  8  7  6

   TRACTION 5.0
     SURFTRACTION 2.0 2.0 2.0  SURFACE 1  3  5  8
     SURFTRACTION 2.0 2.0 2.0  SURFACE 1  8  7  6

   TRACTION 6.0
     SURFTRACTION 1.0 1.0 1.0  SURFACE 1  3  5  8
     SURFTRACTION 1.0 1.0 1.0  SURFACE 1  8  7  6

   TRACTION 8.0
     SURFTRACTION 1.0 1.0 1.0  SURFACE 1  3  5  8
     SURFTRACTION 1.0 1.0 1.0  SURFACE 1  8  7  6

   TRACTION 10.
     SURFTRACTION -4.0 -4.0 -4.0  SURFACE 1  3  5  8
     SURFTRACTION -4.0 -4.0 -4.0  SURFACE 1  8  7  6

   TRACTION 11.
     SURFTRACTION 4.0 4.0 4.0  SURFACE 1  3  5  8
     SURFTRACTION 4.0 4.0 4.0  SURFACE 1  8  7  6

   TRACTION 12.
     SURFTRACTION 1.0 1.0 1.0  SURFACE 1  3  5  8
     SURFTRACTION 1.0 1.0 1.0  SURFACE 1  8  7  6

OUTPUT
 MESH
 REACTIONS ? NO
 ELASTIC YES
 OUTIMES 1..2..3..4..5..6..7..8..9..10..11..12..13.
 SUBELASTIC NO
```

SPECTROM-32 Input File for the Hydrostatic Compaction of TRU Waste Problem (VP29-Axisymmetric)-Cont.

```
 PLOTDBASE YES   PLOTSTRAIN
  RESTDBASE NO
SUPDEF NO
EXECUTE YES
ENDATA
```

SPECTROM-32 Input File for the Hydrostatic Compaction of TRU Waste Problem (VP29-Plane Strain)

VERIFICATION PROBLEM 29 - CRUSHABLE FOAM MODEL (TRU WASTE)

```
PROBTYPE 2          PLSTRAIN          ELEMTYPE 8    INTORD 2
MAXSTEPS 29             MAXTIME 17.0      LOCONVERGENCE = YES
MAXITER = 500     CONVERGENCE = 0.005       MAXFAIL = 0
TIMESTEP 1..1..0.0.1.    STEPRFAC 1.0
```

MATERIAL 1 "CRUSHABLE FOAM/TRU WASTE"

```
    BULKMODULUS 100.0  SHRMODULUS 60.0    DENSITY 542.
    CRFOAM  1 0.0 0.0 50.0  0.0  0.00  0.01
```

FUNCTION 1

```
    0.0001   0.0001
    0.1525   0.5
    0.255    1.0
    0.3283   1.5
    0.3832   2.0
    0.4255   2.5
    0.4591   3.0
    0.4862   3.5
    0.5084   4.0
    0.5269   4.5
    0.5424   5.0
```

TEMP0 23.85 CENTIGRADE

NODES

```
    1        0.0      0.0
    2        0.5      0.0
    3        1.0      0.0
    4        0.0      0.5
    5        1.0      0.5
    6        0.0      1.0
    7        0.5      1.0
    8        1.0      1.0
```

ELEMENTS

```
    1   1   2   3   5   8   7   6   4   1
```

KINBC 0.0

```
 FIXDISP 0..
   NODELIST 1.4.6
 FIXDISP ..0.
   NODELIST 1.2.3
```

SPECTROM-32 Input File for the Hydrostatic Compaction of TRU Waste Problem (VP29-Plane Strain)-Cont.

```
TRACTION 0.0
   SURFTRACTION 1.0 1.0 1.0  SURFACE 1  3  5  8
   SURFTRACTION 1.0 1.0 1.0  SURFACE 1  8  7  6

TRACTION 2.0
   SURFTRACTION 1.0 1.0 1.0  SURFACE 1  3  5  8
   SURFTRACTION 1.0 1.0 1.0  SURFACE 1  8  7  6

TRACTION 4.0
   SURFTRACTION -2.0 -2.0 -2.0  SURFACE 1  3  5  8
   SURFTRACTION -2.0 -2.0 -2.0  SURFACE 1  8  7  6

TRACTION 6.0
   SURFTRACTION 2.0 2.0 2.0  SURFACE 1  3  5  8
   SURFTRACTION 2.0 2.0 2.0  SURFACE 1  8  7  6

TRACTION 8.0
   SURFTRACTION 1.0 1.0 1.0  SURFACE 1  3  5  8
   SURFTRACTION 1.0 1.0 1.0  SURFACE 1  8  7  6

TRACTION 10.0
   SURFTRACTION 1.0 1.0 1.0  SURFACE 1  3  5  8
   SURFTRACTION 1.0 1.0 1.0  SURFACE 1  8  7  6

TRACTION 12.
   SURFTRACTION -4.0 -4.0 -4.0  SURFACE 1  3  5  8
   SURFTRACTION -4.0 -4.0 -4.0  SURFACE 1  8  7  6

TRACTION 14.
   SURFTRACTION 4.0 4.0 4.0  SURFACE 1  3  5  8
   SURFTRACTION 4.0 4.0 4.0  SURFACE 1  8  7  6

TRACTION 16.
   SURFTRACTION 1.0 1.0 1.0  SURFACE 1  3  5  8
   SURFTRACTION 1.0 1.0 1.0  SURFACE 1  8  7  6

OUTPUT
 MESH
 REACTIONS ? NO
 ELASTIC YES
 OUTIMES 1.,2.,3.,4.,5.,6.,7.,8.,9.,10.,11.,12.,13.,14.,15.,16.,17.
 SUBELASTIC NO
```

SPECTROM-32 Input File for the Hydrostatic Compaction of TRU Waste Problem (VP29-Plane Strain)-Cont.

```
  PLOTDBASE YES    PLOTSTRAIN
  RESTDBASE NO
SUPDEF NO
EXECUTE YES
ENDATA
```

SANCHO Input File for the Uniaxial Creep Consolidation of Crushed Salt

```
SANCHO Solution of NonLin Elas CrpConsol Prob (S32): UNIAX 10
CONTROL. 1, 4, 0, 3          $# material: # press BC pts; # disp pts; Cauchy
DXSCALE.0.01                 $crit time step mltplr to insure stability
SOLUTION. 0.005, 100, 2500, 0.01 $toler; soln prnt intrvl; maxiter;maxtoler
AXISYM                       $axisymmetric
TIMESTEP. 0.,20,1000., 40,2000., 40,1.E4, 10,2.5E4, 15,1.0E5*
         15,4.E5, 12,1.0E6                $start time:num steps:end
TIMEPRNT. 0.,50.,250., 250.,1000., 500.,2500., 2500.,1.E4*
         1.5E4,2.5E4, 2.5E4,1.E5, 1.E5,1.E6      $print time:increment:end
TIMEPLOT. 0.,100.,1000., 1000.,1.E4, 1.5E4,2.5E4, 2.5E4,1.0E5*
         5.E4,4.E5, 1.E5,1.0E6            $start time:num steps:end
PLOT.GLOBAL.RMAG.ITER
PLOT.ELEMENT.STRESS.STRAIN.STATE
PLOT.NODAL.DISP.RESIDUAL.TEMP
NODES                        $data written to print file for all nodes
ELEMENTS                     $data written to print file for all elements
ENDSET                       $end of problem definition set
MATERIAL. 7, 1., 0.,0.,0.    $Mat type: density (kg/m^3); gravx,gravy.omega
   Creep Consolidation / Crushed Salt
   10600.,0.00653,17600.,0.00653,5.79E-36,4,9.20.13*
   -0.0173.,1.3E8,0.82E-6,1700.,2140.,0.002
S                            SG0.G1.K0.K1.Ac.N,Q/RT,A.A1.B0.B1.RHO1.RHOFC.DTSUB
ENDSET                       $end of material definition set
DISPZ. 111.                  $lower boundary restrained vertically
PRESSURE.222.0.0.0.          $right boundary traction
PRESSURE.333.1.0.0.          $top boundary traction
DISPR. 444.                  $left vertical boundary is axis of symmetry
DISPRZ.999.                  $center node on-axis pinned
PHISTORY. 0.,0., 1000.,1.E6, 2000.,10.E6, 2.E6,10.E6
END
```

SPECTROM-32 Input File for the Uniaxial Creep Consolidation of Crushed Salt

CRUSHED SALT UNIAXIAL COMPRESSION/WIPP SS.

PROBTYPE 1   AXISYMMETRIC   ELEMTYPE 8   INTORD 2

MAXSTEPS 20000.1   MAXTIME 1.0001E+6

TIMESTEP 1..10000..0.0.10000. STEPRFAC .10   GLOCONVERGENCE = YES

MAXITER = 0   MAXFAIL = 2   CONVERGENCE = 0.0005

MATERIAL 1 "NONLINELAS/CREEPCON-WIPP SS"

  NONLINELASTIC 0.0176.0.0106.1700..0.00653.0.00653

        20700..12425..10..025

  MUNDAW

   A1 = 1.4544E-6 Q1DIVR = 5978.61 N1 = 4.9 MU = 1.0

   CONCRP 1.3E+8.0.82.-0.0173.2140..2

  MXSHEAR

MATERIAL 2 "WIPP STEADY-STATE"

    2395.04   0.2492 1.   2140.

  MUNDAW

   A1 = 1.4544E-6 Q1DIVR = 5978.61 N1 = 4.9 MU = 1.0

  MISEQSTRESS

TEMP0 23.85 CENTIGRADE

NODES

1	0.0	0.0
2	0.5	0.0
3	1.0	0.0
4	0.0	0.5
5	.1.0	0.5
6	0.0	1.0
7	0.5	1.0
8	1.0	1.0

ELEMENTS

  1 1 2 3 5 8 7 6 4 1

KINBC 0.0

 FIXDISP 0..

  NODELIST 1.4.6

 FIXDISP ..0.

  NODELIST 1.2.3

TRACTION

 SURFTRACTION 10.00 10.00 10.00 SURFACE 1 8 7 6

SPECTROM-32 Input File for the Uniaxial Creep
Consolidation of Crushed Salt-Cont.

```
OUTPUT
 REACTIONS ? NO
 MESH
 ELASTIC YES
 OUTIMES 100..1.E+4..33E+5..5E+5..66E+5..867E+5
       1.E+5.1.5E+5.2E+5.3E+5.4E+5.5E+5.6E+5.7E+5.8E+5.9.E+5.1.E+6
 SUBELASTIC NO
 PLOTDBASE YES   PLOTSTRAIN
 RESTDBASE NO

SUPDEF NO
EXECUTE YES
ENDATA
```

SPECTROM-32 Input File for Stress Initialization of the WIPP Disposal Room Problem

JOB 217 SPECTROM-32 COMPARISON TO SANCHO...776 EL/4 NODED-INITIAL STRESS

MXELEX = 227

PROBTYPE 2   PLSTRAIN   INTORD 2

MAXSTEPS 4   MAXTIME 200.   GLOCONVERGENCE = YES

MAXITER = 6   CONVERGENCE = 0.005   MAXFAIL = 1

TIMESTEP 1.0   2.0   STEPRFAC 1.   PRESCO YES

OUTPUT = DISPLACE STRESS   MESH   ELASTIC   LASTRESS

OUTINT = 1

OUTIMES = 1.0

NODELIST 1 19 116 163 316 318 320 322 324 326 328 426 428 430 340

ELEMLIST = 1 12 79 80 163 48 74 73 72 161 753 774 772 770 263 259

        81 82 83 179 180 181 186 188 344 595 639

PLOTDBASE = YES PLOTSTRAIN

MATERIAL 1 "PSEUDO AIR/TRU-WASTE"

     0.10 0.0   1. 0.0

MATERIAL 2 "PSEUDO AIR/C-SALT"

     0.10 0.0   1. 0.0

MATERIAL 3 "INTACT SALT"

     31000.   0.25   1.   2140.

MATERIAL 4 "AIR-GAP"

     0.10 0.0   1. 0.0

READ

  GENMESH

KINBC = 0.0

  FIXDISPL = 0.,   NODESET = 2,3

  FIXDISPL = .0.   NODESET = 1

GRAVITY = 9.79E-6

OVERBURDEN = -14.8

LAYER 54.0 0.0 1.0 1.0

INISURFACE

  SURFTRACTION 0.0 0.0 0.0 0.0

  SURFSET = 1

EXCAVATION 1.0

  ELSETEX = 1 2 4

```
TRACTION 2.0
 SURFTRACTION 0.01  0.01  0.0  0.0
 SURFSET 2

EXECUTE = YES
SUPDEF NO
ENDATA
```

SPECTROM-32 Input File for the WIPP Disposal Room Problem

JOB 217 SPECTROM-32 COMPARISON TO SANCHO...776 EL/4 NODED

! NOTE: Initial stress field established in separate run.

MXELEX = 227

PROBTYPE 3	PLSTRAIN	INTORD 2
MAXSTEPS 20	MAXTIME 2000.	GLOCONVERGENCE = YES
MAXITER = 150	CONVERGENCE = 0.001	MAXFAIL = 5
TIMESTEP 1.0E-14 .50	STEPRFAC 0.03	PRESCO YES

READ

  GENMESH

  INISTRESS

KINBC = 0.0

  FIXDISPL = 0., NODESET = 2,3

  FIXDISPL = .0. NODESET = 1

MATERIAL 1 "TRU WASTE"

  BULKMODULUS = 222. SHRMODULUS = 333. DENSITY = 790.4

  CRFOAM 1 0.0 0.0 3.0 0.0 0.0 0.02

FUNCTION 1

  0.000000 0.010

  0.031493 0.028

  0.523363 0.733

  0.592620 1.133

  0.642640 1.667

  0.692720 2.800

  0.784760 10.170

  0.800000 20.000

MATERIAL 2 "CRUSHED-SALT"

  NONLINELAST 0.001408.0.000846.1300..0.00653.0.00653

       1656..992..1..025

  MUNDAW

   A1 = 45.86   Q1DIVR = 6039.   N2 = 1.0

   N1 = 4.9   MU = 1.0

   CONCRP 4.10E+15. 0.82. -.0173. 2140.. 3

  MISEQSTRS

MATERIAL 3 "INTACT SALT"

   2480.   0.25 1. 2140.

```
    MUNDAW
     AI = 45.86    QIDIVR = 6039.
     NI = 4.9      MU = 1.0
    MISEQSTRS


    MATERIAL 4 "AIR-GAP/CRUSHED SALT"
        0.10  0.0   1.  0.0


    GAPMATI 3
      ELEMSET 4
    GAPTOLERANCE = 0.01


    TEMP0 27.00 CENTIGRADE


    GASGENERATION
      R = 8.314E-6   GASTEMP = 300.15   POROSITY = .6626
      IDEALGAS
      GASCONSTANT = 2. 18.60
      ELEMSET 1 2 4   SURFSET 1


    FUNCTION  2
      0.   0.
      550.   1100.
      1050.   1600.
      2000.   1600.


    OUTPUT = DISPLACE  STRESS  MESH  ELASTIC
    OUTINT = 1
    OUTIMES = .001  .1  .25  .50  .75  1.  2.5  5.  7.5  10.  12.5  &
            15.  17.5  20.  22.5 25. 27.5  30. 32.5 35. 40.  50. 60.  &
            70.  80.  85.  90.  100.  125.  150.  200. 250. 300. 350. &
            400. 450. 500. 600. 700. 800. 900. 1000. 1250. 1500. 1750. &
            2000.
    NODELIST  1 19 116 163 316 318 320 322 324 326 328 426 428 430 340
    ELEMLIST = 1 12 79 80 163 48 74 73 72 161 753 774 772 770 263 259
            81 82 83 179 180 181 186 188 344 595 639


    PLOTDBASE = YES  PLOTSTRAIN


    RESTDBASE
      SAVINTERVAL = 20000
```

SPECTROM-32 Input File for the WIPP Disposal Room Problem-Cont.

```
SAVTIMES = 15. 25. 50. 75. 100. 150. 200. &
           500. 1000. 1500. 2000.

EXECUTE = YES
SUPDEF NO
ENDATA
```

E-132